

École polytechnique de Louvain

Joint evaluation of performance and environmental impacts of a microfabricated device.

VO₂-based device

Author: **Pauline RAUX**

Supervisors: **Jean-Pierre RASKIN, Noémie BIDOUL, Alex PIP**

Readers: **Jean-Pierre RASKIN, Laurent FRANCIS, Noémie BIDOUL,
Alex PIP**

Academic year 2022-2023

Master [120] in Electrical Engineering

Abstract

VO₂-based devices are particularly intriguing due to their capacity to undergo a phase change from insulator to metal in response to temperature variations. The potential applications for such devices are extensive and involves switches, memories, photodetectors, smart windows, sensors, oscillators etc. In this work, a cradle-to-gate approach was employed to evaluate the environmental impact of the microfabrication of the VO₂-based device, from the extraction of raw materials to the exit of the WINFAB laboratory. The objective was to identify the hotspots and propose energy-efficient alternatives, while also assessing the impact of these alternatives on device performance. The process involved a standard cleaning step, followed by wet thermal oxidation to create a SiO₂ layer. Subsequently, a VO₂ sputtering step and VO₂ annealing step were conducted to trigger crystallization. This was followed by lithography, metallization, and lift-off. The Primary Energy Demand (PED) in [MJ/cm²] was chosen as the indicator for the Life Cycle Assessment (LCA). Several assumptions were made to obtain conclusive results, with one of the major assumptions being the utilization of Boyd's work as source for the Energy Intensity (EI) values, except for the metals where the EduPack software was used. Real-time power consumption measurements revealed that the equipment consumed less power than stated in the datasheet, which was also taken into consideration and slightly reduced the final result. The overall PED of the process was determined to be $1.37 \cdot 10^2$ [MJ/cm²]. The most significant impact was observed during the metallization step, primarily due to gold deposition and its associated EI, representing 99.27% of the total PED. The methodology used in this work and the results obtained were discussed with the research laboratory, CEA-Leti. An alternative approach proposed replacing the gold metal layer with copper, resulting in a 99.25% reduction in the total PED to 1.03 [MJ/cm²]. In this alternative process, the VO₂ sputtering step has the highest impact due to the EI of vanadium. Following the reduction in impact, a performance analysis was conducted, considering the $R_{contact}$ and the R_{ins}/R_{met} ratio for both gold and copper evaporation. The use of copper evaporation exhibited a lower $R_{contact}$, indicating smoother current flow across the junction. Moreover, the greater R_{ins}/R_{met} ratio for copper evaporation resulted in a larger negative differential resistance (NDR) zone, representing the wanted region for oscillations, that we desire maximum. A proposed virtual process suggests substituting the gold deposit with aluminum, along with the utilization of different equipment, and replacing wet thermal oxidation with PECVD. The implementation of this virtual process results in a total PED of $7.07 \cdot 10^{-1}$ [MJ/cm²], leading to a remarkable reduction in the overall impact by 99.48%. The biggest challenge faced during this work revolves around obtaining the necessary data for EI. This factor significantly impacts the ultimate outcome. Collaboration between industry, researchers, and other stakeholders is necessary to facilitate the sharing of such information.

Keywords : VO₂-based device, Life Cycle Assessment (LCA), Primary Energy Demand (PED), Energy Intensity (EI), contact resistance, negative differential resistance (NDR) zone

Acknowledgments

I would like to express my deep gratitude to the people who made a significant contribution to the completion of this work. Their invaluable support and presence along the way have been of paramount importance.

First of all, I would like to extend my warmest thanks to Professor Jean-Pierre Raskin for giving me the exciting opportunity to work on this topic. From the start, I was captivated by this subject, and I am grateful to have been able to bring it to fruition.

Secondly, I would like to express my deep gratitude to Noémie Bidoul. She was an essential pillar of this project, supporting me from start to finish. Her invaluable guidance at every stage, her unfailing availability and her confidence in my abilities have been invaluable. I am sincerely grateful.

I would also like to thank Alex Pip for his help throughout this work. His sound advice and precious time spent helping me to improve certain aspects that I had less control over were of great value to me. I am grateful for his constant support.

Noémie and Alex, I'd particularly like to thank you for the time you gave me. Your unfailing availability, even in moments of doubt, has been a source of comfort and encouragement.

I would also like to express my gratitude to Sebastien Faniel and Christian Renaux for their invaluable help with my questions about the WINFAB laboratory. Thanks to them, I was able to identify each of the sources of energy consumption of the equipment used in my process. Their support was a great help in completing this dissertation. Special thanks go to Christian for the time he generously gave to help me with the measurements on the equipment. His availability and expertise were invaluable.

I would also like to express my gratitude to Alexandre Jérard for his kindness in providing me with two wafers that enabled me to finalise this work on time. I would also like to thank Nicolas Roisin for his enlightening explanations of elements that I no longer mastered so well, and my friend Brock for his invaluable help with Python programming. I would also like to express my gratitude to my father, who dedicated time to proofread this work, despite it being outside his area of expertise.

Finally, I'd like to emphasise that a work of this nature can never really be done alone. Many people have helped me at different times and with various aspects. For this, I am extremely grateful.

Contents

1	Introduction	1
2	State Of The Art	3
2.1	VO ₂ -based devices	3
2.2	LCA of microfabricated devices	5
3	Microfabrication Process of VO₂-based device	11
3.1	Wafer	12
3.2	Standard Cleaning	13
3.3	Wet Thermal Oxidation	15
3.4	VO ₂ Sputtering	16
3.5	VO ₂ Annealing	18
3.6	Lithography	19
3.7	Metallization	21
3.8	Lift-off	22
4	Life Cycle Assessment of the VO₂-based device	24
4.1	Goal & Scope	25
4.2	Methodology	26
4.3	Inventory	30
4.4	Results & Impacts	31
4.5	Interpretation of the results	40
5	Alternative process	42
5.1	Change in environmental impact	47
5.2	Change in performance	49
6	Discussion and Perspectives	53
6.1	Life Cycle Assessment (LCA) of the VO ₂ -based device	53
6.2	Alternative process	60
6.3	Perspectives	64
7	Conclusion	69

A Detailed Worksheet (Inventory)	71
A.1 Standard Cleaning (10 wafers)	71
A.2 Wet Thermal Oxidation (20 wafers)	71
A.3 VO ₂ Sputtering (1 wafer)	72
A.4 VO ₂ annealing (20 wafers)	72
A.5 Lithography (1 wafer)	72
A.6 Metallization - Gold Evaporation (4 wafers)	73
A.7 Lift-off (1 wafer)	73
A.8 Metallization - Copper Evaporation (4 wafers)	73
A.9 PECVD (3 wafers)	74
A.10 Metallization - Aluminum evaporation (16 wafers - VST)	74
B PEL103 measuring device.	75
C VO₂ appearance between insulator and metallic state.	76
D Plasma Enhanced Chemical Vapor Deposition (PECVD)	77

List of Figures

2.1	Hysteresis curve during the insulator-to-metal transition (IMT) of a thin VO ₂ film [42].	4
2.2	I- (yellow) and V-driven (blue) characteristic of the VO ₂ device with the current range for spiking regime (in orange, corresponding to the negative differential resistance (NDR)).	4
2.3	Definition of the different possible scopes in an LCA [36].	6
2.4	Break down of environmental impacts from VRFB manufacturing to battery components and upstream processes without the use of recycled materials [56].	6
2.5	The CED and GWP per cm ² were calculated for the complete process flows of the pressure sensors developed by Kumar et al. and Li et al. These process flows encompass the entire production cycle, including the production of silicon wafers, SOI process, and wafer manufacturing steps [14].	9
2.6	Life cycle primary energy requirements [34].	9
2.7	(a) Energy and (b) GWP use per die, by life-cycle stage, over eight technology nodes [8].	10
2.8	Trends at each node reveal the environmental impacts per cm ² in relation to (a) PED, (b) GWP, and (c) water consumption [47].	10
3.1	Microfabrication process of VO ₂ device.	12
3.2	Argon ions from the plasma strike a target made of the material to be deposited. Atoms from the target are ejected and deposited on the substrate [22].	16
3.3	Photolithography with negative resist.	19
3.4	Lift-off process : resist development and metal lift-off.	22
4.1	Scope and boundaries of the study.	25
4.2	Real Time power consumption (in blue) versus datasheet (in orange), in [kW].	29
4.3	PED [J/cm ²] of the complete process, logarithmic scale.	32
4.4	PED [J/cm ²] of the standard cleaning step, logarithmic scale.	33
4.5	PED [J/cm ²] of wet thermal oxidation step, logarithmic scale.	34
4.6	PED [J/cm ²] of the VO ₂ sputtering step, logarithmic scale.	35
4.7	PED [J/cm ²] of the VO ₂ annealing step, logarithmic scale.	36
4.8	PED [J/cm ²] of the lithography step, logarithmic scale.	37
4.9	PED [J/cm ²] of the metallization step, logarithmic scale.	38
4.10	PED [J/cm ²] of the lift-off step, logarithmic scale.	39
4.11	PED [J/cm ²] of the complete process with zoom on the hotspot, logarithmic scale.	41

5.1	Grain size of the initial batch of wafers that exhibited halos, 906.2 nm.	44
5.2	Grain size of wafer with gold (and nickel) evaporation, 245.36 nm.	44
5.3	Grain size of wafer with copper evaporation, 253 nm.	44
5.4	Metal-semiconductor Ohmic contact IV curve.	45
5.5	Measuring pad for the IV transition curves.	45
5.6	I- (yellow) and V-driven (blue) characteristic of the VO ₂ device.	46
5.7	PED [J/cm ²] of the complete process with copper evaporation, logarithmic scale. The solid line in the graph depicts the PED of the initial process (gold and nickel evaporation).	47
5.8	PED [J/cm ²] of the metallization step (copper evaporation), logarithmic scale. The solid line in the graph depicts the PED of the initial metallization step (gold and nickel evaporation).	48
5.9	Pads for the transfer length measurement (TLM). <i>W</i> the width of the pads and <i>L</i> the length between the pads.	49
5.10	Spacing between the different pads [μm].	49
5.11	Linear regression of the transfer length measurement (TLM) method performed at 25°C.	50
5.12	Linear regression of the TLM method performed at 110°C.	51
5.13	Resistance of VO ₂ with temperature to demonstrate the magnitude of hysteresis in the case of gold (and nickel) evaporation and in the case of copper evaporation.	52
6.1	PED [J/cm ²] of the complete process with gold (and nickel) evaporation, logarithmic scale. Energy Intensity (EI) values only from Boyd's work [8]. The solid line in the graph depicts the PED [J/cm ²] with EI from the EduPack software for the metals.	55
6.2	PED [J/cm ²] of the complete process with gold (and nickel) evaporation, logarithmic scale. Without capacity Factor. The solid line in the graph depicts the PED [J/cm ²] with the capacity factor included.	56
6.3	Energy use per 300 mm wafer equivalent, by life-cycle stage [8].	59
6.4	Life cycle primary energy requirements [34].	59
6.5	PED per cm ² in function of the node trends which are derived from an analysis of scientific literature and LCA databases [47].	59
6.6	PED [J/cm ²] of the complete process with copper evaporation, logarithmic scale. The solid line in the graph depicts the PED [J/cm ²] for gold (and nickel) evaporation.	60
6.7	PED [J/cm ²] of the metallization step gold (and nickel, left) versus copper evaporation (right), logarithmic scale.	61
6.8	V-driven characteristic of the Au/VO ₂ device with the current range for spiking regime (in orange, corresponding to the NDR).	62
6.9	V-driven characteristic of the Cu/VO ₂ device with the current range for spiking regime (in orange, corresponding to the NDR).	62
6.10	The green spot indicated by the arrow in the figure shows the oxidation of copper.	62
6.11	PED [J/cm ²] of the metallization step copper versus copper and tantalum nitride evaporation, logarithmic scale.	63
6.12	PED [J/cm ²] of the complete process with copper and tantalum nitride evaporation, logarithmic scale.	63
6.13	PED [J/cm ²] of the metallization step for gold, copper and aluminum evaporation, logarithmic scale.	66
6.14	PED [J/cm ²] of the oxidation step, logarithmic scale. Wet Thermal Oxidation versus PECVD.	66

6.15	PED [J/cm^2] of the wet thermal oxidation vs PECVD (100 Standard cubic centimeters per minute (sccm)) vs PECVD (1000 sccm), logarithmic scale.	66
6.16	PED [J/cm^2] of the complete process with aluminium evaporation and PECVD. The solid line in the graph depicts the PED [J/cm^2] for gold (and nickel) evaporation and wet thermal oxidation. .	67
B.1	Positioning of the PEL103 measuring device.	75
C.1	VO ₂ appearance.	76

List of Tables

3.1	Specifications of the 3 baths.	13
3.2	Process parameters specific for LCA.	14
3.3	Process parameters specific for LCA.	15
3.4	The amounts of inputs based on the chronological sequence of the process.	17
3.5	Process parameters specific for LCA.	17
3.6	Process parameters specific for LCA.	18
3.7	Overview of the various steps, taking into account inputs, equipment, and duration.	20
3.8	Process parameters specific for LCA.	20
3.9	Process parameters specific for LCA.	21
3.10	Process parameters specific for LCA.	23
4.1	Real Time energy consumption versus datasheet, in [MJ].	28
4.2	Inventory of the microfabrication process of VO ₂ -based device.	30
4.3	PED [MJ/cm ²] of the complete process.	32
4.4	PED [MJ/cm ²] of the standard cleaning step.	33
4.5	PED [MJ/cm ²] of the wet thermal oxidation step.	34
4.6	PED [MJ/cm ²] of the VO ₂ sputtering step, logarithmic scale.	35
4.7	PED [MJ/cm ²] of the VO ₂ annealing step.	36
4.8	PED [MJ/cm ²] of the lithography step.	37
4.9	PED [MJ/cm ²] of the metallization step.	38
4.10	PED [MJ/cm ²] of the lift-off step.	39
5.1	Measurement conditions.	45
5.2	PED [MJ/cm ²] of the complete process with copper evaporation.	47
5.3	Total resistance R_{tot} according to pad distances.	50
5.4	$R_{contact}$ at 25°C and 110°C.	51
5.5	R_S at 25°C and 110°C.	52
6.1	Comparison of EI values between Boyd and other sources. EI value for vanadium not present in Boyd.	54
6.2	PED [MJ/cm ²] of the complete process. Energy Intensity (EI) values only from Boyd's work [8].	55

6.3	PED [MJ/cm ²] of the complete process. Energy Intensity (EI) values only from Boyd's work [8] and the EduPack software for metals [4].	55
6.4	PED [MJ/cm ²] of the complete process with gold (and nickel) evaporation. Without capacity Factor.	57
6.5	PED [MJ/cm ²] of the complete process. Energy Intensity (EI) values only from Boyd's work [8] and the EduPack software for metals [4].	57
6.6	PED [MJ/cm ²] of the complete process with copper evaporation.	61
6.7	Comparison of gold, copper and aluminum.	64
6.8	PED [MJ/cm ²] of the complete process with aluminium evaporation and PECVD.	67
A.1	Detailed worksheet of the standard cleaning step.	71
A.2	Detailed worksheet of the wet thermal oxidation step.	71
A.3	Detailed worksheet of the VO ₂ sputtering step.	72
A.4	Detailed worksheet of the VO ₂ annealing step.	72
A.5	Detailed worksheet of the lithography step.	72
A.6	Detailed worksheet of the gold evaporation step.	73
A.7	Detailed worksheet of the lift-off step.	73
A.8	Detailed worksheet of the copper evaporation step.	73
A.9	Detailed worksheet of the PECVD alternative.	74
A.10	Detailed worksheet of the aluminum evaporation in VST alternative.	74

Acronyms

CED Cumulative Energy Demand. 7, 8, 26, 58, 69

DI water de-ionized water. 13, 14, 19, 20, 22, 23, 39, 71–73

EI Energy Intensity. 26, 27, 31, 40, 45, 53–55, 58, 62, 64, 69, I, VI, VIII

HMDS Hexamethyl disilazane. 19, 20, 72

HVAC Heating, ventilation and air-conditioning. 25, 31, 53, 57

IMT insulator-to-metal transition. 3, 4, V

LCA Life Cycle Assessment. 1, 2, 5–8, 14, 15, 17, 18, 20, 21, 23–27, 30, 40, 42, 53, 54, 56–60, 69, 70, I, III, V, VI, VIII

LCI Life Cycle Inventory. 6, 7, 24, 30, 54

LCIA Life Cycle Impact Assessment. 7, 24, 57

NDR negative differential resistance. 4, 51, 52, 61, 62, 70, I, V, VI

PEB post-exposure bake. 20

PECVD Plasma Enhanced Chemical Vapor Deposition. 65–67, 70, 77, 78, IV, VII, IX

PED Primary Energy Demand. 7, 25, 26, 28, 31–40, 47, 48, 53–62, 64, 65, 67, 69–74, I, VI

PEF Primary Energy Factor. 26, 28, 31

PVD Physical Vapor Deposition. 16

rpm revolutions per minute. 13

sccm Standard cubic centimeters per minute. 18, 31, 66, VII

TLM transfer length measurement. 49–51, VI

UPW Ultra Pure Water. 13, 59

UV Ultraviolet. 19, 22

Chapter 1

Introduction

Today, global warming is a pressing issue that demands our immediate attention and action. As a future electrical engineer, I find it particularly intriguing to explore how my knowledge and skills can contribute to help mitigating global warming's effects. When considering global warming, we recognize that human activities significantly impact the environment, and the microelectronics industry is no exception. Within this industry, microfabricated devices are widely utilized in various industrial sectors such as aerospace, healthcare, consumer electronics, and automotive. Unfortunately, the intensive use of chemicals, toxic materials, high energy consumption during extraction and manufacturing processes, and the production of waste contribute to the pollution associated with these microfabricated devices.

Among the emerging microfabricated devices, VO₂-based devices have acquired significant interest due to their unique phase-changing properties. These devices can adapt their behaviour based on temperature variations, offering promising applications in electronics, sensors, and thermal insulation systems.

Nevertheless, it is crucial to acknowledge the environmental impact associated with the production of these microfabricated devices. The sustainability of the microelectronics research and industry is constrained by some critical factors. The fabrication step of microelectronic devices is often pointed at as the most harmful step of their life cycle to the environment planetary limits: depletion of material resources, high environmental impact of microfabrication processes (polluting gases, toxic products, high energy intensity, high water consumption, ...). Therefore, it becomes imperative to take proactive measures to minimize the environmental footprint throughout the life cycle of these devices.

One approach to achieving this objective is through the implementation of a Life Cycle Assessment (LCA) specific to VO₂-based microfabricated devices. LCAs provide a comprehensive evaluation of a product's entire life cycle, involving material production, usage, and end-of-life considerations. By conducting LCAs on VO₂-based microfabricated devices, we can identify critical areas contributing to greenhouse gas emissions and other environmental impacts. This knowledge enables us to focus our efforts on targeted improvements, develop strategies to reduce environmental impact, and promote the adoption of sustainable practices in device manufacturing.

In conclusion, addressing global warming requires collective efforts, and the microelectronics industry, including VO₂-based microfabricated devices, has a role to play in reducing pollution in general and greenhouse gas emissions

in particular. Incorporating LCAs into the development and manufacturing processes of these devices is crucial in identifying opportunities for improvement, minimizing environmental impact, and actively contributing to the fight against global warming. By combining technological innovation with a strong commitment to environmental responsibility, we can pave the way for a sustainable future that preserves and protects our planet for generations to come.

This master thesis, hereafter described as the 'work', is part of the development of a methodology for systematic impact assessment of a microfabrication processes, through the joint evaluation of figures of merit (FoM) based on technical performance and environmental impacts. This methodology is developed by taking the microfabrication process of the VO₂-based device in the WINFAB cleanrooms of UCLouvain as case study.

The following structure is adopted for this work. First, the context is explored through literature and some field research. Subsequently, a detailed examination of the entire process of the VO₂-based devices is given. The subsequent chapter focuses on a comprehensive review of the LCA conducted on this process, involving the underlying assumptions made to ensure accurate and identifiable results. Additionally, we propose an alternative process and present a comparative assessment of its environmental impact and selected performance indicators. To conclude, we present a chapter dedicated to discussion, followed by an outlook on future prospects and a conclusion. We hope you will enjoy reading this presentation.

Chapter 2

State Of The Art

This chapter establishes the context that will be further explored in the subsequent chapters of this work through a literature review. It also introduces and elucidates the fundamental concepts employed throughout this work.

2.1 VO₂-based devices

VO₂-based devices are composed of a thin film of vanadium dioxide (VO₂) that undergoes a reversible phase transition driven by temperature, transitioning from an insulating state to a metallic state, commonly referred to as an insulator-to-metal transition (IMT). These devices find extensive applications in various fields, including switches, memories, photodetectors, actuators, smart windows, camouflages, passive radiators, resonators, sensors, field-effect transistors, magnetic refrigeration, and oscillators [30]. The VO₂ film switches from a semiconducting, monoclinic phase to a metallic, tetragonal phase. The exact mechanism behind the IMT in VO₂ is still a subject of debate, with two proposed possibilities : a crystalline phase transition (from monoclinic to tetragonal), or electron-electron correlations leading to a pure electronic Mott transition. Both experimental and theoretical studies on bulk VO₂ suggest that the IMT mechanism is a combination of a pure Mott transition and a spin-Peierls lattice instability, indicating strong correlations ([42], [32]). This transition occurs at approximately 68°C and is accompanied by a sudden change in resistivity (Figure 2.1). During heating, the resistivity decreases as the material undergoes the IMT and transitions to the metallic state. However, during cooling, the resistivity remains in the metallic state until a lower critical temperature is reached, at which point the material undergoes another transition back to the insulating state, resulting in an abrupt increase in resistivity. This hysteresis behaviour is due to the presence of structural and electronic instabilities within the material during the phase transition, leading to different resistivity values for heating and cooling cycles. In addition to thermal activation, the IMT in VO₂ thin films can be triggered electrically (through charge injection or Joule heating), optically (via photon excitation), or even through the application of high pressure or stress. The optically and electrically induced transitions are known to occur rapidly, often within 1 picosecond ([11], [12]). The transition properties of VO₂ can vary significantly, influenced by factors such as the growth technique, crystal size (nanoparticles, thin films, bulk, etc.), annealing, doping, deformation, and other variables [13].

In terms of the electrical transition, once the electrical triggering of the IMT phase occurs, a nucleation process initiates. When the applied voltage surpasses a threshold value, the first seed domains transition into a metallic state. As the voltage increases, the filament extends due to the Joule effect, switching the device from high resistance (insulator) to low resistance (metal). At this point, the current experiences a sudden surge, signifying the completion of the transition from insulator to metal (IMT). When reducing the applied voltage, the heat dissipates, causing the filament size to decrease and a the film to transition from a metallic state to an insulating state (MIT) ([58], [7]). This behaviour is reflected in the characteristic IV curves depicted in Figure 2.2. To achieve current/voltage oscillations, a prerequisite is the presence of a distinct NDR regime in the I-V characteristic, between its equilibrium points for metallic and insulating states [30]. For optimal performance, the current flowing through the device should fall within the NDR range. The extent of this NDR region may vary based on different factors such as the grain size of the VO₂ film during device production.

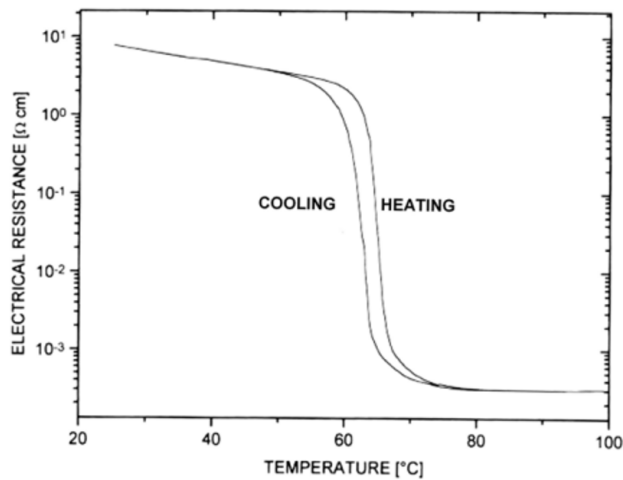


Figure 2.1: Hysteresis curve during the insulator-to-metal transition (IMT) of a thin VO₂ film [42].

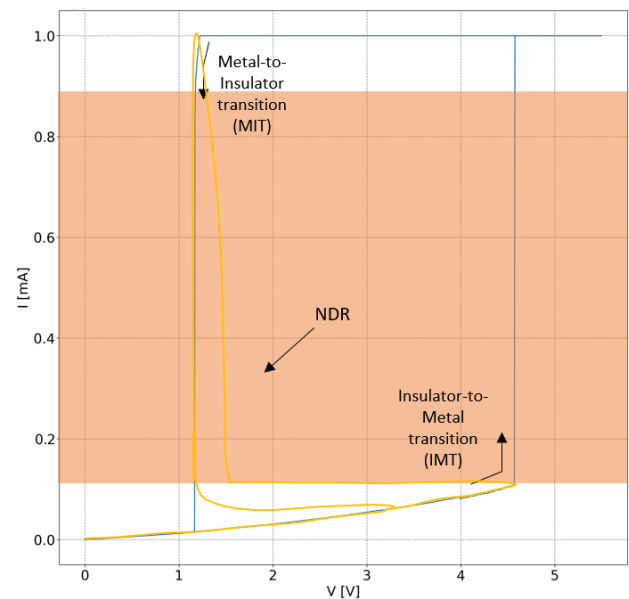


Figure 2.2: I- (yellow) and V-driven (blue) characteristic of the VO₂ device with the current range for spiking regime (in orange, corresponding to the NDR).

2.2 LCA of microfabricated devices

An LCA, which stands for Life Cycle Assessment, is an environmental evaluation technique used to estimate the ecological effects of a product, service, or process throughout its entire life cycle. This life cycle spans from the acquisition of raw materials to the product's end of life, including activities such as manufacturing, transportation, usage, and waste management. The primary objective of conducting an LCA is to quantify various environmental impacts, including greenhouse gas emissions, water consumption, air pollution, waste generation, and more, associated with the evaluated product, service, or process. By analyzing the results of an LCA, it becomes possible to identify the stages of the life cycle that have the greatest environmental impact and to determine the actions to be taken to reduce these impacts. LCA is therefore an essential method for decision-making in eco-design, sustainable development and environmental policy. It allows the assessment of environmental pros and cons of different products, services, or processes, enabling comparisons to identify the most environmentally favorable solution. Today, numerous companies, organizations, and governments rely on LCA to enhance their environmental performance and minimize their ecological footprint [1].

Methodology of LCA

The methodology of LCA is structured around four distinct yet interconnected stages, highlighting the iterative nature of the approach, which requires frequent feedback throughout the study [36]. These stages are as follows:

1. The initial stage of the LCA is **goal and scope definition**. In this step, the study's objectives are clearly stated, and the system under investigation (product, service, or process) is defined, along with the boundaries that include the different stages of the life cycle to be considered in the analysis. The goal of an LCA states the intended application, reasons for conducting the study, target audience, and whether the results will be used for comparative assertions or public disclosure. The scope of the study includes several crucial elements, including product descriptions, the function of the product, and the functional unit, which quantifies the system's function and serves as the basis for comparing scenarios. Additionally, system boundaries are established to specify the material or energy flow and the level of environmental significance associated with unit processes or product systems to be excluded from the study, as defined by ISO 14044:2006 [27]. These system boundaries can be categorized into groups such as cradle to gate, gate to gate, and cradle to grave (Figure 2.3). In the article "Life cycle assessment of Vanadium Redox Flow Battery" the authors state that their LCA methodology involves a cradle-to-gate approach, meaning the battery's entire life cycle from raw material extraction to manufacturing and disposal is considered [56]. According to their findings, the battery components related to the electrolyte (including the electrolyte itself, tanks, and upstream processes) account for over 90% of the overall global warming impacts. In contrast, the stack and peripheral components contribute merely 5% and 2% respectively (Figure 2.4).

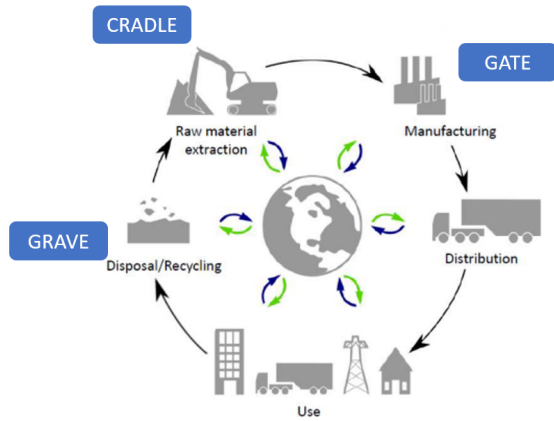


Figure 2.3: Definition of the different possible scopes in an LCA [36].

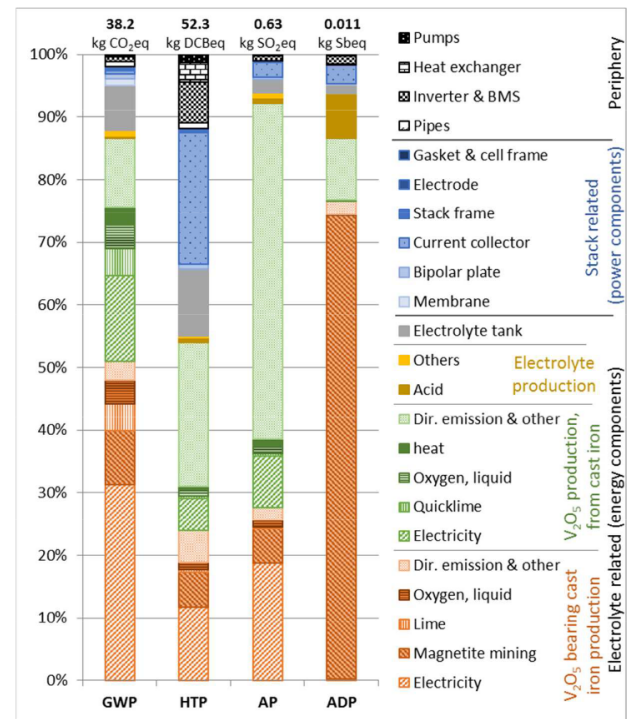


Figure 2.4: Break down of environmental impacts from VRFB manufacturing to battery components and upstream processes without the use of recycled materials [56].

2. The **Life Cycle Inventory (LCI)** stage involves gathering the necessary data (activity factors, data sources) for conducting an environmental assessment throughout the life cycle of the system being studied. These data can be obtained from different sources, such as suppliers, interviews with industry experts, industry reports, public databases, literature reviews or scientific studies [8]. There are three distinct inventory approaches employed.

- The first approach is the *bottom-up* or process-based inventory. It relies on data collected directly from the factory, such as electricity, heat, and water consumption by machines, to compile an inventory of the manufacturing process. While this method can be highly accurate, it does suffer from a systematic underestimation bias known as "truncation error." This bias arises due to practical limitations in estimating factors like maintenance and machine watch, which leads to the exclusion of certain components ([52], [14], [24]). Therefore, this method is more suitable for in-depth studies of specific end-uses or systems aimed at identifying emissions hot spots.
- The second approach is *top-down* LCI, which utilize an economic input-output (EIO) method for inventorying. This involves quantifying the impacts per dollar exchanged between different industrial sectors in the production of goods. Impacts are calculated based on the relationship between monetary flows and energy consumption, specifically energy consumption per dollar/sector. This approach avoids limitations associated with the bottom-up approach, such as chemical production. However, it may

not be ideal when used alone for product production, as the industry can be dynamic with fluctuating prices.

- The third approach involves *hybrid* LCI, which combines bottom-up and top-down data when the bottom-up approach has limitations. Hybrid LCI are considered the most accurate but also require extensive work as both approaches must be integrated. For example, in "A Hybrid Life Cycle Inventory of Nano-Scale Semiconductor Manufacturing", the authors collected industry data, public information, and experimental data to create a hybrid LCI [34]. In "Economic-balance hybrid LCA extended with uncertainty analysis: case study of a laptop computer", a hybrid economic-ecological LCA was performed which combined material flow analysis with economic analysis and sensitivity analysis to assess the environmental and economic impact of a specific product, such as a laptop [15].

3. The **Life Cycle Impact Assessment (LCIA)** stage involves evaluating the environmental impacts associated with each life cycle stage of the system under study. This assessment utilizes environmental indicators such as carbon footprint, ultra-pure water consumption (UPW), waste generation, global warming potential (GWP), Primary Energy Demand (PED), Cumulative Energy Demand (CED), and more. The LCIA typically comprises four key steps. The first step, classification, aims to classify the results of the inventory into impact categories. The second, characterisation, is used to express different pollutants in the same impact category as the equivalent of the same pollutant. The third step, normalisation, aims to express the results in relation to a reference. The final step is weighting, which assigns importance or significance to different impact categories. A higher score indicates a greater environmental impact. For instance, in Sarah Boyd's work, environmental indicators such as greenhouse gas emissions, water consumption, energy consumption, and waste generation were presented [8]. Meanwhile, the authors of "Life cycle assessment of a Vanadium Redox Flow Battery" identified impact categories such as global warming potential, acidification potential, eutrophication potential, photochemical ozone creation potential, and cumulative energy demand [56].
4. The **interpretation of LCA results** is a crucial step that involves analyzing and understanding the findings in relation to the study's objectives. This step makes it possible to determine the life cycle stages with the greatest environmental impacts and to identify opportunities for improvement.
5. The **communication of LCA results** involves effectively presenting the findings to various stakeholders, including customers, suppliers, employees, and others. The objective is to ensure that the results are communicated in a clear and understandable manner. Additionally, this step involves proposing environmental improvement solutions for the system under study, aiming to provide actionable recommendations for enhancing environmental performance.

It is important to note that LCAs can vary depending on the specific product, service, or process under investigation, as well as the objectives of the study. To provide a more comprehensive assessment, LCA can be complemented by analyses of sustainability, social impacts, or economic factors.

LCA in the field of microelectronics

LCA in the field of microelectronics, particularly in relation to semiconductors, is a relatively new and evolving practice [47]. Semiconductors find application in various areas, including electronic devices, solar panels, energy storage systems, electric vehicles, and medical devices. However, semiconductor production is also associated with

significant environmental impacts, such as energy consumption, greenhouse gas emissions, waste generation as well as extensive water and chemical usage ([8], [34], [6]). Obtaining data on microelectronics can be challenging due to various factors: confidentiality, complexity of the field, speed of innovation and cost of data collection. The available data may be fragmented or incomplete, making it difficult to analyze the environmental impacts of the industry and make well-informed decisions regarding sustainability. The difficulty in obtaining comprehensive data is not limited to microelectronics but also extends to other industries within the broader context of LCA, which is much criticized.

For instance, the authors highlights in "Life Cycle Assessment of Metals: A Scientific Synthesis" the challenges in assessing the life cycle of metals, including data variability, complex supply chains, and the difficulty of considering all environmental impacts [45]. In "Integrative approaches to environmental life cycle assessment of consumer electronics and connected media", Paul Teehan discusses the difficulties in applying integrative LCA, such as the lack of standardized methods and data for assessing environmental impacts [52]. In "The Environmental Footprint of IC Production: Review, Analysis, and Lessons From Historical Trends", the authors point out the lack of transparent and detailed data on manufacturing processes and energy sources utilized [47]. Lastly, Sarah Boyd explains the complexities of manufacturing processes, data uncertainties, the variability of environmental impacts, and the necessity of analyzing the entire supply chain [8].

So, what do these authors suggest? They point out the significance of transparency and data availability to ensure precise LCAs. As a result, they recommend collaboration between companies, governments, researchers, and standardization organizations to develop more accurate and standardized approaches for assessing environmental impacts ([52], [47]). Sarah Boyd's work, being a reference source itself, highlights that the outcomes of such assessments can guide strategic decisions and policies aimed at reducing the environmental impact of the electronics industry.

Where do we stand now ?

Now, the key question arises : where do we stand in terms of semiconductor LCA? Microelectronic integrated circuits are produced in controlled environments known as cleanrooms, using high-purity silicon substrates called wafers. These wafers undergo various stages in the manufacturing process, starting from the extraction and processing of raw materials. Then the life cycle of a microelectronic product includes the Front-End manufacturing phase, where integrated circuits are produced on silicon wafers, and the Back-End phase, involving testing, cutting, and encapsulating the circuits. The next phase involves integrating the circuits into electrical and electronic equipment, followed by their use. Finally, the end-of-life phase is reached.

Silicon wafers, which are polished discs of ultra-pure silicon, serve as the foundation for microelectronic integrated circuits. These wafers are manufactured from sand, which contains silicon dioxide (SiO₂) in the form of silica. The process of producing ultra-pure wafers involves multiple steps, including sand extraction, silica separation, silicon purification, crystal production, ingot cutting, and wafer polishing. The production of wafers consumes significant resources, particularly energy. Studies have shown that the energy consumption for wafer production is considerable, with specific values depending on the diameter of the wafers. According to Delhaye and al., for wafers 300 mm in diameter, the CED is 0.4 [kWh/cm²], or 1.44 [MJ/cm²], while the GWP is 180 [g.CO_{2eq}/cm²] [14]

(Figure 2.5). This energy consumption coincides with the results of Krishnan, who estimates that 2900 [MJ/wafer] (for the same 300 mm diameter wafers) or 2.05 [MJ/cm²] of primary energy is used throughout the silicon wafer production chain [34] (Figure 2.6). The manufacture of wafers for the semiconductor industry therefore consumes a lot of energy, mainly because of the high levels of purity required by microelectronic processes.

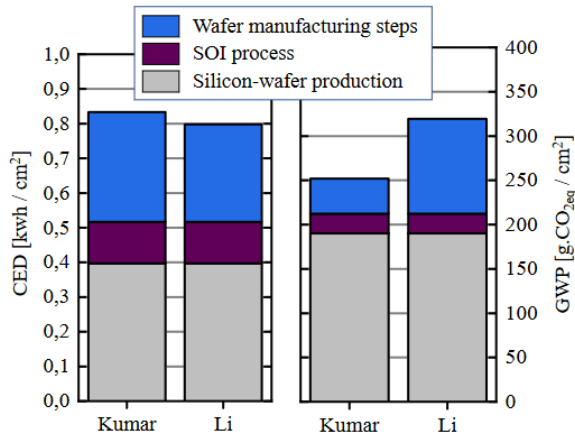


Figure 2.5: The CED and GWP per cm² were calculated for the complete process flows of the pressure sensors developed by Kumar et al. and Li et al. These process flows encompass the entire production cycle, including the production of silicon wafers, SOI process, and wafer manufacturing steps [14].

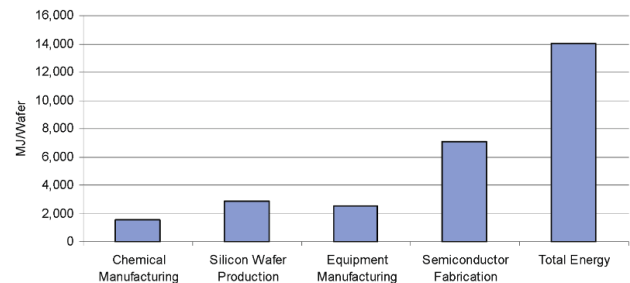


Figure 2.6: Life cycle primary energy requirements [34].

Chemical products play a vital role in the manufacturing of integrated circuits, with various toxic liquid and gaseous chemicals being utilized in substantial quantities. These chemicals include resins, developers, acids, solvents, slurries, dopants, and perfluorocarbons (PFCs) [34]. The microelectronics industry requires highly pure chemical substances, and the purification processes for these chemicals consume substantial energy [6]. The energy consumption associated with the production of ultra-pure chemicals is significantly higher than that of conventional products, although the exact levels are not as extensively studied as those for silicon wafer manufacturing. Krishnan study provides us with the value of 1510 [MJ/wafer] (for the same 300 mm diameter wafers) or 1.07 [MJ/cm²], which is lower as the wafer production as can be seen in Figure 2.6. In Boyd's work, we observe a more or less identical value for the same wafer size (300 mm), the energy associated with chemicals is 2 [GJ/wafer] or 1.41 [MJ/cm²] (Figure 2.7) [8].

The production phase of microelectronic products, particularly semiconductor manufacturing, has various environmental impacts. These include energy and water consumption, greenhouse gas emissions, atmospheric emissions, water discharges, and waste generation. Studies have shown that the energy consumption per wafer during manufacturing is significant, and primary energy requirements for semiconductor manufacturing are greater than those for wafer production. Boyd's work shows that energy consumption per wafer for the fab is around 10 [GJ/wafer], or 7.07 [MJ/cm²] for all the technology nodes (Figure 2.7). Krishnan shows that the primary energy required for semiconductor manufacturing is 7000 [MJ/wafer], or 4.95 [MJ/cm²] (Figure 2.6). Pirson and al.'s give different values based on data from the scientific literature and the LCA databases. Their study shows the environmental

impacts per cm^2 with respect to PED (going from 0 to 100 $[\text{MJ}/\text{cm}^2]$), GWP (going from 0 to 7 $[\text{kgCO}_{2\text{eq}}/\text{cm}^2]$), and water consumption (going from 0 to 100 $[\text{L}/\text{cm}^2]$) [47].

Overall, the production of microelectronic integrated circuits involves complex processes, extensive energy consumption, and the use of chemical substances, all of which have environmental implications that need to be considered.

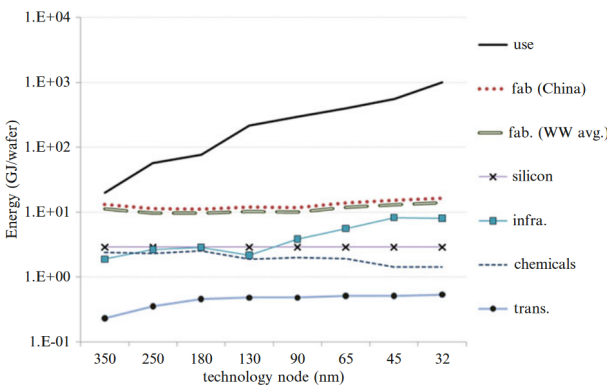


Figure 2.7: (a) Energy and (b) GWP use per die, by life-cycle stage, over eight technology nodes [8].

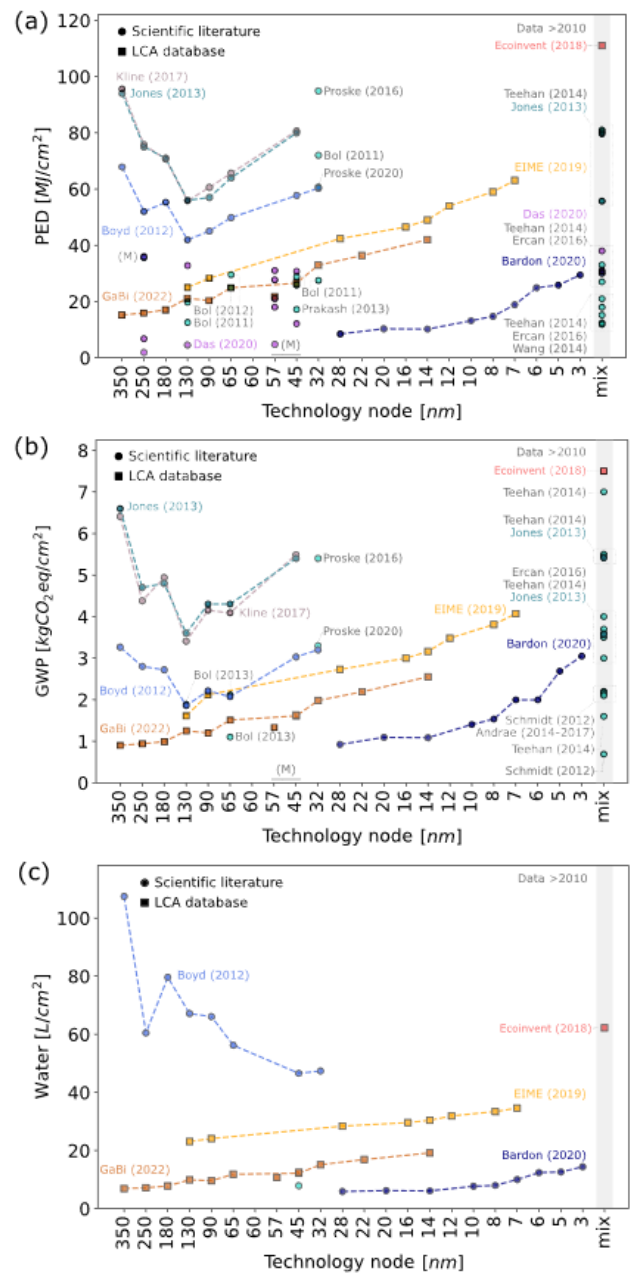


Figure 2.8: Trends at each node reveal the environmental impacts per cm^2 in relation to (a) PED, (b) GWP, and (c) water consumption [47].

Chapter 3

Microfabrication Process of VO₂-based device

In this chapter, we will describe the microfabrication process of a VO₂-based device produced in the WINFAB cleanroom, the Wallonia infrastructure for micro and nano fabrication at the Université catholique de Louvain. Unlike large industrial laboratories that have access to considerable resources and equipment, universities often have to deal with more modest resources for their research work. In research cleanrooms, dedicated equipment for each specific process is not available. Instead, the same equipment is utilized for multiple processes interchangeably which can lead to contamination. However, this does not prevent them from developing innovative microfabrication techniques to produce high quality functional devices. Moreover, these research cleanrooms provide enhanced flexibility for such device developments. Several factors contribute to this flexibility. Firstly, there is no profit-driven motive, reducing the necessity for achieving high yield (the number of functional dies on a wafer) or maintaining high equipment 'up time' (the proportion of the year the equipment is actively producing dies). Consequently, researchers can afford to undertake more experimental actions, such as utilizing the same equipment for depositing different materials, despite the inherent risks of contamination.

The microfabrication process of our VO₂-based device, as shown in Figure 3.1, starts with a standard cleaning to remove all impurities on the substrate surface. Next, we perform wet thermal oxidation to form an oxide layer on the substrate, which serves as a buffer layer for VO₂ growth and as an electrical insulator. We then apply a layer of VO₂ by sputtering, followed by high temperature annealing to trigger the crystallinity of the VO₂. Electrical contacts are defined through reversal photolithography, followed by a gold evaporation (metallization step) and lift-off step. As the VO₂ layer itself is not patterned, the device geometry are defined by the electrode dimensions [22]. We will now detail each step of the microfabrication process, highlighting the **inputs** in blue and the corresponding **equipment** used in our university's cleanroom in orange. This color differentiation aims to enhance clarity, facilitating understanding in the subsequent chapter.

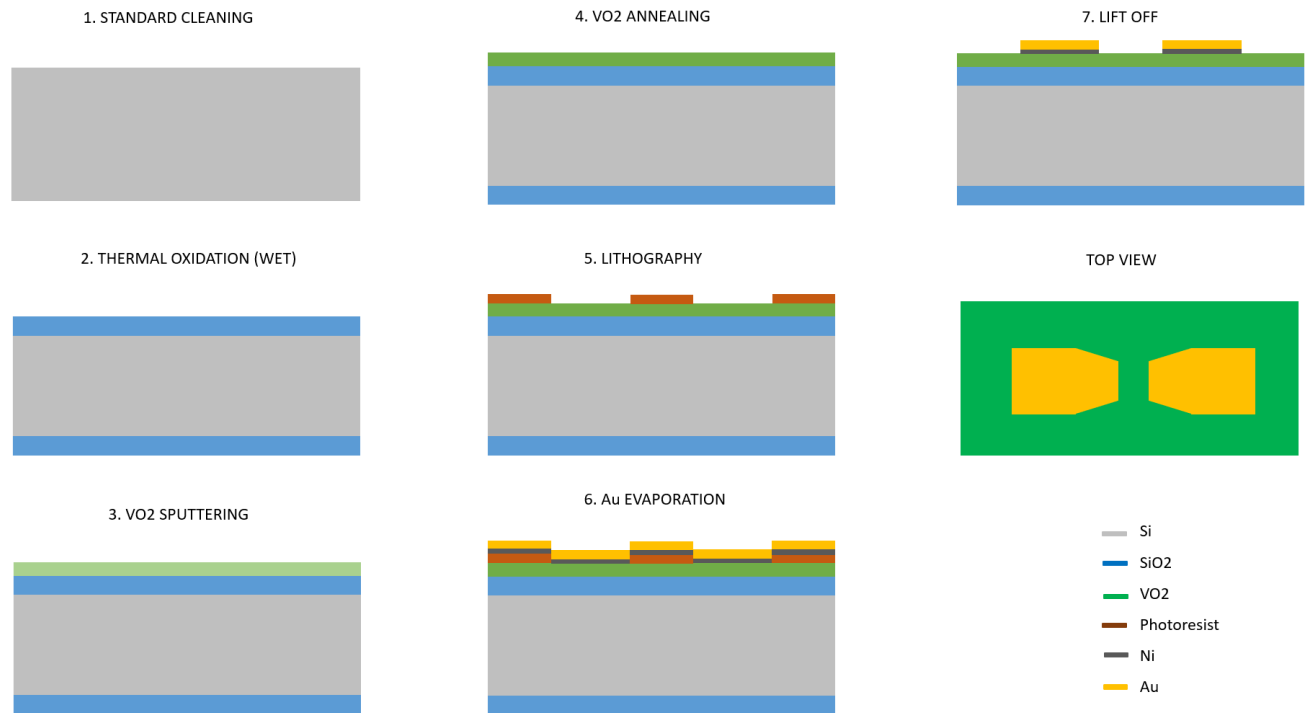


Figure 3.1: Microfabrication process of VO₂ device.

3.1 Wafer

The wafers used for the VO₂ device are standard silicon wafers provided by SIEGERT WAFER GmbH [55]. The specifications are the following : 380 μm thickness and 3 inch (76.2 mm) diameter with a resistivity of 10 Ω·cm.

3.2 Standard Cleaning

Operating Principle

The standard cleaning step is an essential step in the microfabrication process of semiconductor devices on wafers due to the sensitivity of semiconductors to impurities and the presence of a native oxide layer. Contamination of wafer surfaces can disrupt the electrical properties of devices and lead to malfunctions or manufacturing failures. Because of device size downscaling, contamination becomes evermore critical. The objective is therefore to obtain a clean, contaminant-free surface by eliminating particles and reducing atomic contamination before continuing with the microfabrication process.

Process Parameters

In this step, a batch of 10 wafers is immersed successively in 3 baths, each with specific specifications outlined in Table 3.1. Each of these baths is followed by a rinse with [de-ionized water \(DI water\)](#), also called Ultra Pure Water (UPW) and [N₂](#) bubbles at 25°C for 10 minutes.

	Bath 1	Bath 2	Bath 3
Name of the bath	<i>first wash</i>	<i>ultra clean wash</i>	<i>etch</i>
Bath composition	H_2SO_4 and H_2O_2	H_2SO_4 and H_2O_2	2% HF
Temperature	110°C	110°C	25°C
Immersion time	10 minutes	10 minutes	15 seconds

Table 3.1: Specifications of the 3 baths.

The *first and ultra clean wash* are used to remove any organic compounds that may be present on the wafers. The *etch step* aims to remove the native SiO₂ oxide present on the surfaces of the silicon wafer. On top of that, HF treatment leads to a hydrogen-terminated hydrophobic surface. The rinsing between the different baths is intended to eliminate any remaining chemical residue.

The baths are located in so-called "[wet benches](#)", namely tables under hoods where gas extraction is provided by a ventilation system. These benches also contain a system of [heating resistances](#) which are designed to heat the baths to the desired temperature.

The drying step after standard cleaning is essential to ensure that the wafer surface is completely dry before continuing with the microfabrication process. To this end there are a number of methods available in WINFAB : spinning and nitrogen blowing. The [rinser-dryer](#), whose operating principle is based on spinning, is used to achieve this objective in the standard cleaning stage. The centrifuge is working at 880 revolutions per minute (rpm) for 240 seconds.

LCA Parameters

In the Chapter 4, a life cycle analysis will be conducted, and the following Table 3.2 displays the parameters necessary for this analysis.

	Standard Cleaning
Number of wafers	10
Duration of the process	approx. 1 hour
Inputs	H ₂ SO ₄ , H ₂ O ₂ , HF (2%) DI water and N ₂
Equipment	Wet benches, heating resistances and rinsing-dryer
Equipment on standby	No

Table 3.2: Process parameters specific for LCA.

3.3 Wet Thermal Oxidation

Operating Principle

The thermal oxidation step is used for the production of silicon oxide (SiO₂) layer on the surface of wafers. This technique involves heating the wafers to high temperatures in a controlled atmosphere of oxygen and water vapour. First, during what is called a pre-treatment, the wafer is placed in a high-temperature, high-pressure oven containing pressurised water. The wafer is exposed to an oxygen atmosphere to remove the last traces of contaminants from the wafer surface. After the pre-treatment, the growth of the SiO₂ layer begins, which occurs at high temperature in the presence of water. The water molecules are dissociated into oxygen and hydrogen atoms at high temperatures, which then react with the wafer surface to form the SiO₂ layer



The wet thermal oxidation step results in faster growth of the silicon oxide layer compared to dry thermal oxidation. The resulting high quality silicon oxide layer can be used as an electrical insulator in electronic devices.

Process Parameters

A maximum of 20 wafers are put in a vertical **KOYO furnace** (JTEKT Thermo Systems VF1000). The oven is heated at 1000°C under a mixed atmosphere of **O₂**, **H₂** and **N₂**. The full process to get 400 nm of SiO₂ takes 3 hours and 47 minutes and is composed of a total of 16 steps involving different pressures, gas mixtures, temperatures and step times. H₂O (made from combination of H₂ and O₂ gases) is introduced into the furnace so that the water vapour molecules can diffuse into the silicon wafer surface, yielding a SiO₂ thin film at its surface. Nitrogen (N₂) is used as a background gas to regulate the pressure. The temperature (and hence power consumption) is not constant during the whole process (there are upwards and downwards ramps to maintain the temperature of the oven at 1000°C in between oxidations). The KOYO furnace is always on standby mode keeping a temperature of 750°C.

LCA Parameters

In the Chapter 4, a life cycle analysis will be conducted, and the following Table 3.3 displays the parameters necessary for this analysis.

	Wet Thermal Oxidation
Number of wafers	20
Duration of the process	3 hours 47 minutes
Inputs	O ₂ , H ₂ and N ₂
Equipment	KOYO furnace
Equipment on standby	Yes

Table 3.3: Process parameters specific for LCA.

3.4 VO₂ Sputtering

Operating Principle

The sputtering step deposits a thin layer of VO₂ on the surface of the substrate using a Physical Vapor Deposition (PVD) technique. Sputtering, which is the main method of PVD, uses a plasma of ions or atoms which is created by applying a high DC voltage (Figure 3.2). Argon ions (Ar⁺) are attracted to the cathode (target, which is the negatively charged electrode) and collide with it. With the impact energy, atoms are ejected from the target, travel through the plasma, and finally deposit on the wafer as a thin film. When oxygen is added to the sputtering atmosphere intentionally, oxide films result. This method is called reactive sputtering. It is important to note that the growth of the VO₂ layer depends on several factors, such as the power of the DC voltage source, the pressure of the inert gas in the vacuum chamber, the distance between the target and the substrate, and the substrate temperature. These parameters must be carefully controlled to obtain a uniform and optimal quality VO₂ layer.

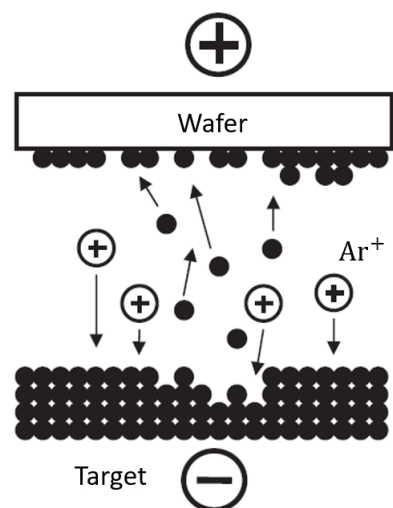


Figure 3.2: Argon ions from the plasma strike a target made of the material to be deposited. Atoms from the target are ejected and deposited on the substrate [22].

Process Parameters

The sputtering is performed at room temperature in the [AJA equipment](#) which has two connected chambers: the loading chamber and the deposition chamber. The pressure in each chamber is controlled by a [set of 2 pumps; a primary pump and a turbo pump](#) (four in total). The primary pump evacuates the chamber to a sufficiently low base pressure (around 10^{-2} mTorr). The turbo pump allows even higher vacuum pressures to be achieved.

The wafers are put (one at a time) into the loading chamber where the pressure is lowered using the first set of pumps (turbo + primary). When the pressure is close to the pressure in the deposition chamber (5 mTorr, set by the second set of pumps), the [transfer valve](#) between the loading chamber and the deposition chamber is opened, and the wafer is introduced into the main chamber (the transfer valve is then closed).

During the first 5 minutes the [argon](#) gas is introduced, the deposition pressure is regulated and the plasma is turned on at 200 W ([DC voltage](#) applied between two electrodes, which will ionize the gas in the chamber). Then the argon flow is lowered at the same time as the [oxygen](#) is introduced. Finally, the shutter covering the [vanadium](#) target is opened. When the plasma ions bombard the target, vanadium particles are ejected from it. Subsequently, these particles undergo a reaction with the O₂ reactive gas, resulting in their oxidation and transformation into VO₂ particles. These VO₂ particles are then deposited onto the wafer to form a 130 nm thick layer. The exact amounts are given in Table 3.4.

ΔT [min]	Ar [sccm]	O ₂ [sccm]	V [kg]
5	50	0	0
5	43.25	6.75	0
17.33	43.25	6.75	$4.07 \cdot 10^{-3}$

Table 3.4: The amounts of inputs based on the chronological sequence of the process.

The four pumps are always on in order to keep the vacuum into the chamber, even when no deposition is performed. The DC source controlling the plasma is only turned on during the deposition.

LCA Parameters

In the Chapter 4, a life cycle analysis will be conducted, and the following Table 3.5 displays the parameters necessary for this analysis.

	VO₂ Sputtering
Number of wafers	1
Duration of the process	approx. 43 minutes
Inputs	Ar, O ₂ and V
Equipment	4 pumps, transfer valve and DC source
Equipment on standby	Only the 4 pumps

Table 3.5: Process parameters specific for LCA.

3.5 VO₂ Annealing

Operating Principle

The annealing step allows the properties of the VO₂ thin film deposited to be controlled. The VO₂ layer deposited by sputtering is at this stage amorphous. Annealing is necessary to trigger crystallisation and obtain a polycrystalline VO₂ layer. Annealing allows control over the grain size, transition temperature and electrical resistance of the VO₂ layer according to the application requirements.

Process Parameters

For this purpose, the wafers (maximum 20) are placed into an horizontal tubular furnace. A **turbo pump** is turned on to lower the pressure up to 20 mTorr (the pressure is measured by two pressure gauges with different ranges). **Argon** gas is then introduced into the chamber with a flow of 30 sccm, increasing the pressure to 165 mTorr. Argon, unlike oxygen which is reactive, is an inert gas that does not react chemically with VO₂ or other elements present in the annealing furnace [43]. Therefore, it is often used as a shielding or inert gas to avoid unwanted chemical reactions. The chamber is then heated by an **external resistor** controlled by a PID, up to 650°C (30 min ramp from 25°C to the target temperature, then 1 hour annealing at target temperature). Finally, the equipment is left to cool for another 1 hour under controlled atmosphere.

LCA Parameters

In the Chapter 4, a life cycle analysis will be conducted, and the following Table 3.6 displays the parameters necessary for this analysis.

	VO₂ Annealing
Number of wafers	20
Duration of the process	2 hours and 30 minutes
Inputs	Ar
Equipment	Pump and heater
Equipment on standby	No

Table 3.6: Process parameters specific for LCA.

3.6 Lithography

Operating Principle

The lithography step allows the definition of the patterns and shapes of the devices at the micrometer scale. This step consists of transferring a pattern onto a surface using a photolithography technique. Photolithography, uses Ultraviolet (UV) lamps to expose photosensitive film through photomasks. The photosensitive films, or resists can be either negative or positive. For negative resists, unlike positive resists, the unexposed areas are developed while the exposed areas remain after development (Figure 3.3).

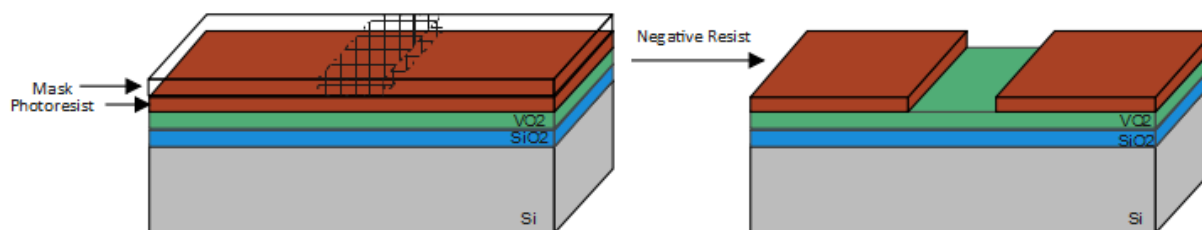


Figure 3.3: Photolithography with negative resist.

Process Parameters

The photolithography process is as follows. First, *wafers priming*, also called adhesion promotion. **Hexamethyl disilazane (HMDS)** vapor ($(CH_3)_3SiNHSi(CH_3)_3$) adhesion promoter is a coating used to improve the adhesion of photoresists to wafers. It is commonly used in photolithography processes in microelectronics to improve the quality and accuracy of the patterns created. On water-free surfaces, HMDS chemically binds its silicon atom to the oxygen of oxidised surfaces, resulting in the release of ammonia (NH₃). A hydrophobic surface is created by the methyl groups of the HMDS molecule and this improves adhesion and resistance to wetting [39]. In a so-called bubbler, water-free nitrogen is saturated at room temperature by HMDS vapours. The N₂ + HMDS flows onto the heated (100°C, for 23 minutes), water-free substrate, forming a thin layer of chemically bonded $Si(CH_3)_3$ groups responsible for the desired hydrophobic characteristics. In WINFAB, this is done in the **LP111 oven**. In the meantime, the photomask is cleaned using **acetone**, **methanol** and **DI water**. Then dried using a **N₂ gun**. All of this is performed on a **wet bench** under hoods where gas extraction is provided by a ventilation system, especially to avoid inhalation by the user.

Next in order, *spin coating* which is the standard resist application method. The wafers are coated (one by one) by negative **photoresist AZnLof5510** through spincoating of a few millilitres at 3000 rpm (1000 rpm/s acc) during 60 seconds. About 3 mL of photoresist is deposited per wafer. During this step, they are put on and removed from the coater support using a robotic arm (automated process). They hold on the coater thanks to a small hole where vacuum is applied. A soft bake, *pre-exposure bake*, is then performed at 90 °C for 60 seconds to dry the resist and to drive out most of the solvent still present in the spin-coated resist. Once again, the wafers are put in and removed from the ovens using a robotic arm. All of this is performed in the **SUSS Gamma** equipment.

The wafer and photomask are *aligned* and brought into close contact (vacuum) and then exposed under UV light

(lamp) using the **SUSS MA6**. The exposure dose is around 90-140 mJ. Overall, the lamp will stay on for 15 min pre-heating.

A *post-exposure bake (PEB)* is then performed at 105°C for 120 seconds to trigger the diffusion of photogenerated molecules. During the bake, these molecules are responsible for changing the solubility of the resist in the developer and produce the difference in solubility between the exposed and unexposed resist. Again this is done in the SUSS Gamma equipment. Finally, the resist is developed and the soluble parts of the resist are removed by immersing the wafer with approximately 10 to 15 mL of **developer AZ 726 MIF (TMAH)** during 45 seconds. It is then rinsed with DI water. In negative resists, the exposed parts have been cross-linked and made stable, and the unexposed parts are removed.

The wafer is then cleaned using methanol and DI water, then dried using a N₂ gun. The whole process is done in what we call the *yellow room* because of the yellow light used as the photoresists are sensitive below 450 nm only.

An overview of the different steps is given in Table 3.7.

	Inputs	Equipment	Duration
Wafer Priming	HMDS	LPIII oven	23 min
Photomask Cleaning	Acetone, Methanol, DI water	/	approx. 5 min
Spin Coating	Photoresist	SUSS Gamma	1 min
Exposure	/	MA6	approx. 1 hour 30 min
PEB	/	SUSS Gamma	2 min
Development	Developer, DI water	Wet Bench	45 seconds
Wafer Cleaning	Methanol, DI water	Wet Bench	approx. 1 min

Table 3.7: Overview of the various steps, taking into account inputs, equipment, and duration.

LCA Parameters

In the Chapter 4, a life cycle analysis will be conducted, and the following Table 3.10 displays the parameters necessary for this analysis.

	Lithography
Number of wafers	1
Duration of the process	approx. 2 hours
Inputs	HMDS, Acetone, Methanol, DI water, Photoresist, Developer, N ₂
Equipment	LPIII oven, SUSS Gamma, SUSS MA6, Wet Bench
Equipment on standby	No

Table 3.8: Process parameters specific for LCA.

3.7 Metallization

Operating Principle

All electrical devices need a layer of metallization for the future use phase. The metallization step, also known as metal deposition, consists of depositing a thin layer of metal on the surface of the chip to create electrical contacts. In the specific case of VO₂-based device manufacturing, the metallization step is performed using Electron Beam Physical Vapour Deposition (EBPVD), referred to as "gold evaporation", which involves spraying a thin layer of gold onto the surface of the wafer. This technique produces a uniform, high quality metal layer. Gold is used as an electrical contact material because of its excellent electrical properties and resistance to oxidation.

Process Parameters

The wafers (maximum 4) are loaded into the chamber of the VACOTEC equipment, and a few pellets (small balls) of nickel (Ni) and gold (Au) are put each into a dedicated crucible. The chamber is then pumped during several hours (with a cryo, primary and root pump) until the pressure reaches a value below $4 \cdot 10^{-7}$ mbar. Once the pressure is low enough, the crucible is heated using an electron gun (with ramping power applied). The electron gun has a maximum power of 3 kW and its use time is approximately 30 minutes. Once the crucible is hot enough, it starts evaporating. At the time the deposition rate, measured with a piezoelectric crystal, is stable, the shutter protecting the substrate is opened. First a layer of 5 nm of nickel is deposited which serves as an adhesive layer as gold is a noble metal and cannot be deposited directly on the surface and prevents the diffusion of gold atoms into the substrate. After that, gold particles start to condense on the wafer surface. The deposition of gold itself takes 12 minutes for a 100 nm layer. In between two metallization, the two pumps (root and primary) are always on.

LCA Parameters

In the Chapter 4, a life cycle analysis will be conducted, and the following Table 3.9 displays the parameters necessary for this analysis.

	Metallization
Number of wafers	4
Duration of the process	4 hours 30 minutes
Inputs	Ni, Au
Equipment	Primary, Root and Cryo Pump and Electron gun
Equipment on standby	Root and Primary Pump

Table 3.9: Process parameters specific for LCA.

3.8 Lift-off

Operating Principle

The gold lift-off step selectively removes the previously deposited metal layer from the chip surface, leaving behind the desired regions. This technique is used to create precise metal patterns and to form the electrical contact regions with the VO₂. The lift-off usually takes place in two stages : the first step, the lithography step explained above, consists of depositing a layer of photoresist on the surface of the chip. This (negative) resist is then exposed to UV light through a mask. This step makes it possible to create precise patterns in the resist layer. After that, there is the metallization. The second step is to immerse the wafer in a solvent, such as acetone, which dissolves the exposed resist layer. The metal layer deposited on the surface of the chip in the areas covered by the resist then peels off, creating the desired patterns and structures (Figure 3.4).

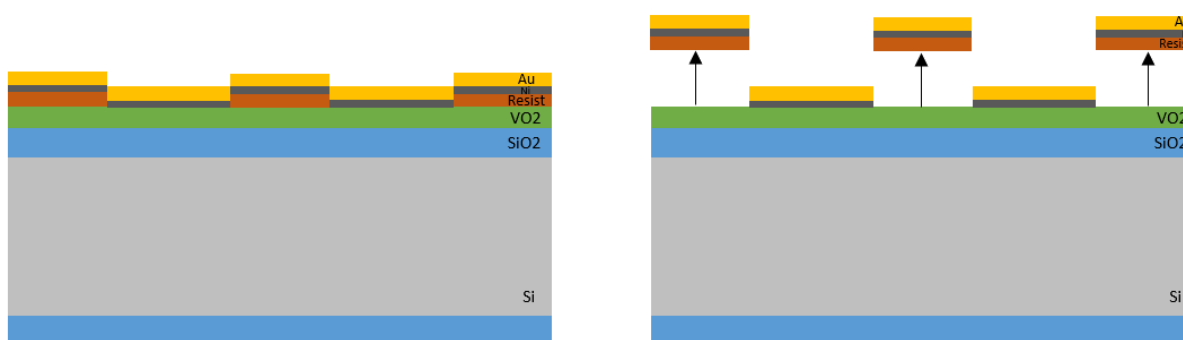


Figure 3.4: Lift-off process : resist development and metal lift-off.

Process Parameters

In the WINFAB laboratories, the wafer is immersed in a beaker containing 700 mL of [acetone](#) which dissolves the photoresist for 5 minutes. The gold layer deposited on the photoresist is therefore "lifted off" leaving only the gold patterns deposited on the edge where there is no photoresist. It is possible that sometimes the gold does not peel off easily. The beaker is then placed in an [ultrasonic vibration waterbath](#), which can also be heated, to facilitate peeling for approximately 5 minutes. Finally, the wafer is removed from the beaker and cleaned with a wash bottle containing acetone followed by [methanol](#) and [DI water](#). The wafers are then dried using an [N₂ gun](#). Like the standard cleaning, this step is performed on a [wet bench](#) under a hood with a ventilation system.

LCA Parameters

In the Chapter 4, a life cycle analysis will be conducted, and the following Table 3.10 displays the parameters necessary for this analysis.

	Lift-off
Number of wafers	1
Duration of the process	apprx. 10 minutes
Inputs	DI water, Acetone, Methanol, N ₂
Equipment	Ultrasound waterbath
Equipment on standby	No

Table 3.10: Process parameters specific for LCA.

Chapter 4

Life Cycle Assessment of the VO₂-based device

LCA is a tool that allows a global and multi-criteria evaluation of the environmental impacts of a product or service by identifying and quantifying the flows of materials and energy associated with human activities. Depending on the scope of the study, all stages of a product's life cycle are taken into account, and several criteria are used to analyze incoming and outgoing flows, such as raw materials, water, oil and gas, as well as waste, gaseous emissions, and discharged liquids. The flows are quantified at each stage of the cycle and correspond to indicators of potential environmental impacts. LCA provides an overall view of the impacts generated by the fabrication, use and end-of-life of a product, and its results can be used to make choices about the design and improvement of the product. Although LCA was considered experimental in the early 1990s, its international ISO standardisation has led to harmonisation of the methodology used, greater robustness and reliability of results and more formalized communication. In particular, ISO 14040 is an international standard that establishes the principles and framework for LCA in environmental management. The standard provides guidelines for conducting an LCA, including defining the purpose and scope of the study, collecting data, modelling the system and interpreting the results. It also specifies the basic principles that should guide a LCA, including transparency, comparability, completeness, relevance and consistency [28].

As mentioned in Chapter 2, LCA has four interdependent and iterative stages. The first step is to define the objectives of the LCA and specify the rules and boundaries of the study, that is the *goal* and the *scope*. The second step is to make the LCI, an *inventory* of the material and energy inputs and outputs associated with the life cycle stages. The inventory can be carried out using LCA software or a spreadsheet. The third step, the LCIA, determines the potential *impacts* of the inventoried flows using environmental impact indicators. The fourth and final step is to *interpret the results* obtained according to the objectives decided earlier and to check that the results meet those objectives. This stage allows the robustness of the results to be assessed [1]. In this chapter, we will first define the goal and scope of the study. Then, we will explain the calculation methodology. Next, we will provide a detailed inventory, and finally, we will present and analyze the results, which will allow us to highlight the stage(s) that dominate in terms of environmental impacts.

4.1 Goal & Scope

The LCA conducted in this study is a model that assesses the environmental impact of the VO2 device from the extraction of the raw materials to the exit of the WINFAB laboratory. It is more commonly referred to as **cradle-to-gate** LCA which, in our particular case, has been simplified. Its objective is to identify the hotspot in order to propose an alternative that consumes less energy and to evaluate the impact of this alternative on the performance of the device. The primary objective of this hotspot search is to be able to play with this lever. Our analysis will concentrate on adaptable variable parameters rather than mandatory fixed parameters, which must be imposed for the completion of the process. The scope and the boundaries of the study, as shown in Figure 4.1, are thus focused on the variable parameters of the process. Inputs, such as materials flows and chemical reagents as well as electrical equipment are taken into account to give the PED indicator. The general infrastructure of the fab (specifically, Heating, ventilation and air-conditioning (HVAC)) as well as the wafer production are neglected as they are fixed parameters and therefore cannot be modified. The study was restricted to quantifying the energy consumption thanks to the PED in MJ, which is a well-known indicator in the LCA community, and not other environmental indicators such as Global Warming Potential (GWP) and Ultra Pure Water (UPW) use.

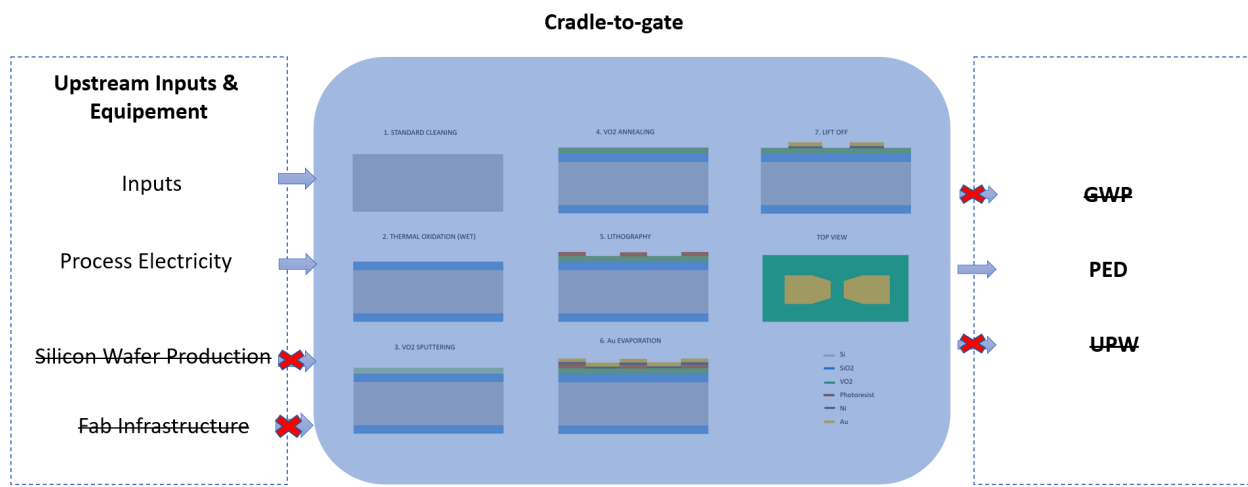


Figure 4.1: Scope and boundaries of the study.

4.2 Methodology

Primary Energy Demand (PED)

In this LCA, the PED is used to assess the total amount of gross energy required to produce the VO2-based device, from the extraction of raw materials to the gate of the WINFAB cleanroom. By using PED in an LCA, one can estimate the relative contribution of different types of energy (fossil fuels, renewable energy, etc.) to the overall environmental impact. PED can also be used to weigh the energy efficiency of a system or product.

The impact indicator PED is calculated on the basis of the CED and the Primary Energy Factor (PEF) (equation 4.1). The PEF considers losses in the generation and transmission of electricity. In this study, the European PEF of 2.5 is chosen [19].

$$PED [MJ] = 2.5 \cdot CED = CED_{inputs}(EI) + 2.5 \cdot CED_{equipment} \quad (4.1)$$

This PED is normalised per cm^2 of wafer surface $[MJ/cm^2]$. This is done by dividing the obtained PED by the surface of the wafer (equation 4.3) multiplied by the number of wafers present during the process (equation 4.2).

$$PED [MJ/cm^2] = \frac{PED [MJ]}{(wafer\ surface [cm^2]) \cdot (number\ of\ wafers)} \quad (4.2)$$

with the wafer surface :

$$\pi \cdot r^2 = \pi \cdot \frac{7.62^2}{2} = 45.60 [cm^2] \quad (4.3)$$

Cumulative Energy Demand (CED)

CED is a measure of the amount of energy required to produce a product or service. In order to calculate the CED, the life cycle stages of the VO2-device which are the extraction of raw materials and production process, must first be identified and quantified. Next, the amount of energy required for each stage is calculated, taking into account the different incoming energy sources. Finally, the total amount of energy required for the whole process is calculated by adding up the energy requirements of each stage. The units used to measure energy can vary, but most often the CED is expressed in megajoules [MJ], which is the case in this study. The CED is calculated on the basis of the EI and the process electricity.

The general formula used to calculate the CED is as follows:

$$CED = CED_{mat} + CED_{proc} = \Sigma[m_{mat} \cdot e_{mat}] + \Sigma[m_{chem} \cdot e_{chem} + e_{proc}] \quad (4.4)$$

where :

- m_{mat} : Raw material flows [kg]
- e_{mat} : Raw material EI [MJ/kg]
- m_{chem} : Chemical flows [kg]
- e_{chem} : Chemical EI [MJ/kg]
- e_{proc} : Energy associated with electricity use in the process [MJ]

Energy Intensity

The Energy Intensity (EI) is the amount of energy required to produce one unit of mass of a product or material. In other words, it measures the energy efficiency of a production process. The higher the EI value, the more energy is required for production and therefore the greater the environmental impact of production. To calculate the EI, the total amount of energy used to produce a unit of mass of the product or material is divided by that unit of mass. The unit of measurement is the megajoule per kilogram [MJ/kg].

The values of EI can be found in many different resources ([45]-[4]-[54]-[8]). As a result, the values found can be, and usually are, quite different, with large disparities existing. These differences depends on several factors such as how the products are extracted, the energy used to extract them, the assumptions made, etc. This is one of the main concerns of LCA research. In this work, we extracted EI values from two main sources: Sarah Boyd's work [8] and the EduPack software [4]. It is assumed that the EI values obtained for each of the inputs from the above 2 sources is a primary energy value. This assumption is made as the energy needed for the production of materials is rarely electrical but rather fossil (ore reduction, extraction,...).

Use of Sarah Boyd's work [8]

As already mentioned in Chapter 2, Sarah Boyd's book is considered a reference manual for LCA in microelectronics. The data collection method used in Boyd's study involves the use of process descriptions when available and data from the Carnegie Mellon EIO-LCA database when cost information is known. If there is a lack of process LCA data or cost information, an estimation of chemical manufacturing's energy intensity created by Overcash is used [33]. For high value specialty chemicals with a purchase price over 1,000 per kg, the "pharmaceuticals and medicines" sector is used in the EIO analysis, as it better represents their economic value. Organic and inorganic chemicals are used for the remaining materials as appropriate. While EIO-LCA results for toxic releases or other impacts may have a lower precision, an uncertainty range of 10% is assumed for EIO-LCA energy consumption based on the sources used by the CMU model for energy data. Chemicals using EIO-LCA data and data from the Kim/Overcash study have an uncertainty of +25%/-75% for the latter. The data collected through the last mentioned method is found to underestimate the energy intensity of metals used in our process, such as gold and nickel. Boyd acknowledges this uncertainty related to the Overcash study. Additionally, various sources indicate that the energy intensity of gold is significantly higher compared to other inputs, contrary to what Boyd suggests ([45]-[4]-[54]-[44]). To address this issue, EI of metals were obtained from the EduPack database.

Use of the EduPack software [4]

Granta EduPack is a educational software developed by Granta Design, now part of ANSYS. It is designed to help teachers and students understand and teach material properties and material selection for products. The software includes data on material properties, tools for material selection and performance comparison, and information on manufacturing processes and environmental considerations. Granta EduPack is used in universities such as ours to support the teaching of materials science, engineering and product design. It obtains its environmental property values (eco properties) from an integrated database called "Materials Data" from Granta Design based on the ecoinvent v3.8 release. This database is fed by reliable and verified sources, such as LCAs, scientific publications, industry reports and data provided by the manufacturers themselves. The values are established using standardised methodologies, such as ISO standards.

Process Electricity

The energy associated with electricity consumption is taken directly from the datasheets on the equipment used for each stage of the process. This correspond to the e_{proc} part in equation 4.4 and is multiplied by the PEF (2.5) to obtain the PED. However, at the next point, we were able to measure the real time power consumption on the KOYO furnace during the step of wet thermal oxidation in order to be aware of the real consumption of the equipment used.

Real Time Measurements on Equipment - Capacity Factor

Real-time power measurement was carried out using the PEL103 measuring device and allowed us to obtain the capacity factor of the equipment. The capacity factor or utilisation factor is the ratio of the electrical energy actually produced over a given period to the energy it would have produced if it had been operating at its rated power during the same period [41]. The PEL103 recorders are power and energy measurement recorders for all electrical installations. The recorder is connected to the three-phase electrical system using current clamps to measure current and voltage probes to measure voltage. The current clamps are placed around the electrical conductors without interrupting them, allowing the current to be measured non-invasively. For a clearer view on the precise positioning of the measuring device, refer to Chapter B in the appendix. The measurements allow all electrical parameters to be visualised and the measurement, energy metering and communication functions to be used [5].

In Figure 4.2, the real-time power of the KOYO furnace (JTEKT Thermo Systems VF1000) is plotted alongside its nominal power. Furthermore, the capacity factor is calculated as the ratio of the energies, using the following formula :

$$Energy [MJ] = (Power [W] \cdot time [h]) \cdot Conversion Factor \cdot PEF \quad (4.5)$$

with :

- Conversion Factor (from [Wh] to [MJ]) : $1 [Wh] = 0.0036 [MJ]$
- $PEF = 2.5$
- $P_{nom} = 17.1[kW]$

Table 4.1 shows the results we get.

	Real Time	Datasheet
Energy [MJ]	134.04	582.25

Table 4.1: Real Time energy consumption versus datasheet, in [MJ].

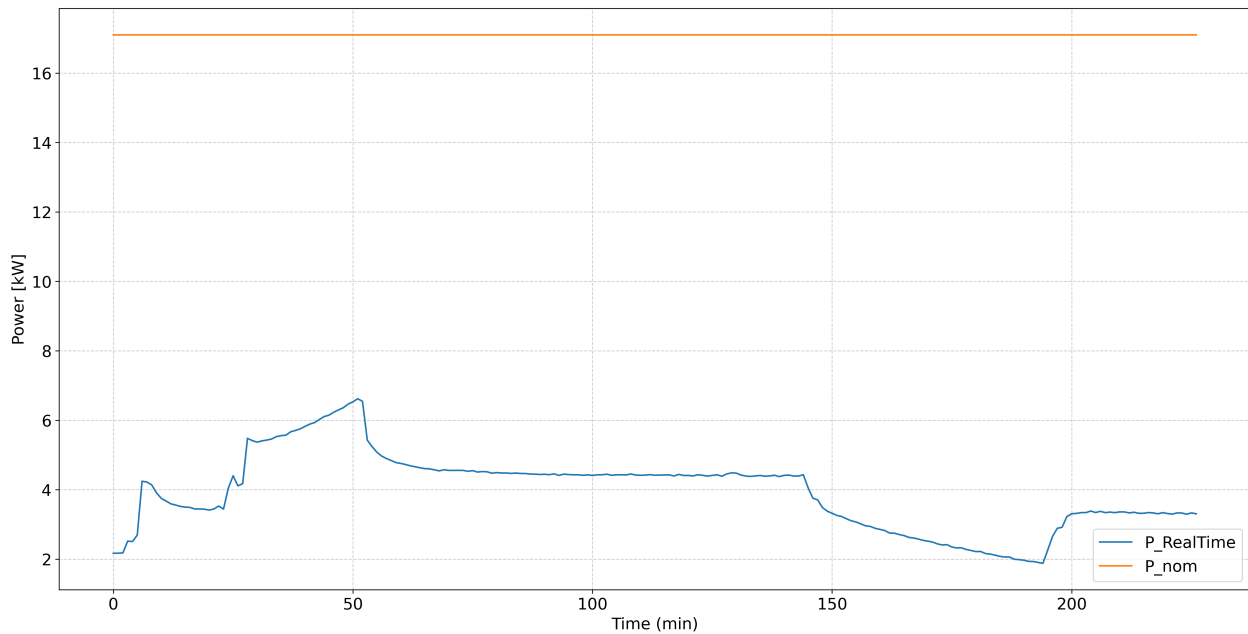


Figure 4.2: Real Time power consumption (in blue) versus datasheet (in orange), in [kW].

The capacity factor is

$$\frac{134.08}{582.25} = 0.23$$

This implies a 77% reduction in the energy consumption of the equipment.

Due to the unavailability of access to the electrical panel of the other equipment, we were unable to repeat the measurement process for all the machines. Nevertheless, we have chosen to apply this coefficient of 0.23 to the rest of the equipment used in the process from now on.

4.3 Inventory

The inventory makes it possible to collect all the data in order to identify potential sources of environmental impacts. In the framework of this cradle-to-gate LCA, a bottom-up LCI was done. The inputs as well as the equipment used during the microfabrication process are listed in Table 4.2.

Step	Inputs	Equipment
Standard Cleaning	H ₂ SO ₄ (l), H ₂ O ₂ (l), HF 2% (l), DI water (l)	Heaters for the baths, Rinser-dryer
Wet Thermal Oxidation	N ₂ (g), H ₂ (g), O ₂ (g)	Furnace heaters
VO₂ Sputtering	O ₂ (g), Ar (g), V (g)	Primary and turbo pump (Load chamber), Primary and turbo pump (Main chamber), Transfer valve, DC source
VO₂ Annealing	Ar (g)	Furnace heaters, Pump
Lithography	DI water (l), HMDS (g), Photoresist AZnLof5510 (Novolac) (l), Developer AZ726MIF (TMAH) (l), Acetone (l), Methanol (l)	LP111 Oven, Suss Gamma Suss MA6
Metallization	Au (s), Ni (s)	Cryo pump, Compressor, Primary Pump Root pump, Electron gun
Lift-off	DI water (l), Acetone (l), Methanol (l)	Ultrasound vibration waterbath

Table 4.2: Inventory of the microfabrication process of VO₂-based device.

4.4 Results & Impacts

In this section, the results will be presented, initially for the entire process, followed by a step-by-step breakdown. The results were achieved based on a set of assumptions, which can be categorized into two subgroups. First, there are overall assumptions that include every step of the process. Secondly, there are specific assumptions made for each individual step. The general assumptions are :

- Inputs :

$$PED_{Inputs} [MJ/cm^2] = \frac{EI[MJ/kg] \cdot mass [kg]}{wafer\ surface [cm^2] \cdot number\ of\ wafers} \quad (4.6)$$

where

- the following formula was used to convert litres to kg

$$mass [kg] = \frac{volume [l] \cdot density [kg/m^3]}{1000} \quad (4.7)$$

knowing $1[L] = 10^{-3}[m^3]$.

- The following formula was used to convert sccm to kg

$$mass [kg] = \frac{sccm [cm^3/min] \cdot density [kg/m^3] \cdot time [s]}{10^6 \cdot 60} \quad (4.8)$$

knowing that $1 [cm^3] = 10^{-6} [m^3]$ and $1 \text{ min} = 60 \text{ s}$.

- EI [MJ/kg] values are sourced from Sarah Boyd's work [8], with the exception of Au, Ni, and V, which are obtained from the EduPack software [4].

- Equipment :

$$PED_{Equipment} [MJ/cm^2] = \frac{(Power [W] \cdot time [h]) \cdot Conversion\ Factor \cdot PEF \cdot Capacity\ Factor}{wafer\ surface [cm^2] \cdot number\ of\ wafers} \quad (4.9)$$

with :

- Conversion Factor (from [Wh] to [MJ]) : $1 [Wh] = 0.0036 [MJ]$
- $PEF = 2.5$
- Capacity Factor = 0.23
- Time [h] : only the duration of the process is considered

- Facility infrastructure (HVAC), wafer production, N2 input and computers to run the process are neglected

For the reader's convenience, all histograms are presented in $[J/cm^2]$, whereas the values in the tables, as mentioned above, are in $[MJ/cm^2]$. The inputs will be shown in blue and the corresponding equipment used in our university's cleanroom in orange.

Complete Process

In Figure 4.3, the inputs (in blue) and equipment (in orange) per process step are displayed in $[J/cm^2]$ with a logarithmic scale. The values of these are shown in Table 4.3 in $[MJ/cm^2]$. The overall PED for the entire process is $1.37 \cdot 10^2 [MJ/cm^2]$.

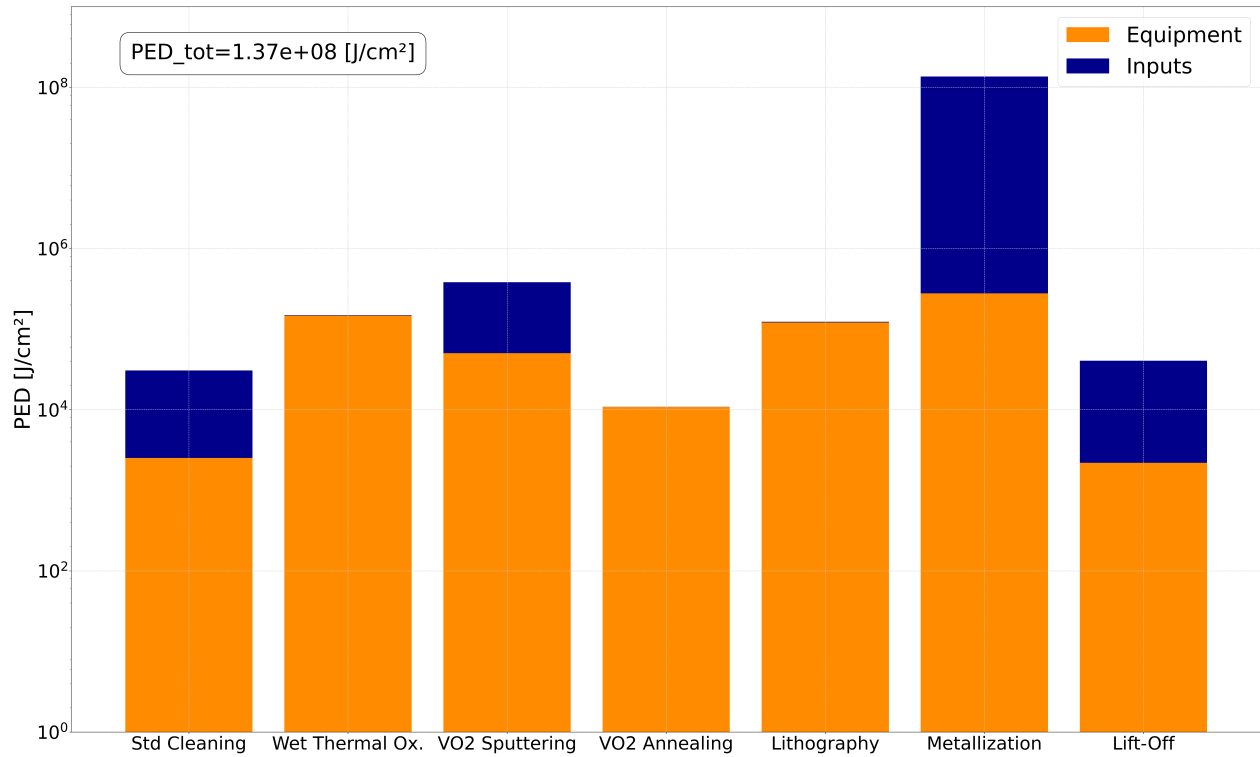


Figure 4.3: PED $[J/cm^2]$ of the complete process, logarithmic scale.

PED $[MJ/cm^2]$	Standard Cleaning	Thermal Oxidation	VO2 Sputtering	VO2 Annealing	Lithography	Metallization	Lift-off
Inputs	$2.81 \cdot 10^{-2}$	$2.26 \cdot 10^{-3}$	$3.32 \cdot 10^{-1}$	$3.17 \cdot 10^{-5}$	$2.26 \cdot 10^{-3}$	$1.36 \cdot 10^2$	$3.83 \cdot 10^{-2}$
Equipment	$2.52 \cdot 10^{-3}$	$1.47 \cdot 10^{-1}$	$5.02 \cdot 10^{-2}$	$1.08 \cdot 10^{-2}$	$1.21 \cdot 10^{-1}$	$2.78 \cdot 10^{-1}$	$2.19 \cdot 10^{-3}$
PED_{tot}	$3.06 \cdot 10^{-2}$	$1.49 \cdot 10^{-1}$	$3.82 \cdot 10^{-1}$	$1.08 \cdot 10^{-2}$	$1.23 \cdot 10^{-1}$	$1.36 \cdot 10^2$	$4.05 \cdot 10^{-2}$

Table 4.3: PED $[MJ/cm^2]$ of the complete process.

Standard Cleaning

In Figure 4.4, the inputs (in blue shades) and equipment (in orange shades) are displayed in [J/cm^2] with a logarithmic scale. The values of these, as well as the overall PED for the entire process step, are shown in Table 4.4 in [MJ/cm^2]. The PED of the standard cleaning step represents $2.23 \cdot 10^{-4}\%$ of the complete process's PED. No other specific assumptions were made for this step of the process. For a more comprehensive overview of this stage of the process, please refer to Section A.1 in Chapter A (appendix), which provides a detailed worksheet.

Inputs	PED [MJ/cm^2]
$\text{H}_2\text{SO}_4(\text{l})$	$2.86 \cdot 10^{-4}$
$\text{H}_2\text{O}_2(\text{l})$	$2.65 \cdot 10^{-2}$
$\text{HF } 2\% (\text{l})$	$1.36 \cdot 10^{-3}$
DI water (l)	0
Equipment	PED [MJ/cm^2]
Heaters for the baths	$1.52 \cdot 10^{-3}$
Rinser-dryer	$9.99 \cdot 10^{-4}$
PED_{tot}	$3.06 \cdot 10^{-2}$

Table 4.4: PED [MJ/cm^2] of the standard cleaning step.

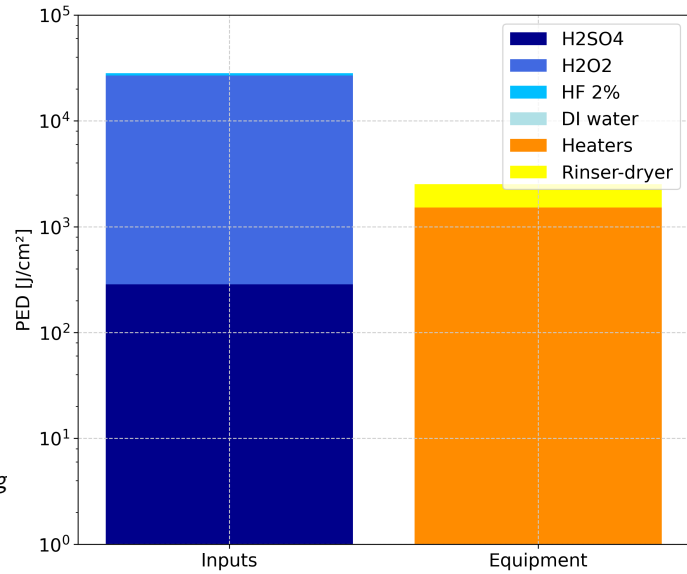


Figure 4.4: PED [J/cm^2] of the standard cleaning step, logarithmic scale.

Wet Thermal Oxidation

In Figure 4.5, the inputs (in blue shades) and equipment (in orange shades) are displayed in $[J/cm^2]$ with a logarithmic scale. The values of these, as well as the overall PED for the entire process step, are shown in Table 4.5 in $[MJ/cm^2]$. The PED of the wet thermal oxidation step represents $1.09 \cdot 10^{-3}\%$ of the complete process's PED. No other specific assumptions were made for this step of the process. For a more comprehensive overview of this stage of the process, please refer to Section A.2 in Chapter A (appendix), which provides a detailed worksheet.

Inputs	PED $[MJ/cm^2]$
$N_2(g)$	$5.75 \cdot 10^{-4}$
$H_2(g)$	$3.79 \cdot 10^{-4}$
$O_2(g)$	$1.31 \cdot 10^{-3}$
Equipment	PED $[MJ/cm^2]$
Furnace heaters (KOYO)	$1.47 \cdot 10^{-1}$
PED_{tot}	$1.49 \cdot 10^{-1}$

Table 4.5: PED $[MJ/cm^2]$ of the wet thermal oxidation step.

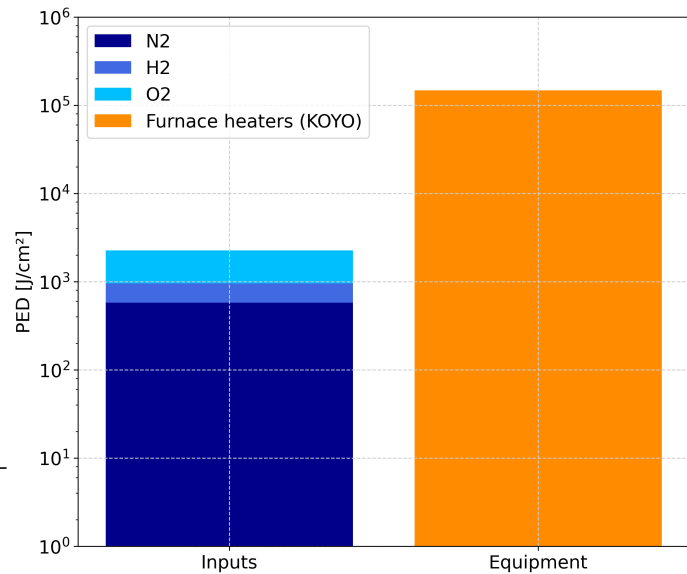


Figure 4.5: PED $[J/cm^2]$ of wet thermal oxidation step, logarithmic scale.

VO2 Sputtering

In Figure 4.6, the inputs (in blue shades) and equipment (in orange shades) are displayed in $[J/cm^2]$ with a logarithmic scale. The values of these, as well as the overall PED for the entire process step, are shown in Table 4.6 in $[MJ/cm^2]$. The PED of the VO2 sputtering step represents $2.79 \cdot 10^{-3}\%$ of the complete process's PED. To determine the mass of vanadium (V) deposited during the process, the following formula was employed as an assumption :

$$mass [kg] = Surface [m^2] \cdot thickness [m] \cdot density [kg/m^3] \quad (4.10)$$

with

- Surface = $2\pi r^2 + 2\pi r h$, radius (r) = 0.165 [m], height (h) = 0.5 [m]
- Thickness = 130 [nm]
- Density (V) = 6100 $[kg/m^3]$

For a more comprehensive overview of this stage of the process, please refer to Section A.3 in Chapter A (appendix), which provides a detailed worksheet.

Inputs	PED $[MJ/cm^2]$
$O_2(g)$	$8.88 \cdot 10^{-6}$
$Ar(g)$	$3.72 \cdot 10^{-4}$
$V(s)$	$3.32 \cdot 10^{-1}$
Equipment	PED $[MJ/cm^2]$
Primary Pump (Load chamber)	$1.44 \cdot 10^{-2}$
Turbo Pump (Load chamber)	$3.52 \cdot 10^{-3}$
Primary Pump (Main chamber)	$1.44 \cdot 10^{-2}$
Turbo Pump (Main chamber)	$1.35 \cdot 10^{-2}$
Transfer Valve	$2.52 \cdot 10^{-4}$
DC Source	$4.14 \cdot 10^{-3}$
PED_{tot}	$3.82 \cdot 10^{-1}$

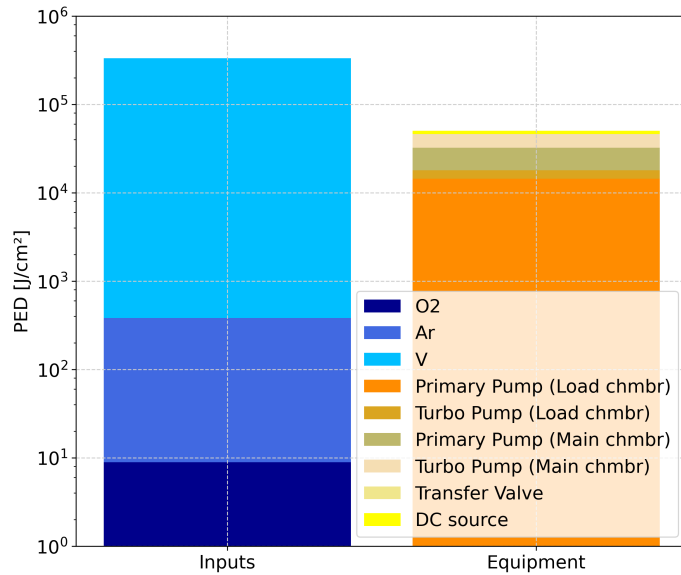


Table 4.6: PED $[MJ/cm^2]$ of the VO2 sputtering step, logarithmic scale.

Figure 4.6: PED $[J/cm^2]$ of the VO2 sputtering step, logarithmic scale.

VO₂ annealing

In Figure 4.7, the inputs (in blue shades) and equipment (in orange shades) are displayed in [J/cm^2] with a logarithmic scale. The values of these, as well as the overall PED for the entire process step, are shown in Table 4.7 in [MJ/cm^2]. The PED of the VO₂ annealing step represents $7.88 \cdot 10^{-5}\%$ of the complete process's PED. No other specific assumptions were made for this step of the process. For a more comprehensive overview of this stage of the process, please refer to Section A.4 in Chapter A (appendix), which provides a detailed worksheet.

Inputs	PED [MJ/cm^2]
Ar(g)	$3.17 \cdot 10^{-5}$
Equipment	PED [MJ/cm^2]
Furnace heaters	$8.51 \cdot 10^{-3}$
Pump	$2.27 \cdot 10^{-3}$
PED_{tot}	$1.08 \cdot 10^{-2}$

Table 4.7: PED [MJ/cm^2] of the VO₂ annealing step.

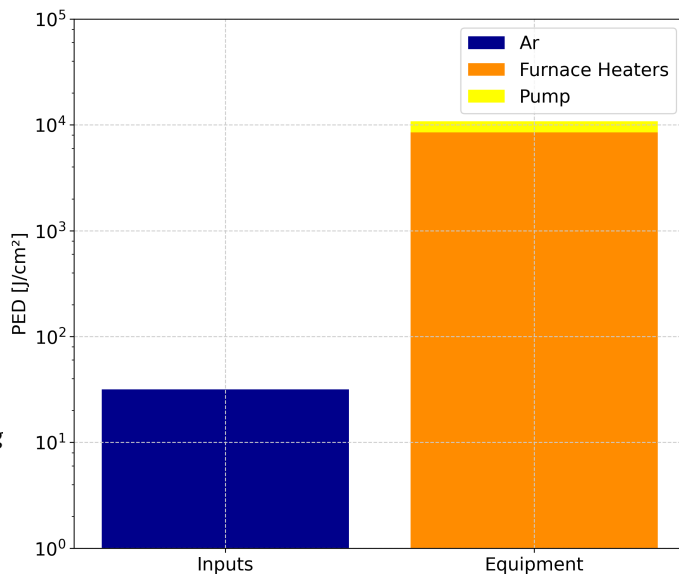


Figure 4.7: PED [J/cm^2] of the VO₂ annealing step, logarithmic scale.

Lithography

In Figure 4.8, the inputs (in blue shades) and equipment (in orange shades) are displayed in $[\text{J}/\text{cm}^2]$ with a logarithmic scale. The values of these, as well as the overall PED for the entire process step, are shown in Table 4.8 in $[\text{MJ}/\text{cm}^2]$. The PED for the lithography step represents $8.98 \cdot 10^{-4}\%$ of the complete process's PED. To determine the mass of HMDS utilized, the known consumption for 400 lithography processes was employed : $500\text{mL}/400 = 1.25\text{mL}$ of HMDS. For a more comprehensive overview of this stage of the process, please refer to Section A.5 in Chapter A (appendix), which provides a detailed worksheet.

Inputs	PED $[\text{MJ}/\text{cm}^2]$
DI water (l)	0
HMDS (g)	$6.54 \cdot 10^{-5}$
Photoresist (Novolac) (l)	$2.55 \cdot 10^{-4}$
Developer (TMAH) (l)	$8.62 \cdot 10^{-4}$
Acetone (l)	$5.37 \cdot 10^{-4}$
Methanol (l)	$5.38 \cdot 10^{-4}$
Equipment	PED $[\text{MJ}/\text{cm}^2]$
LP111 Oven (HMDS)	$2.09 \cdot 10^{-2}$
Suss Gamma (Robotic arm, oven, coater)	$3.18 \cdot 10^{-2}$
Suss MA6 (UV lamp)	$6.81 \cdot 10^{-2}$
PED_{tot}	$1.23 \cdot 10^{-1}$

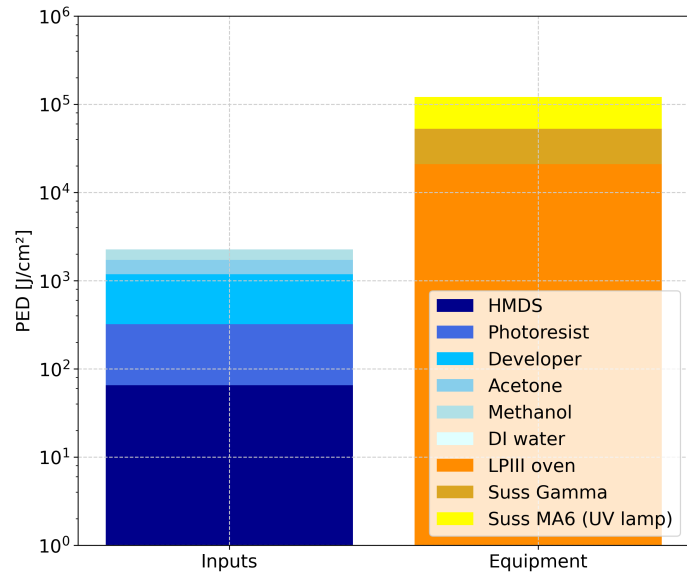


Table 4.8: PED $[\text{MJ}/\text{cm}^2]$ of the lithography step. Figure 4.8: PED $[\text{J}/\text{cm}^2]$ of the lithography step, logarithmic scale.

Metallization

In Figure 4.9, the inputs (in blue shades) and equipment (in orange shades) are displayed in $[\text{J}/\text{cm}^2]$ with a logarithmic scale. The values of these, as well as the overall PED for the entire process step, are shown in Table 4.9 in $[\text{MJ}/\text{cm}^2]$. The PED of the metallization step represents 99.27% of the complete process's PED. To determine the mass of gold (Au) and nickel (Ni) deposited during the process, the following formula was employed as an assumption :

$$mass [kg] = Surface [m^2] \cdot thickness [m] \cdot density [kg/m^3] \quad (4.11)$$

with

- Surface = $2lw + 2lh + 2wh$, length (l) = 0.64 [m], width (w) = 0.84 [m], height (h) = 0.66 [m].
- Thickness (Au) = 100 [nm], Thickness (Ni) = 5 [nm]
- Density (Au) = 19300 $[\text{kg}/\text{m}^3]$, Density (Ni) = 8900 $[\text{kg}/\text{m}^3]$

For a more comprehensive overview of this stage of the process, please refer to Section A.6 in Chapter A (appendix), which provides a detailed worksheet.

Inputs	PED $[\text{MJ}/\text{cm}^2]$
Au(s)	$1.36 \cdot 10^2$
Ni(s)	$1.53 \cdot 10^{-4}$
Equipment	PED $[\text{MJ}/\text{cm}^2]$
Cryo pump + compressor	$2.04 \cdot 10^{-1}$
Primary pump	$2.06 \cdot 10^{-2}$
Root pump	$4.40 \cdot 10^{-2}$
Electron gun	$9.79 \cdot 10^{-3}$
PED_{tot}	$1.36 \cdot 10^2$

Table 4.9: PED $[\text{MJ}/\text{cm}^2]$ of the metallization step.

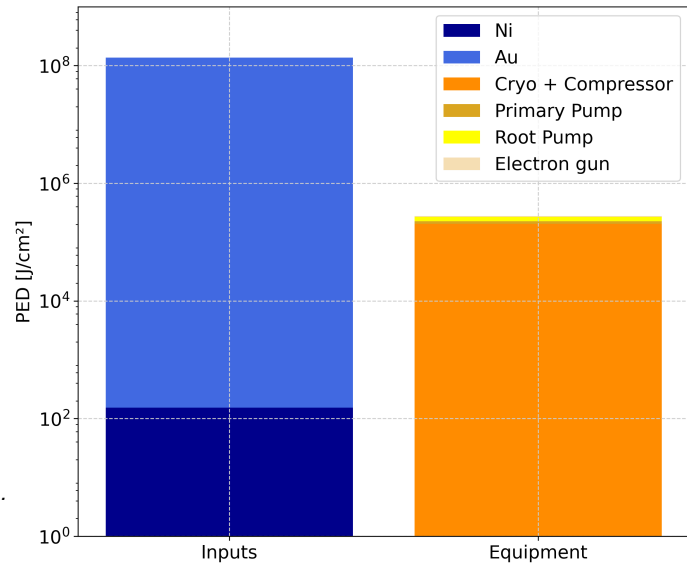


Figure 4.9: PED $[\text{J}/\text{cm}^2]$ of the metallization step, logarithmic scale.

Lift-off

In Figure 4.10, the inputs (in blue shades) and equipment (in orange shades) are displayed in [J/cm^2] with a logarithmic scale. The values of these, as well as the overall PED for the entire process step, are shown in Table 4.10 in [MJ/cm^2]. The PED of the lift-off step represents $2.96 \cdot 10^{-4}\%$ of the complete process's PED. No other specific assumptions were made for this step of the process. For a more comprehensive overview of this stage of the process, please refer to Section A.7 in Chapter A (appendix), which provides a detailed worksheet.

Inputs	PED [MJ/cm^2]
DI water (l)	0
Acetone (l)	$3.76 \cdot 10^{-2}$
Methanol (l)	$6.73 \cdot 10^{-4}$
Equipment	PED [MJ/cm^2]
Ultrasound vibration waterbath	$2.19 \cdot 10^{-3}$
PED_{tot}	$4.05 \cdot 10^{-2}$

Table 4.10: PED [MJ/cm^2] of the lift-off step.

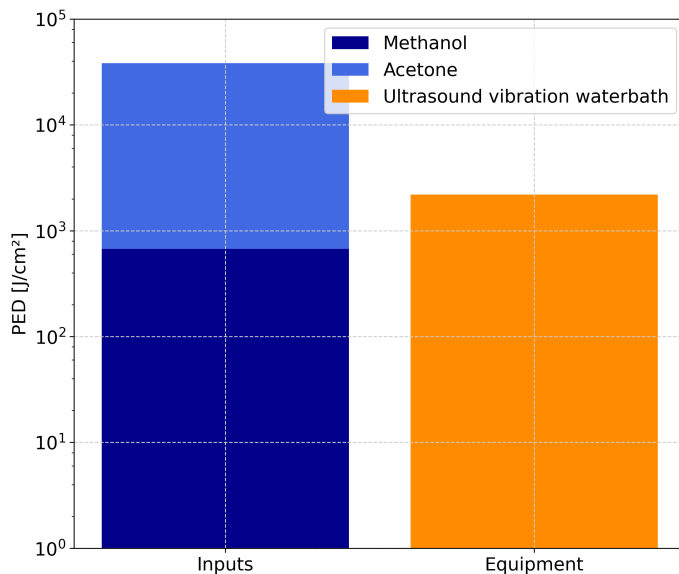


Figure 4.10: PED [J/cm^2] of the lift-off step, logarithmic scale.

4.5 Interpretation of the results

As stated in Section 4.1, *the objective of this LCA is to identify the hotspot in order to propose an alternative that consumes less energy and to evaluate the impact on the performance of the device.* From the results outlined in Section 4.4, we have the capability to establish a ranking of the ten most influential elements, arranged in descending order from the highest impact to the lowest.

1. Metallization, use of gold : $1.36 \cdot 10^2$ [MJ/cm²]
2. VO₂ Sputtering, use of vanadium : $3.32 \cdot 10^{-1}$ [MJ/cm²]
3. Metallization, equipment (Vacotec) : $2.78 \cdot 10^{-1}$ [MJ/cm²]
4. Wet Thermal Oxidation, equipment (KOYO) : $1.47 \cdot 10^{-1}$ [MJ/cm²]
5. Lithography, equipment (Suss MA6) : $6.82 \cdot 10^{-2}$ [MJ/cm²]
6. VO₂ Sputtering, equipment (AJA) : $5.02 \cdot 10^{-2}$ [MJ/cm²]
7. Lift-off, use of acetone : $3.76 \cdot 10^{-2}$ [MJ/cm²]
8. Standard Cleaning, use of H₂O₂ : $2.65 \cdot 10^{-2}$ [MJ/cm²]
9. VO₂ Annealing, equipment : $1.08 \cdot 10^{-2}$ [MJ/cm²]
10. Lift-off, equipment (waterbath) : $2.19 \cdot 10^{-3}$ [MJ/cm²]

From previous ranking and as shown in Figure 4.11, it is evident that the metallization stage stands out as the dominant hotspot, responsible for 99.27% of the overall process's PED. This dominance can be largely attributed to the exceptionally high EI linked to gold. This particular element opens the door to improvement via substitution of gold by another material, and it will be the central point of discussion in the subsequent chapter.

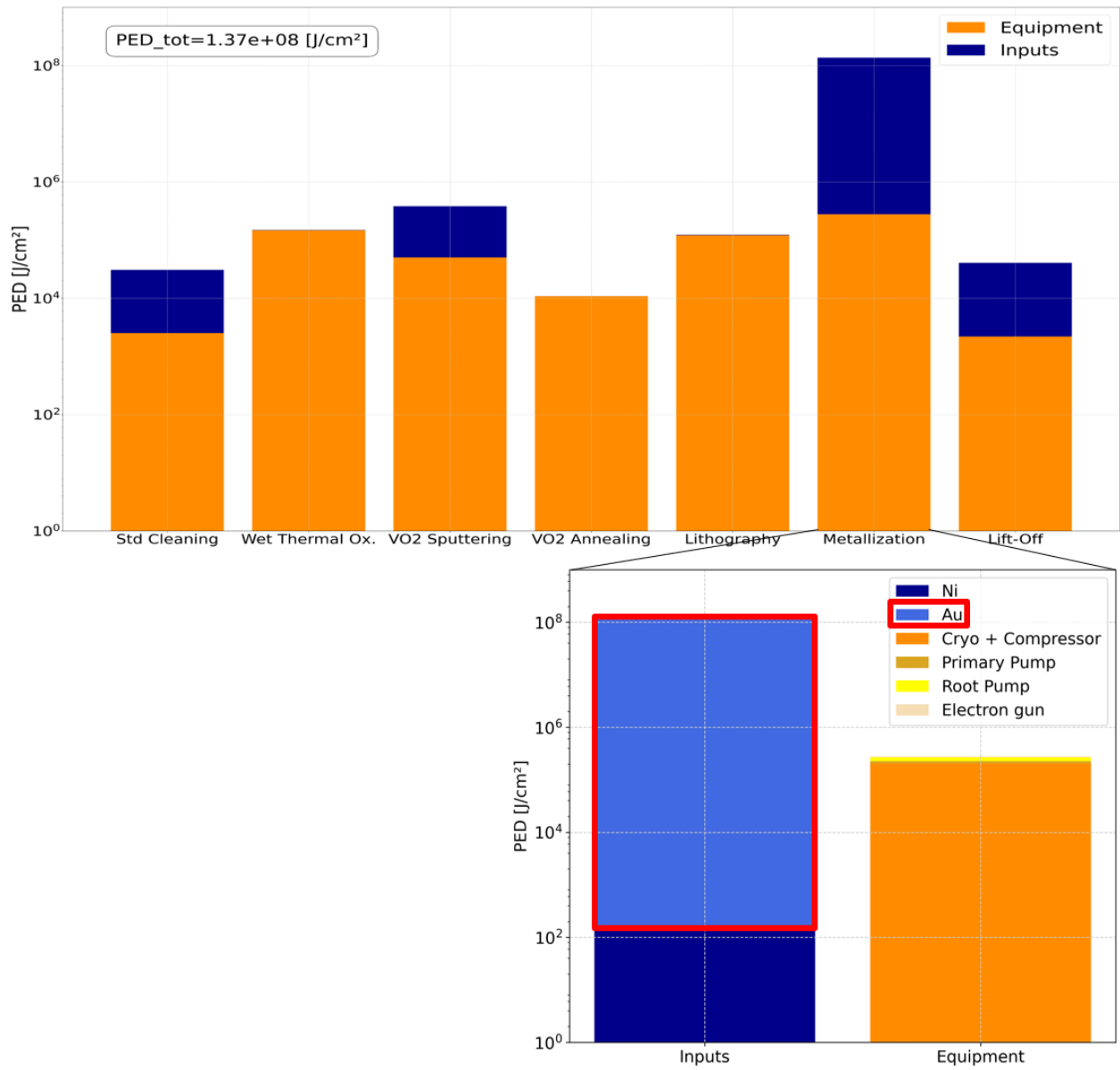


Figure 4.11: PED [J/cm²] of the complete process with zoom on the hotspot, logarithmic scale.

Chapter 5

Alternative process

In Chapter 4, the LCA was conducted on the microfabrication process of the VO₂-based device. This assessment revealed the hotspot, which corresponds to the most energy-intensive element : the use of gold in the metallization step for contact creation. The objective of this chapter is twofold: to suggest an alternative to gold that can decrease the overall energy consumption of the entire process, and to examine the impact of this substitution on performance. However, certain elements need to be taken into account when selecting this alternative. As a primary concern, it is necessary to reduce the environmental impact of the microfabrication process. Furthermore, it is imperative to guarantee that the selected metal as a substitute for gold fulfills the same criteria. This involves establishing Ohmic contact with the semiconductor layer (VO₂) and to ensure the VO₂ IV-characteristic transition as well.

Ohmic contacts between metal and semiconductor facilitate efficient current flow, with low resistance and the establishment of a continuous conductive path. They enable current passage from metal to semiconductor or vice versa and exhibit equal conductivity for both polarities. This is due to majority carriers crossing a low barrier height at the junction. Ohmic contacts are electrical connections with a linear current-voltage (I-V) characteristic, meaning that the current through the contact is proportional to the applied voltage (Figure 5.4a). This characteristics are essential for many electronic devices and circuits, as it allows for reliable electrical connections and efficient performance. Poor Ohmic contact can lead to high resistance, low conductivity, electrical instability, and even failures in device operation ([46], [53]). To form an Ohmic contact, there are two approaches available. The first one involves utilizing different metals with work functions adapted to the carriers you want to collect. The other solution, mainly used in industry, is to strongly dope the material and take advantage of the tunnel effect. High doping narrows the depletion region at the interface and allow electrons to flow in both directions easily at any bias by tunneling through the barrier [48]. Tunneling in an Ohmic contact refers to the quantum phenomenon where charge carriers can cross a potential barrier, allowing current to flow despite a high potential difference [16].

The work function, denoted ϕ , represents the minimum energy needed to remove an electron from a material's surface and move it just outside the material, without providing any additional energy to the electron [17]. It essentially overcomes the attractive forces that keep the electron bound within the material. To form the Ohmic contact the following conditions must be satisfied based on majority carriers, with ϕ_m being the work function of the metal and ϕ_{sc} the work function of the semiconductor :

- N-doped semiconductor : $\phi_m < \phi_{sc}$
- P-doped semiconductor : $\phi_m > \phi_{sc}$

However, in the case of VO₂ being an intrinsic semiconductor, these conditions are not relevant. We can achieve an Ohmic contact for both carriers by obeying to the following conditions :

- $\phi_m < \phi_{sc} \rightarrow$ Ohmic contact for electrons (n)
- $\phi_m > \phi_{sc} \rightarrow$ Ohmic contact for electron holes (p)

Multiple values for the work functions are found in the literature. To obtain a representative value, we calculate an average from these values :

- $\phi_{VO_2} = 5.12$ eV ([31], [57], [50], [10]),
- $\phi_{Au} = 4.95$ eV ([31], [57], [3], [37])

Gold has a lower work function than the VO₂ semiconductor in the original microfabrication process, resulting in Ohmic contact for electrons.

The second requirement that the alternative metal must meet is to guarantee the characteristic transition. As a reminder, the characteristic transition mentioned in Chapter 2 is observable in the IV curves (see Figure 2.2 in Chapter 2). It reflects the change of the VO₂ film from a semiconducting (insulating) state to a metallic state in response to electrical triggering.

Alternative process

The proposed alternative process suggests replacing the gold deposit, as well as the adhesive nickel layer, with a copper layer.

To implement this alternative process, we went to the WINFAB cleanroom to create nearly identical wafers. The only difference was in the metallization stage, where half of the wafers received a gold and nickel layer, while the other half received a copper layer through evaporation. The complete process included standard cleaning, wet thermal oxidation for oxide layer formation, sputtering of the VO₂ layer, annealing for crystallization, lithography for contact patterns, metallization, and lift-off to remove unwanted areas. However, we encountered an issue after the annealing step. The wafers exhibited non-uniformity, with a halo-like appearance in the center due to large and discontinuous grains (Figure 5.1). This could be attributed to either the vanadium target nearing the end of its lifespan during the sputtering step or contamination in the furnace used for annealing. As mentioned in Chapter 3, equipment sharing is a common practice in the WINFAB laboratory, which may contribute to such issues. These wafers were considered unusable.

If large and disconnected grains are present, the SiO₂ layer beneath the VO₂ layer will dominate, resulting in high substrate resistance and the prevention of current flow. This is an undesirable outcome. Our goal is to have rather small grains that are closely packed together. Small grains provide more grain joints, also known as defects and serve as pathways for current. Therefore, the smaller the grains and the closer, the more conductive the VO₂ film becomes. This highlights the impact of grain size on the resistivity of VO₂. Fortunately, another researcher working on a similar process kindly provided us with two wafers. These wafers had a 500 nm SiO₂ layer (thicker than our original process, but it doesn't affect the comparison between gold and copper deposition), a 130 nm VO₂ layer, and were annealed at 650°C. Subsequently, we returned to the lithography step to generate the desired patterns. A layer of nickel and gold was deposited on one wafer, while a layer of copper was deposited on the other. It was observed that the grain size of these two new wafers was the desired one, small grains close to each other (Figure 5.2 and Figure 5.3). Our research will be based on these two wafers.

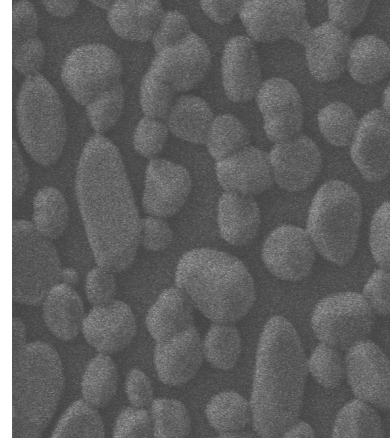


Figure 5.1: Grain size of the initial batch of wafers that exhibited halos, 906.2 nm.

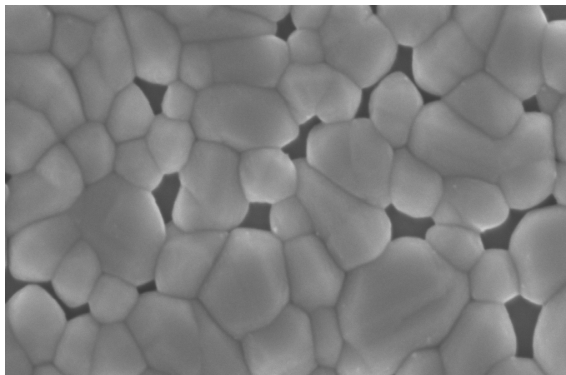


Figure 5.2: Grain size of wafer with gold (and nickel) evaporation, 245.36 nm.

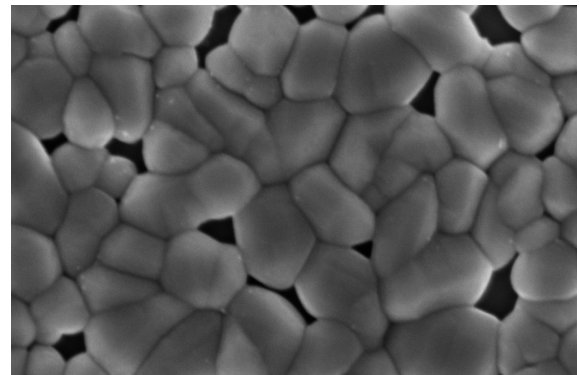


Figure 5.3: Grain size of wafer with copper evaporation, 253 nm.

Before addressing the modifications in impact and performance, let us verify that the alternative process satisfies the aforementioned requirements (i.e. impact reduction, Ohmic contact and IV transition). Copper (Cu) has an EI of 98.3 [MJ/kg] [4] which is lower compared to gold (which has an EI $4.25 \cdot 10^5$ [MJ/kg] [4]). This will reduce the impact of the metallization step, which was the most energy intensive step of the process. The work function of copper is $\phi_{Cu} = 4.60$ eV ([37], [40], [2]), ensuring an Ohmic contact for electrons, as shown in Figure 5.4.

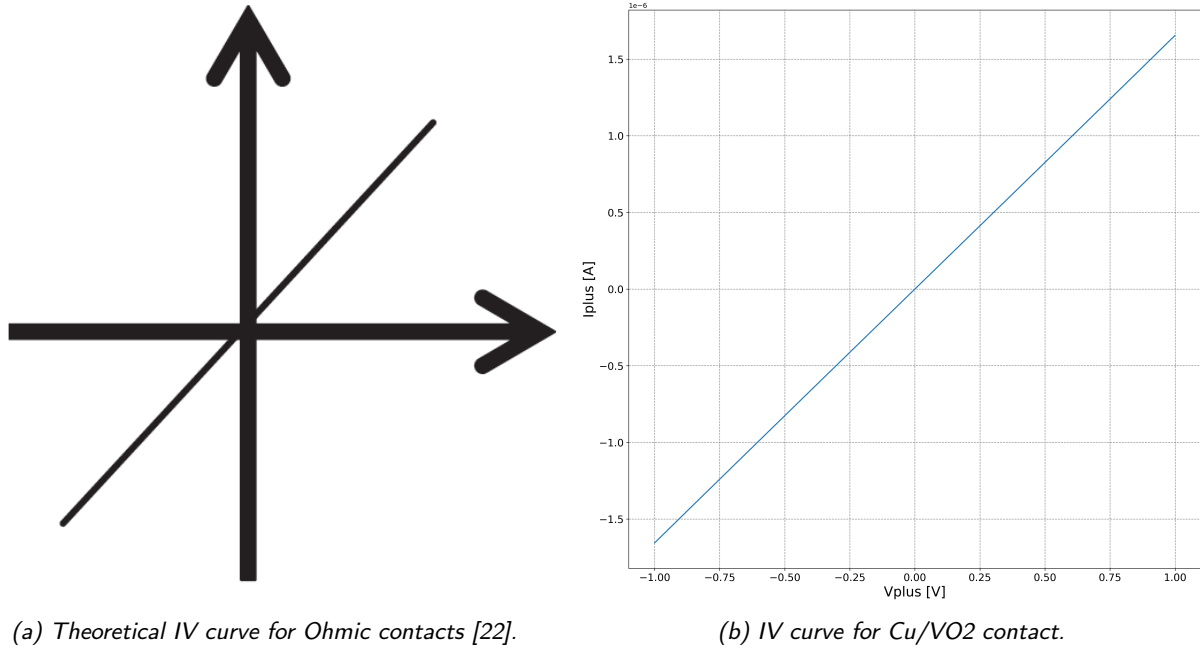


Figure 5.4: Metal-semiconductor Ohmic contact IV curve.

To observe the characteristic transition in the IV curves, we conducted DC measurements driven by both current and voltage on the device illustrated in Figure 5.5, with dimensions of $L=1.6 \mu\text{m}$ and $W=100 \mu\text{m}$.

	Au	Cu
I_{driven}	$I_{sweep} = 0 - 300[\mu A]$ $V_{compl} = 5[V]$	$I_{sweep} = 0 - 1[mA]$ $V_{compl} = 50[V]$
V_{driven}	$V_{sweep} = 0 - 3[V]$ $I_{compl} = 300[\mu A]$	$V_{sweep} = 0 - 4[V]$ $I_{compl} = 500[\mu A]$

Table 5.1: Measurement conditions.

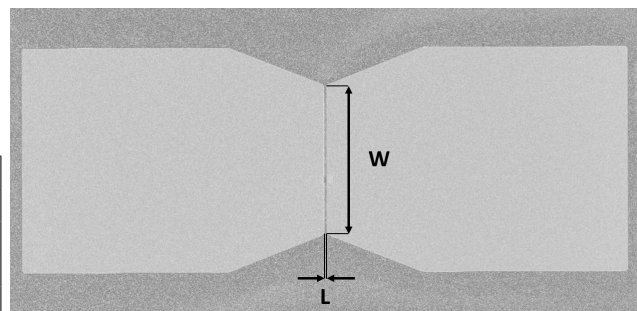


Figure 5.5: Measuring pad for the IV transition curves.

It is evident that the transitions, while not flawless, are observable, affirming that both wafers are functioning as intended as shown in Figure 5.6.

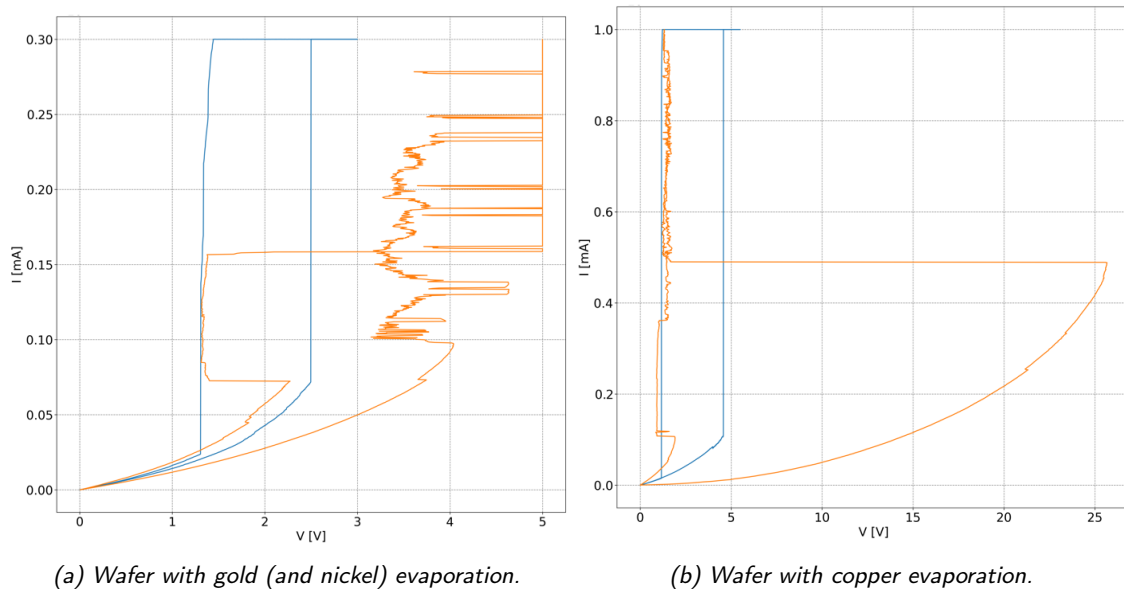


Figure 5.6: I- (yellow) and V-driven (blue) characteristic of the VO₂ device.

Furthermore, at a price of 5.2 euros per kilo, copper is a more economical material compared to gold, which costs 51,000 euros per kilo [4]. This cost advantage makes copper a favorable choice for large-scale manufacturing.

5.1 Change in environmental impact

Changing the deposited metal leads to a noticeable reduction in the environmental impact of the microfabrication process, as depicted in Figure 5.7. Specifically, the total PED decreases from $1.37 \cdot 10^2$ [MJ/cm²] for the gold deposit with its nickel adhesive layer to 1.03 [MJ/cm²] for the copper deposit, which corresponds to a decrease of 99.25%. Table 4.3 provides the exact PED values [MJ/cm²] per process step for the initial process (Au and Ni), while Table 5.2 presents the corresponding values for the alternative process.

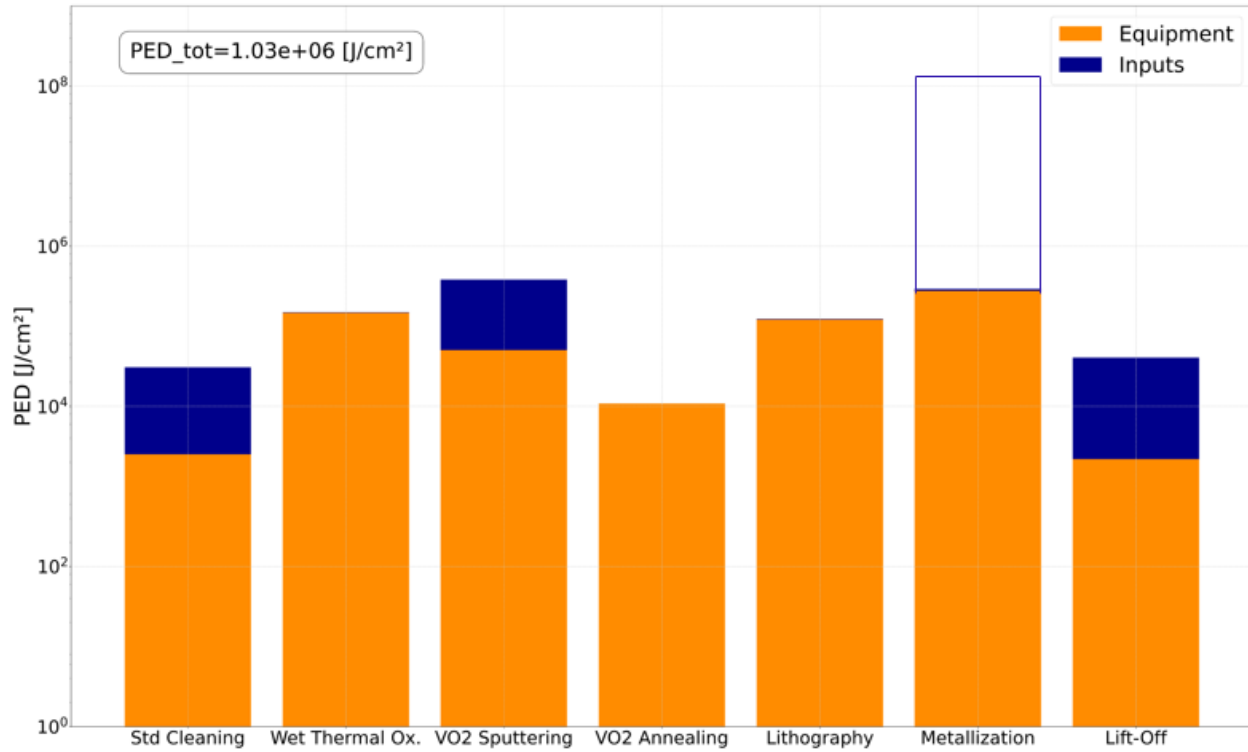


Figure 5.7: PED [J/cm²] of the complete process with copper evaporation, logarithmic scale. The solid line in the graph depicts the PED of the initial process (gold and nickel evaporation).

PED [MJ/cm ²]	Standard Cleaning	Thermal Oxidation	VO2 Sputtering	VO2 Annealing	Lithography	Metallization	Lift-Off
Inputs	$2.81 \cdot 10^{-2}$	$2.26 \cdot 10^{-3}$	$3.32 \cdot 10^{-1}$	$3.17 \cdot 10^{-5}$	$2.26 \cdot 10^{-3}$	$1.46 \cdot 10^{-2}$	$3.83 \cdot 10^{-2}$
Equipment	$2.52 \cdot 10^{-3}$	$1.47 \cdot 10^{-1}$	$5.02 \cdot 10^{-2}$	$1.08 \cdot 10^{-2}$	$1.21 \cdot 10^{-1}$	$2.78 \cdot 10^{-1}$	$2.19 \cdot 10^{-3}$
PED_{tot}	$3.06 \cdot 10^{-2}$	$1.49 \cdot 10^{-1}$	$3.82 \cdot 10^{-1}$	$1.08 \cdot 10^{-2}$	$1.23 \cdot 10^{-1}$	$2.93 \cdot 10^{-1}$	$4.05 \cdot 10^{-2}$

Table 5.2: PED [MJ/cm²] of the complete process with copper evaporation.

Upon closer examination of the process stage that undergoes reduction, it becomes evident that copper consumes significantly less energy than gold due to its considerably lower energy intensity, as shown in Figure 5.8. The PED for copper evaporation is $2.93 \cdot 10^{-1}$ [MJ/cm²], whereas for gold (and nickel evaporation), it is $1.36 \cdot 10^2$ [MJ/cm²]. This metallization step exhibits a significant decrease of 99.78%. For a more comprehensive overview of this stage of the process, please refer to Section A.8 in Chapter A, which provides a detailed worksheet.

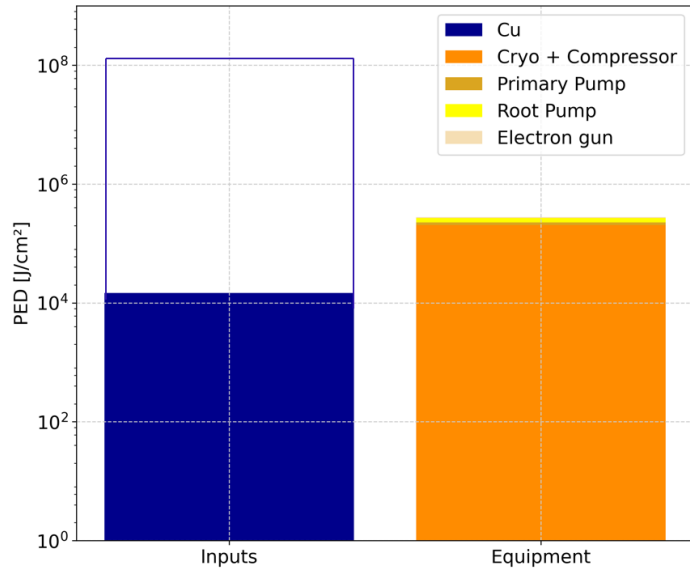


Figure 5.8: PED [J/cm²] of the metallization step (copper evaporation), logarithmic scale. The solid line in the graph depicts the PED of the initial metallization step (gold and nickel evaporation).

The same formula was employed as an assumption to calculate the mass of copper deposited :

$$mass [kg] = Surface [m^2] \cdot thickness [m] \cdot density [kg/m^3] \quad (5.1)$$

with

- Surface = $2lw + 2lh + 2wh$, length (l) = 0.64 [m], width (w) = 0.84 [m], height (h) = 0.66 [m].
- Thickness (Cu) = 100 [nm]
- Density (Au) = 8940 [kg/m³]

In this new process, the most energy-intensive aspects have shifted from the inputs of the metallization step to the next identified hotspots as stated in Section 4.5 in Chapter 4. Both Table 5.2 and Figure 5.7 highlight that the vanadium input in the VO₂ sputtering step, the equipment used in the metallization step, and the equipment of the wet thermal oxidation step play a dominant role in determining the environmental impact of the alternative process.

5.2 Change in performance

To evaluate the impact of the alternative process on performance, we conducted contact resistance measurements between the metal and the semiconductor (VO₂) using the transfer length measurement (TLM) technique ([20], [25]). To determine the specific contact resistivity, a series of rectangular metal pads (Au and Ni for the original process, Cu for the alternative process), are deposited on the surface of the VO₂ semiconductor substrate, as depicted in the accompanying Figure 5.9. The distance between the pads increases from the left to the right (Figure 5.10).



Figure 5.9: Pads for the transfer length measurement (TLM). W the width of the pads and L the length between the pads.

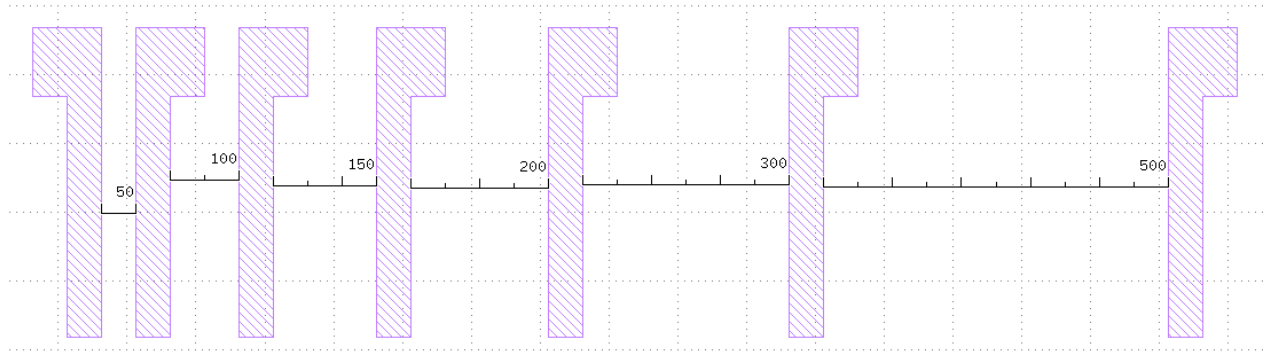


Figure 5.10: Spacing between the different pads [μm].

When the resistance between adjacent pads is measured, the total resistance correspondingly increases. The total measured resistance includes 3 components :

$$R_{tot} = R_{SC} + 2R_C + 2R_m \quad (5.2)$$

In this context, R_m represents the resistance attributed to the contact metal, R_C is related to the metal/semiconductor interface, and R_{SC} represents the typical resistance of the semiconductor itself. Nevertheless, in the majority of cases, the resistivity of the metal at the contact is significantly lower than R_C so that R_m can be ignored. The contribution of the VO₂ semiconductor layer can be described by the formula $R_{SC} = \frac{R_S}{W} d_i$, where d_i represents

the distance between the pads and W denotes the width of the metal pads. The total resistance is thus :

$$R_{tot} = \frac{R_S}{W} \cdot d_i + 2R_C \quad (5.3)$$

By calculating the total resistance for the different distances (Table 5.3) and doing a linear regression, the y-intercept ($d_i = 0$) provides twice the contact resistance, $2R_C$. This allows us to determine the contact resistance accurately.

R_{tot}	50 [μm]	100 [μm]	150 [μm]	200 [μm]	300 [μm]	500 [μm]
Gold (25°C)	$7.2158 \cdot 10^5$	$9.7319 \cdot 10^5$	$1.4827 \cdot 10^6$	$1.8423 \cdot 10^6$	$2.2022 \cdot 10^6$	$2.8169 \cdot 10^6$
Copper (25°C)	$6.0531 \cdot 10^5$	$8.1558 \cdot 10^5$	$1.2553 \cdot 10^6$	$1.5678 \cdot 10^6$	$1.8854 \cdot 10^6$	$2.4666 \cdot 10^6$
Gold (110°C)	$1.7663 \cdot 10^2$	$2.2636 \cdot 10^2$	$3.6333 \cdot 10^2$	$4.5891 \cdot 10^2$	$5.6206 \cdot 10^2$	$7.2894 \cdot 10^2$
Copper (110°C)	$6.6616 \cdot 10^1$	$8.9399 \cdot 10^1$	$1.3878 \cdot 10^2$	$1.7415 \cdot 10^2$	$2.1303 \cdot 10^2$	$2.8243 \cdot 10^2$

Table 5.3: Total resistance R_{tot} according to pad distances.

Contact Resistance

Contact resistance refers to the level of resistance encountered when electric current passes through the interface between a metal and a semiconductor. It serves as an indicator of the ease or difficulty with which the current can traverse this junction. In Figure 5.11, the linear regressions of the total resistance values, previously calculated and displayed in Table 5.3, are shown for gold and copper at 25°C. Figure 5.12 presents the same analysis but at 110°C. The resulting contact resistance values obtained at both temperatures are summarized in Table 5.4. Notably, copper exhibits a lower contact resistance compared to gold, of 19.5% at 25°C and of 62.3% 110°C.

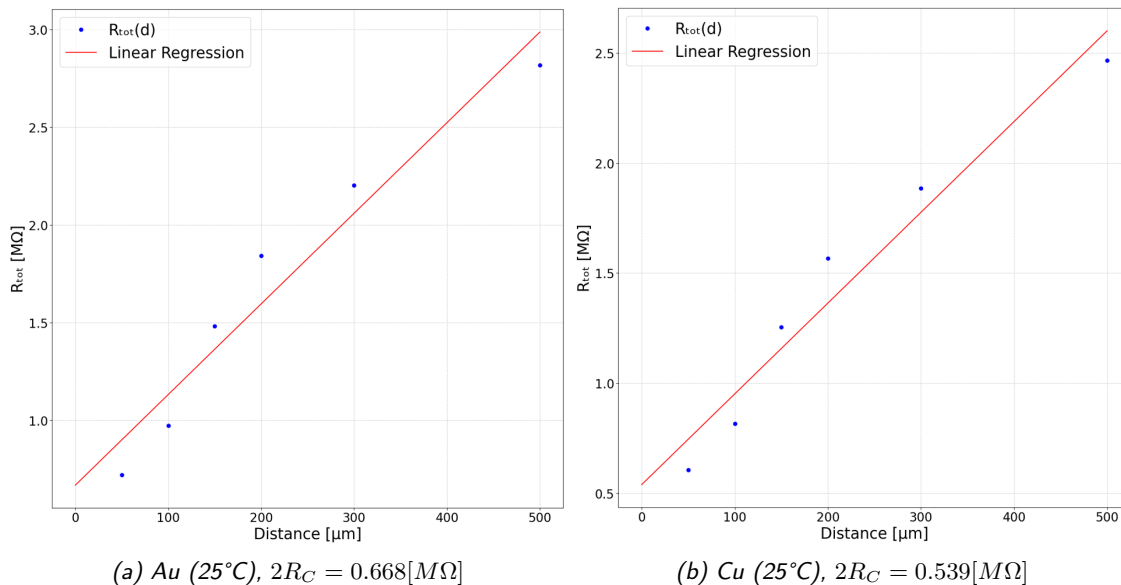


Figure 5.11: Linear regression of the TLM method performed at 25°C.

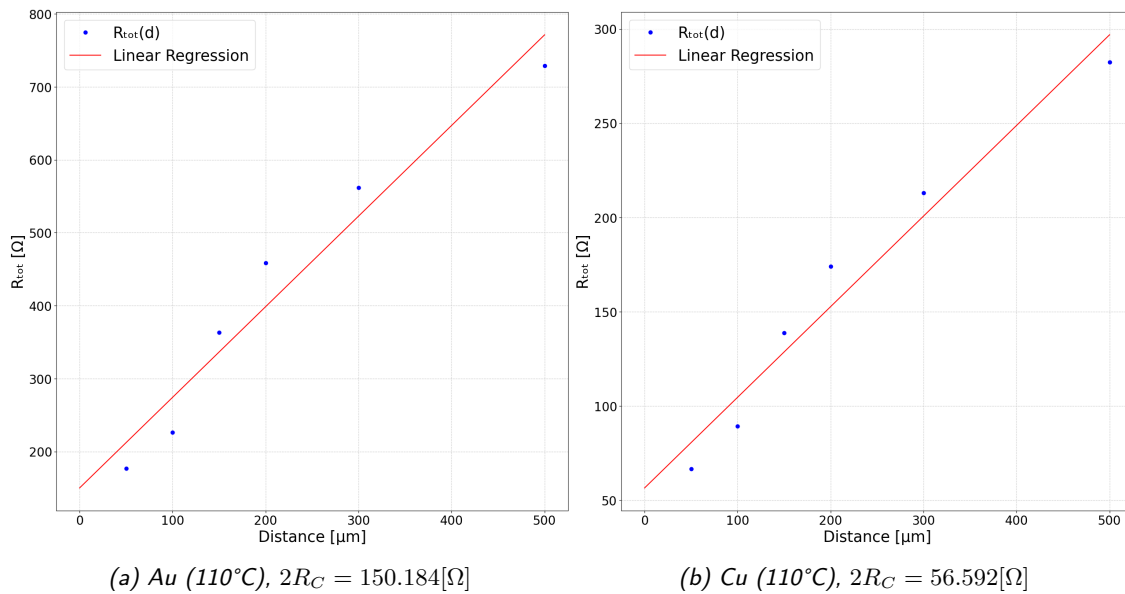


Figure 5.12: Linear regression of the TLM method performed at 110°C.

	$R_{\text{contact}} [M\Omega]$ at 25°C	$R_{\text{contact}} [\Omega]$ at 110°C
Gold evaporation	0.334	75.092
Copper evaporation	0.269	28.296

Table 5.4: R_{contact} at 25°C and 110°C.

Resistance of VO2 with Temperature

To enable the VO2 resistor to enter the spiking regime, it must be biased within an astable region where it oscillates between its metallic and insulating equilibrium points. This requires the current flowing through the device to fall within its negative differential resistance (NDR) range, which can be observed in the current- and voltage-driven measurement of the I-V characteristic Figure 2.2 in Chapter 2. The NDR region expands with an increase in the $\frac{R_{\text{ins}}}{R_{\text{met}}}$ ratio. Additionally, the size of the NDR zone can be correlated with the hysteresis of the resistance as a function of temperature (Figure 2.1 in Chapter 2). A larger hysteresis height, which signifies a greater disparity between R_{ins} and R_{met} , implies an extended duration in the metallic phase and a higher $\frac{R_{\text{ins}}}{R_{\text{met}}}$ ratio, resulting in a larger NDR zone. On the other hand, a smaller $\frac{R_{\text{ins}}}{R_{\text{met}}}$ leads to a narrower NDR zone, making it more likely for the current to deviate from the desired range when subjected to external stimuli, ultimately contributing to device aging [7].

Hence, we compute the fraction $\frac{R_{\text{ins}}}{R_{\text{met}}}$ in this context. To do this, we previously obtained the values of R_{contact} at 25°C and 110°C. At 25°C, VO2 is in its insulating phase, while at 110°C, it is in its metallic phase (with a phase transition point around 68°C [42]). Because of the phase-transition, the aspect of the VO2 film changes. This can be seen in Figure C.1. We selected a specific distance between the pads (the same for both cases) and used the equation 5.3 to determine the resistance of the VO2 substrate at both temperatures. Once the resistance values

of the semiconductor obtained at 25 and 110°C, we calculate $\frac{R_{ins}}{R_{met}}$.

$$R_S = \frac{W}{d_i} \cdot (R_{tot} - 2R_C) \quad (5.4)$$

with :

- $W = 200[\mu m]$
- distance 1 : $d_1 = 50[\mu m]$
- $R_S(25) = R_{ins}$
- $R_S(110^\circ C) = R_{met}$

Figure 5.13 illustrates the resistance of the semiconductor in both the insulating state (at 25°C) and the metallic state (at 110°C) for gold and copper deposits while Table 5.5 confirms that the copper evaporation, with its $\frac{R_{ins}}{R_{met}} = 6614.5$ exhibits a higher ratio than the gold evaporation $\frac{R_{ins}}{R_{met}} = 2025.7$ (almost 3 times larger), leading to an expanded NDR zone.

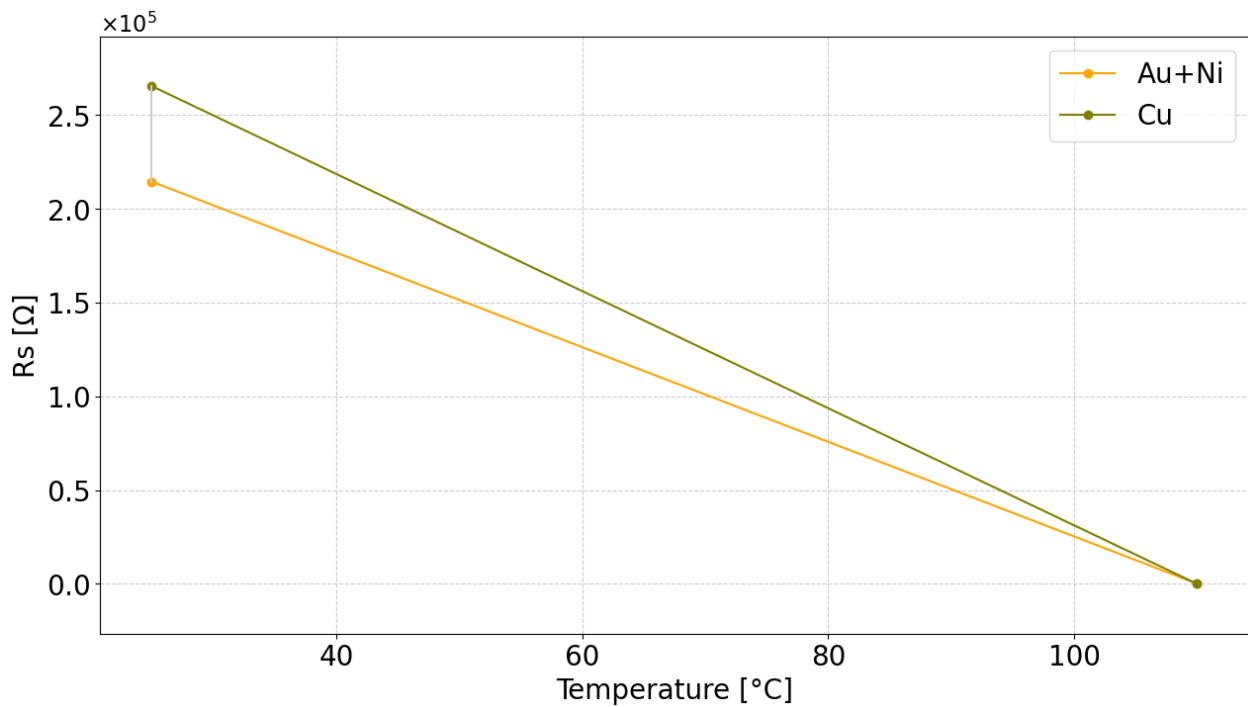


Figure 5.13: Resistance of VO2 with temperature to demonstrate the magnitude of hysteresis in the case of gold (and nickel) evaporation and in the case of copper evaporation.

	$R_S [\Omega]$ at 25°C	$R_S [\Omega]$ at 110°C	R_{ins}/R_{met}
Gold evaporation	214320	105.8	2025.7
Copper evaporation	265240	40.1	6614.5

Table 5.5: R_S at 25°C and 110°C.

Chapter 6

Discussion and Perspectives

In this study, several assumptions were made to achieve conclusive results. However, it is important to acknowledge that these assumptions should be approached with a certain level of nuance.

6.1 LCA of the VO₂-based device

Let us review the assumptions that were made in order to obtain the results for the LCA in Chapter 4 :

- EI [MJ/kg] values are sourced from Boyd's work [8], with the exception of Au, Ni, and V, which are obtained from the EduPack software [4].
- The Capacity Factor of 0.23 has been imposed to all equipment.
- The calculation of PED consumption for the equipment is based on the duration of the process.
- Facility infrastructure (HVAC), wafer production, N₂ input and computers to run the process are neglected.

Mix of Boyd's work and the EduPack software for EI values

To begin with, one of the biggest assumptions made was the use of the EduPack software for the EI [MJ/kg] of metals used in our process (ie Au, Ni and V). We made the decision not to rely on Boyd's work for EI values of metals due to significant underestimation (that is 3.1 [MJ/kg] compared to 425,000 [MJ/kg] for gold for example) as further described in this section. As mentioned in Chapter 4, Boyd referenced Overcash as the source for her energy intensity value for gold and nickel [8]. Overcash's study indicates that *for more than half of the inorganic chemicals, the energy required for the process ranges from -1 to 3 MJ per kg, representing gate-to-gate process energy for producing a specific chemical product* [33]. Overcash estimates these energy values based on the design methodology described in Jimenez-Gonzalez et al [29]. The methodology for obtaining gate-to-gate data for the life cycle of chemical substances involves several steps, including research and process selection, detailed process definition, material balance calculation, evaluation of energy consumption (considering various factors such as heat of reaction, sensible heat, separation units, material transport, energy losses, and potential energy recovery). Boyd acknowledges the common use of Overcash's estimated energy intensity for chemical manufacturing due to the lack of process LCA data and cost information (as explained in Chapter 4). However, concerns arise regarding the

justification for Boyd assigning this value specifically to gold and nickel. Despite the methodology's comprehensiveness, the reasoning behind this choice remains uncertain.

As previously mentioned in Chapter 4, we additionally compared these EI for metals with those from other sources, which confirmed the underestimation and provided higher values for the metals in our process as shown in Table 6.1.

EI [MJ/kg]	Au	Ni	V
Boyd [8]	3.1	3.1	/
Nuss [45]	208,000	206.5	516
EduPack[4]	425,000	206.5	3715
UNEP [54]	310,000	180-200	3700

Table 6.1: Comparison of EI values between Boyd and other sources. EI value for vanadium not present in Boyd.

Moreover, we had the opportunity to collaborate with CEA-Leti, one of the world's leading centres for applied research in microelectronics and nanotechnologies, with a larger-scale research laboratory. They replicated our process and conducted an LCA, using the database ecoinvent for their EI values. Ecoinvent is a widely used database that provides detailed LCI for many products, materials and industrial processes. At first, the determined value of EI for gold using ecoinvent in the CEA-Leti study confirmed our hypothesis (underestimation of EI values for metals used in our process) while highlighting the potential variations and inaccuracies in EI values from different sources.

If we had relied exclusively on Boyd's reference work and only considered her EI values, along with Nuss's and Eckelman's EI for vanadium [45], as it was not covered in Boyd's work, the results would have differed. In this scenario, not only would the total PED be lower, but the VO₂ sputtering step would have emerged as the most energy-intensive. To summarize, when considering the EduPack data, the total PED is $1.37 \cdot 10^2$ [MJ/cm²], with the metallization step (involving gold) being the most energy-intensive at a value of $1.36 \cdot 10^2$ [MJ/cm²] (see Figure 4.3 in Chapter 4 and Table 6.3). However, in this particular case, the total PED is reduced to $7.30 \cdot 10^{-1}$ [MJ/cm²] (Figure 6.1), and the sputtering step now emerges as the most energy-consuming as can be seen in Table 6.2. There is a decrease of 99.47%. Besides, the equipment utilized in the thermal oxidation, lithography, and metallization stages present promising possibilities for alternative investigation. The change in EI sources has resulted in a shift in hotspots within the process.

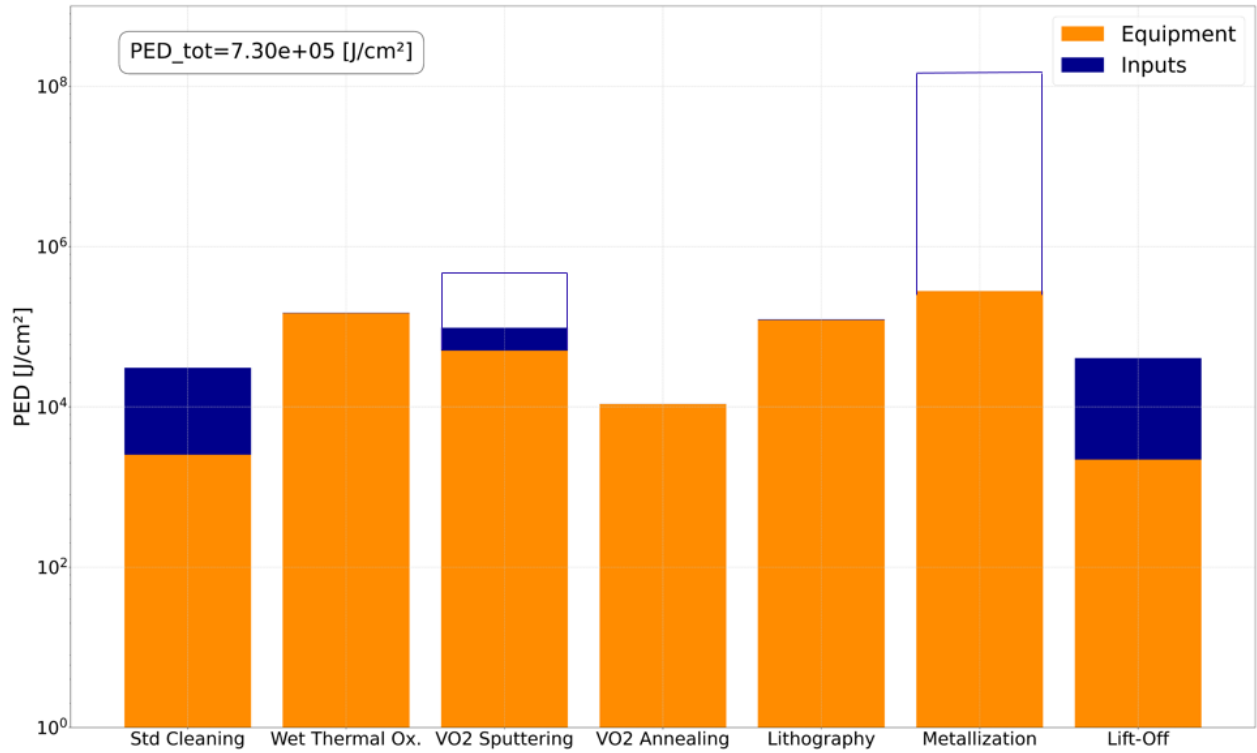


Figure 6.1: PED [J/cm^2] of the complete process with gold (and nickel) evaporation, logarithmic scale. Energy Intensity (EI) values only from Boyd's work [8]. The solid line in the graph depicts the PED [J/cm^2] with EI from the EduPack software for the metals.

PED [MJ/cm^2]	Standard Cleaning	Thermal Oxidation	VO2 Sputtering	VO2 Annealing	Lithography	Metallization	Lift-Off
Inputs	$2.81 \cdot 10^{-2}$	$2.26 \cdot 10^{-3}$	$4.64 \cdot 10^{-2}$	$3.17 \cdot 10^{-5}$	$2.26 \cdot 10^{-3}$	$9.96 \cdot 10^{-4}$	$3.83 \cdot 10^{-2}$
Equipment	$2.52 \cdot 10^{-3}$	$1.47 \cdot 10^{-1}$	$5.02 \cdot 10^{-2}$	$1.08 \cdot 10^{-2}$	$1.21 \cdot 10^{-1}$	$2.78 \cdot 10^{-1}$	$2.19 \cdot 10^{-3}$
PED_{tot}	$3.06 \cdot 10^{-2}$	$1.49 \cdot 10^{-1}$	$3.82 \cdot 10^{-1}$	$1.08 \cdot 10^{-2}$	$1.23 \cdot 10^{-1}$	$2.79 \cdot 10^{-1}$	$4.05 \cdot 10^{-2}$

Table 6.2: PED [MJ/cm^2] of the complete process. Energy Intensity (EI) values only from Boyd's work [8].

PED [MJ/cm^2]	Standard Cleaning	Thermal Oxidation	VO2 Sputtering	VO2 Annealing	Lithography	Metallization	Lift-off
Inputs	$2.81 \cdot 10^{-2}$	$2.26 \cdot 10^{-3}$	$3.32 \cdot 10^{-1}$	$3.17 \cdot 10^{-5}$	$2.26 \cdot 10^{-3}$	$1.36 \cdot 10^2$	$3.83 \cdot 10^{-2}$
Equipment	$2.52 \cdot 10^{-3}$	$1.47 \cdot 10^{-1}$	$5.02 \cdot 10^{-2}$	$1.08 \cdot 10^{-2}$	$1.21 \cdot 10^{-1}$	$2.78 \cdot 10^{-1}$	$2.19 \cdot 10^{-3}$
PED_{tot}	$3.06 \cdot 10^{-2}$	$1.49 \cdot 10^{-1}$	$3.82 \cdot 10^{-1}$	$1.08 \cdot 10^{-2}$	$1.23 \cdot 10^{-1}$	$1.36 \cdot 10^2$	$4.05 \cdot 10^{-2}$

Table 6.3: PED [MJ/cm^2] of the complete process. Energy Intensity (EI) values only from Boyd's work [8] and the EduPack software for metals [4].

Capacity factor applied to all equipment and only duration of the process considered

As for our second major hypothesis, we have chosen to apply the calculated capacity factor (0.23) from Chapter 4 to all process equipment (see *Real Time Measurements on Equipment - Capacity Factor* 4.2). However, it was only feasible to calculate it specifically for the wet thermal oxidation step on the KOYO furnace, which might not accurately represent other equipment. Nevertheless, this hypothesis allowed us to realize that, particularly for the oxidation stage, equipment consumption does not align with the values indicated on the datasheet. This is likely applicable to other equipment as well. If we had only relied on material datasheets, the results would have shown a total consumption increase of 1.5% from $1.37 \cdot 10^2$ [MJ/cm²] to $1.39 \cdot 10^2$ [MJ/cm²] as shown in Figure 6.2. Ideally, conducting real-time measurements on each equipment and considering standby energy consumption (our third hypothesis) would be beneficial. The calculation of PED consumption is based on the process duration, despite certain equipment being on standby and continuing to consume energy outside the active process time (as indicated in Chapter 3 for each stage of the process). However, this hypothesis does not impact the identified hotspot determined during the conducted LCA in this study, Chapter 4, as shown in Table 6.4 and Table 6.5.

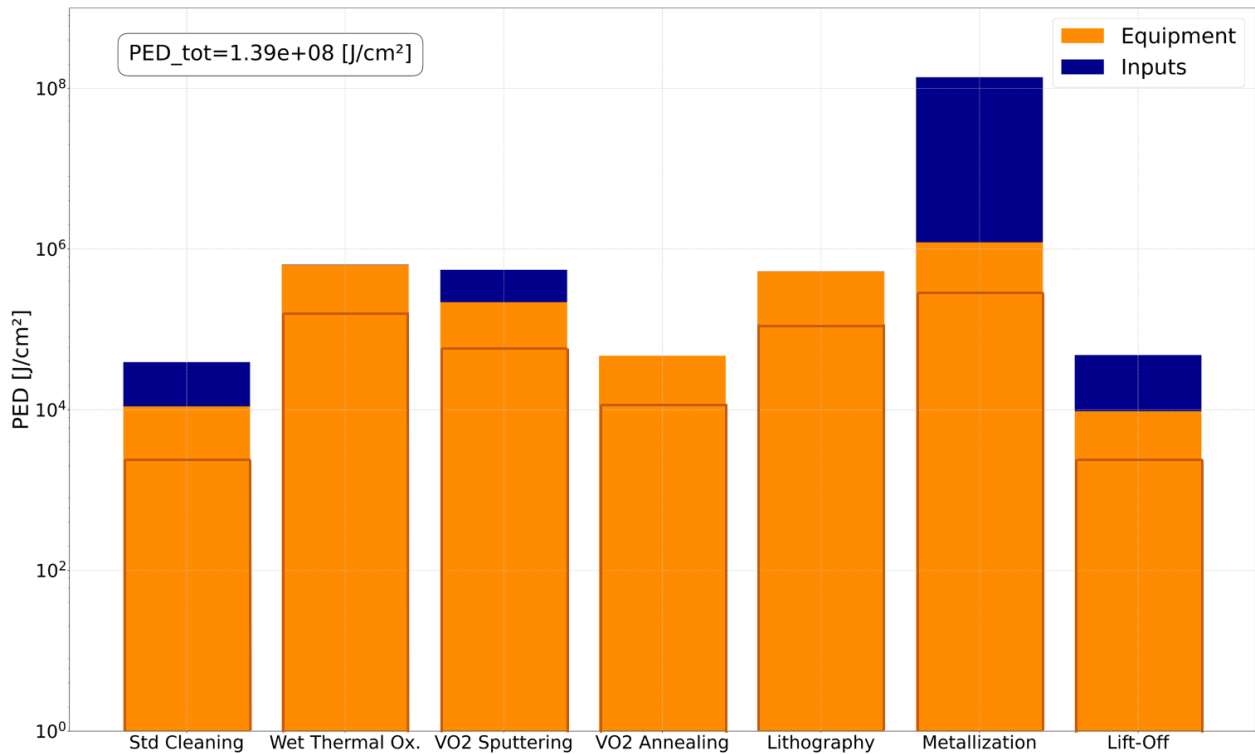


Figure 6.2: PED [J/cm²] of the complete process with gold (and nickel) evaporation, logarithmic scale. Without capacity Factor. The solid line in the graph depicts the PED [J/cm²] with the capacity factor included.

PED [MJ/cm ²]	Standard Cleaning	Thermal Oxidation	VO2 Sputtering	VO2 Annealing	Lithography	Metallization	Lift-Off
Inputs	$2.81 \cdot 10^{-2}$	$2.26 \cdot 10^{-3}$	$3.32 \cdot 10^{-1}$	$3.17 \cdot 10^{-5}$	$2.26 \cdot 10^{-3}$	$1.36 \cdot 10^2$	$3.83 \cdot 10^{-2}$
Equipment	$1.10 \cdot 10^{-2}$	$6.38 \cdot 10^{-1}$	$2.18 \cdot 10^{-1}$	$4.69 \cdot 10^{-2}$	$5.25 \cdot 10^{-1}$	1.21	$9.54 \cdot 10^{-3}$
PED_{tot}	$3.91 \cdot 10^{-2}$	$6.41 \cdot 10^{-1}$	$5.50 \cdot 10^{-1}$	$4.69 \cdot 10^{-2}$	$5.27 \cdot 10^{-1}$	$1.37 \cdot 10^2$	$4.78 \cdot 10^{-2}$

Table 6.4: PED [MJ/cm²] of the complete process with gold (and nickel) evaporation. Without capacity Factor.

PED [MJ/cm ²]	Standard Cleaning	Thermal Oxidation	VO2 Sputtering	VO2 Annealing	Lithography	Metallization	Lift-off
Inputs	$2.81 \cdot 10^{-2}$	$2.26 \cdot 10^{-3}$	$3.32 \cdot 10^{-1}$	$3.17 \cdot 10^{-5}$	$2.26 \cdot 10^{-3}$	$1.36 \cdot 10^2$	$3.83 \cdot 10^{-2}$
Equipment	$2.52 \cdot 10^{-3}$	$1.47 \cdot 10^{-1}$	$5.02 \cdot 10^{-2}$	$1.08 \cdot 10^{-2}$	$1.21 \cdot 10^{-1}$	$2.78 \cdot 10^{-1}$	$2.19 \cdot 10^{-3}$
PED_{tot}	$3.06 \cdot 10^{-2}$	$1.49 \cdot 10^{-1}$	$3.82 \cdot 10^{-1}$	$1.08 \cdot 10^{-2}$	$1.23 \cdot 10^{-1}$	$1.36 \cdot 10^2$	$4.05 \cdot 10^{-2}$

Table 6.5: PED [MJ/cm²] of the complete process. Energy Intensity (EI) values only from Boyd's work [8] and the EduPack software for metals [4].

HVAC, N2, wafer production and computers are neglected when calculating LCIA indicator PED

Regarding the last hypothesis, we discussed the exclusion of certain elements from our LCA calculations, including HVAC, N2 consumption, wafer production and laptop consumption.

- HVAC was not considered primarily due to its fixed parameters, which we were unable to modify. Additionally, its consumption includes various processes, not just ours, making it challenging to accurately attribute the specific proportion to our process alone. The equipment-related PED (i.e. electricity consumption of the room), including HVAC and all equipments present in the WINFAB cleanroom, is $4.31 \cdot 10^3$ [MJ]. This energy consumption corresponds to a daily electricity usage of 4305.6 [MJ], assuming the capacity factor hypothesis is applied. When considering the overall PED of the process equipment, the calculated PED is $2.41 \cdot 10^2$ [MJ].

	Cleanroom	Process for VO2-based device
PED _{equipment} [MJ]	$4.31 \cdot 10^3$	$2.41 \cdot 10^2$

This indicates that our process accounts for 5.6% of the total equipment-related energy consumption in the room. It's important to note that inputs are not considered in this calculation. To make an accurate comparison between this value and the total PED of the process equipment, we would need to know the number of wafers utilizing this room's energy consumption.

It is evident that HVAC consumption is substantial, and it would be worthwhile to investigate it in future studies.

- The consumption of N2 was also omitted from this study for several reasons. First, we lack the means for measurement, and again, it represents a fixed parameter for the process steps. Large quantities of nitrogen are used for sterilization, gas removal, and purging of process chambers [51].
- Regarding wafer production in the context of this study, it represents again a fixed parameter in our specific case. Furthermore, we were able to conclude that this was minimal in relation to the overall process, and

could therefore be disregarded. In a previous study focusing on a MEMs piezoresistive pressure sensor [14], a comprehensive bottom-up LCA was conducted, which included an examination of the CED during wafer production. This analysis revealed a CED value of 0.4 [kWh/cm²] or 1.44 [MJ/cm²] for wafer production. In our case, if we express the final result in terms of CED [MJ/cm²], our process demonstrates a significantly higher CED of $1.3679 \cdot 10^2$ [MJ/cm²].

	Wafer Production	Process for VO ₂ -based device
CED [MJ/cm ²]	1.44	$1.3679 \cdot 10^2$

Considering the inclusion of wafer production in our CED calculation, its contribution would amount to only 1% of the total CED computed for the entire process. Consequently, we can disregard it.

- Lastly, the energy consumption attributed to laptops used during the process was disregarded because it also constitutes a fixed parameter and their energy usage is minimal, even negligible. We are talking about less than 100 [Wh] ([21], [18]).

In conclusion, upon examining the outcomes derived from the aforementioned hypotheses as presented in Chapter 4, it becomes evident that the metallization step stands out as the most energy-intensive in terms of PED, because of the EI of gold. The main reason for this observation is primarily the lower grade of ores utilized in gold production in comparison to the ores used for the production of most other metals [44]. A substantial portion of the embodied energy and greenhouse gas emissions in gold production is attributed to the mining and mineral processing stage, whereas for most other metals, the extraction and refining stage is the primary contributor, considering the current world average ore grades [44]. Additionally, the gold separation process is very energy-intensive and requires huge quantities of cyanide [9].

Evaluation of the result

As previously stated, the French research laboratory CEA-Leti replicated our process, conducted an LCA, and found gold to be the most impactful element. Their conclusions not only validated our assumptions, particularly regarding the accuracy of using the EduPack software for determining the EI values, but also the identification of the dominant element in terms of PED at the process level. In addition, their value obtained in terms of PED also affirmed the approximate magnitude of our calculated total PED for the process.

When considering our overall PED of 1.37×10^2 [MJ/cm²], it is noteworthy to compare it with prior research on semiconductor processes. This becomes particularly intriguing as we contemplate the possibility of integrating the VO₂ resistor directly alongside an NMOS transistor on a single die using a 28 nm technology node. It raises the question of which component will ultimately exert greater influence. Notably, when comparing the VO₂-based devices developed in our work to the 28 nm technological node, Boyd's research on semiconductors (using 300 mm diameter wafers) reports a value of 7.07 [MJ/cm²] [8] for the fab life-cycle stage, as depicted in Figure 6.3.

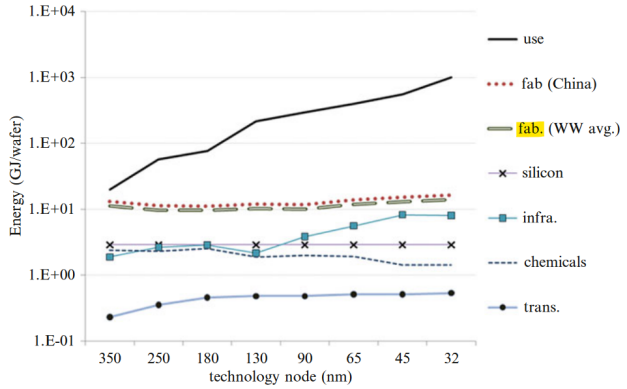


Figure 6.3: Energy use per 300 mm wafer equivalent, by life-cycle stage [8].

Additionally, Krishnan's study, which examines the same wafers as Boyd's, provides a PED value of 4.95 [MJ/cm²] for the semiconductor fabrication [34], as shown in Figure 6.4. Furthermore, the Pirson and al. study investigates the environmental footprint of IC production and highlights node-wise trends based on scientific literature and LCA databases. While this study indicate various values, all of them are lower than the PED of our process. Consequently, it is evident that our total PED value surpasses those of prior studies, indicating the substantial impact associated with the VO₂-based device manufacturing process. This discrepancy is primarily attributed to the use of gold, whereas switching to copper, giving a PED of 1.03 [MJ/cm²] (which will be discussed further in the subsequent section) is closer to the outcomes obtained in the aforementioned studies.

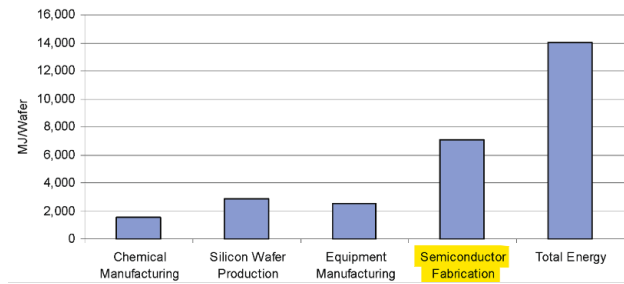


Figure 6.4: Life cycle primary energy requirements [34].

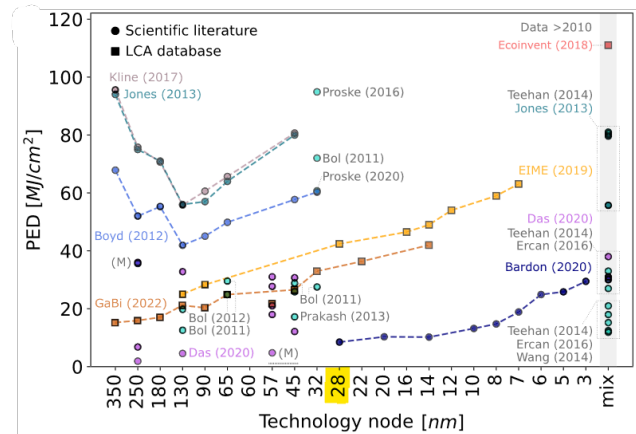


Figure 6.5: PED per cm² in function of the node trends which are derived from an analysis of scientific literature and LCA databases [47].

It is important to note that we have focused on a single impact indicator in this analysis, while there exist numerous other indicators. It is highly probable that the identified hotspot may shift when considering alternative impact indicators. For instance, if we had focused on UPW, the standard cleaning step would have emerged as the prominent contributor as the literature suggests ([14], [6]).

6.2 Alternative process

Change in impact

Considering the objective of the conducted LCA in this work, which aimed to identify an alternative to the aforementioned hotspot, we put forth copper as a potential substitute metal. First, when examining the environmental impact of the alternative process where copper replaces gold, a significant reduction in the PED indicator is observed. This outcome is highly positive and desirable. As depicted in Figure 6.6, the total PED decreases from $1.37 \cdot 10^2$ [MJ/cm²] in the case of gold (and nickel) deposition to 1.03 [MJ/cm²] in the case of copper deposition. This corresponds to a decrease of 99.25%. Focusing on the metallization step, which had the greatest impact due to gold deposition, a significant decrease is evident after switching to copper deposition. Additionally, it is noteworthy that no adhesive layer deposition occurred during the copper process. Figure 6.7 illustrates a substantial 99.78% reduction in the metallization step, with the PED of the inputs decreasing from $1.36 \cdot 10^2$ [MJ/cm²] for the gold (and nickel) deposit to $1.46 \cdot 10^{-2}$ [MJ/cm²] for the copper deposit. In this alternative process the VO2 sputtering step now emerges as the most energy-consuming as can be seen in Table 6.6, because of the inputs, more specifically vanadium, which has a PED of $3.32 \cdot 10^{-1}$ [MJ/cm²]. Furthermore, the equipment utilized in the metallization, thermal oxidation and lithography stages present possibilities for alternative investigation. On top of that, as mentioned in Chapter 5, copper is also more cost-effective, making it advantageous for large-scale manufacturing.

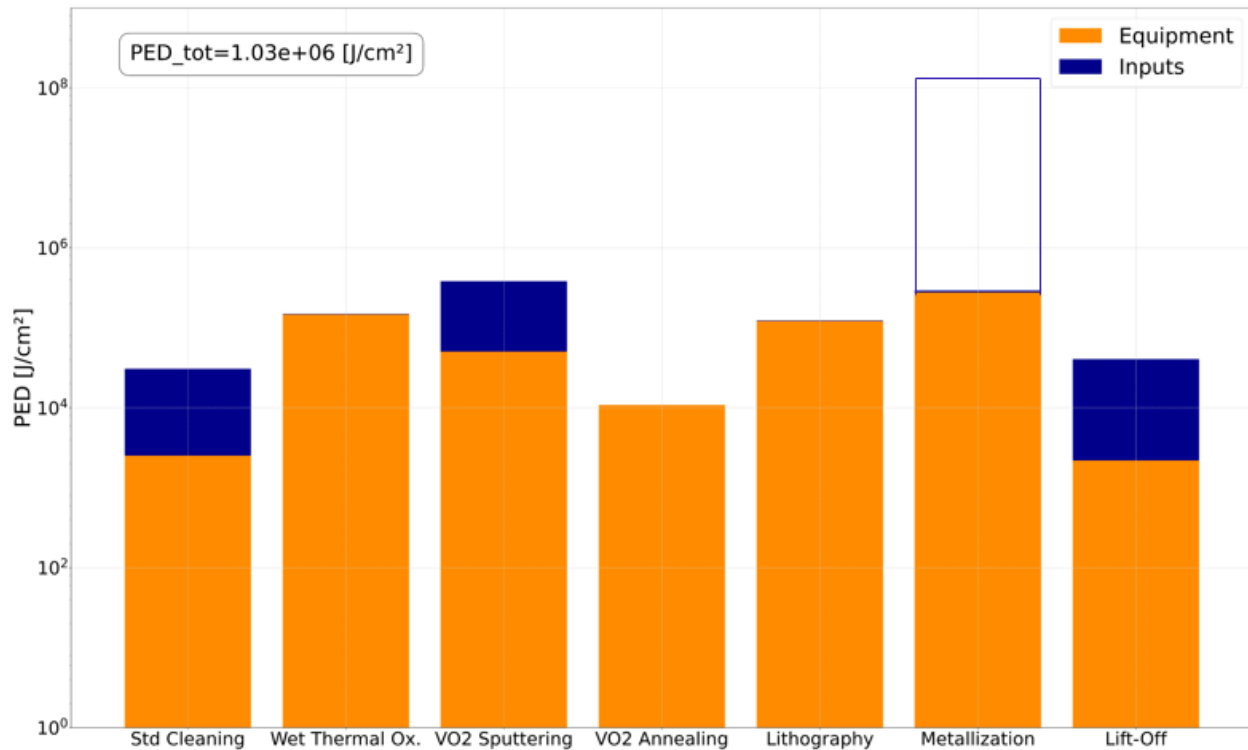
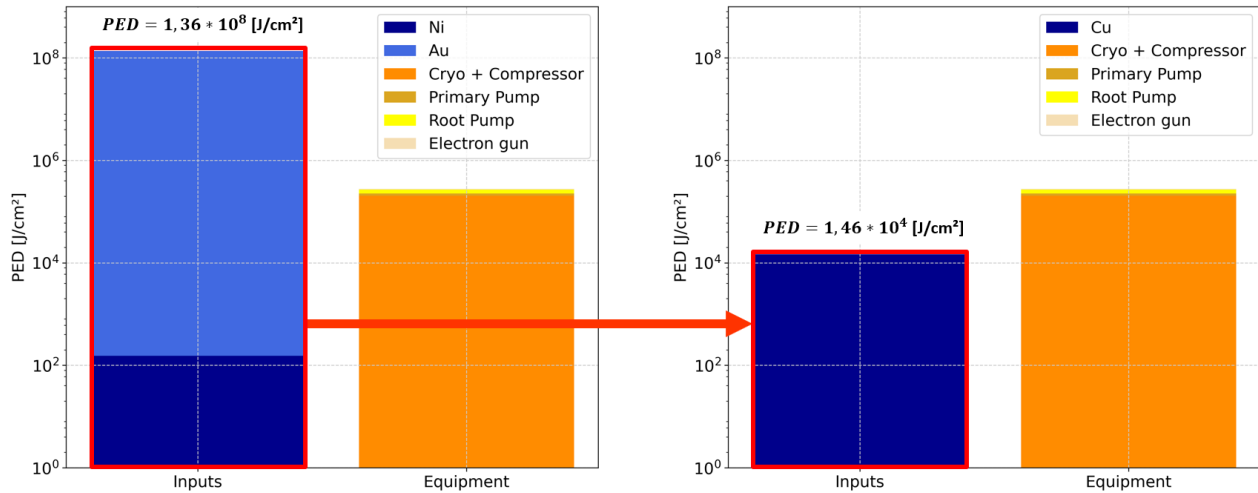


Figure 6.6: PED [J/cm²] of the complete process with copper evaporation, logarithmic scale. The solid line in the graph depicts the PED [J/cm²] for gold (and nickel) evaporation.

PED [MJ/cm ²]	Standard Cleaning	Thermal Oxidation	VO2 Sputtering	VO2 Annealing	Lithography	Metallization	Lift-Off
Inputs	$2.81 \cdot 10^{-2}$	$2.26 \cdot 10^{-3}$	$3.32 \cdot 10^{-1}$	$3.17 \cdot 10^{-5}$	$2.26 \cdot 10^{-3}$	$1.46 \cdot 10^{-2}$	$3.83 \cdot 10^{-2}$
Equipment	$2.52 \cdot 10^{-3}$	$1.47 \cdot 10^{-1}$	$5.02 \cdot 10^{-2}$	$1.08 \cdot 10^{-2}$	$1.21 \cdot 10^{-1}$	$2.78 \cdot 10^{-1}$	$2.19 \cdot 10^{-3}$
PED_{tot}	$3.06 \cdot 10^{-2}$	$1.49 \cdot 10^{-1}$	$3.82 \cdot 10^{-1}$	$1.08 \cdot 10^{-2}$	$1.23 \cdot 10^{-1}$	$2.93 \cdot 10^{-1}$	$4.05 \cdot 10^{-2}$

Table 6.6: PED [MJ/cm²] of the complete process with copper evaporation.Figure 6.7: PED [J/cm²] of the metallization step gold (and nickel, left) versus copper evaporation (right), logarithmic scale.

Change in performance

Comparing exclusively the environmental impact is insufficient. It is essential to consider performance as well. Therefore, we conducted in the second place a comparison between the two processes in terms of performance. We measured the contact resistances, $R_{contact}$, between the respective metal and the semiconductor (VO2), as well as the ratio between the resistance of the semiconductor (VO2) in insulating (R_{ins}) and metallic (R_{met}) states, $\frac{R_{ins}}{R_{met}}$ which determines the size of the NDR zone (as explained in Chapter 5).

In the case of copper deposition, the contact resistance is lower, $R_{contact,25^\circ C}(Cu) = 0.269 [M\Omega]$ compared to $R_{contact,25^\circ C}(Au) = 0.334 [M\Omega]$, indicating that current can flow more easily across the junction, which is desired for electronic components in search of Ohmic contact.

Regarding the relationship between VO2 resistance and temperature, the $\frac{R_{ins}}{R_{met}}$ ratio for copper evaporation is 6614.5, surpassing the ratio of 2025.7 observed for gold evaporation. As a result, the NDR zone is larger for copper evaporation. It is important to note that the NDR zone represents the potential region for oscillations, a wanted behaviour for VO2-based devices, that we desire maximum. By utilizing the measurements conducted on the measurement pads (see Chapter 5, Figure 5.5), we plotted the V-driven characteristics of the VO2 device to visualize the NDR region. Figure 6.8 and 6.9 demonstrates that the NDR zone is significantly greater for copper evaporation, offering a greater zone for the oscillations, nearly eight times larger in size.

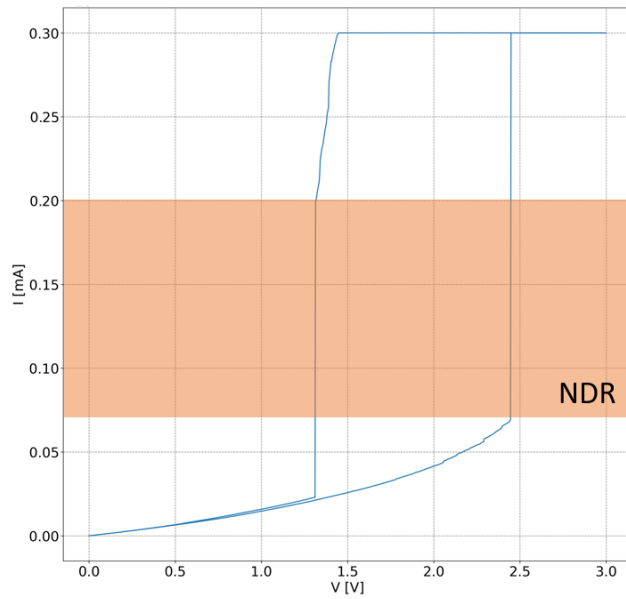


Figure 6.8: V-driven characteristic of the Au/VO₂ device with the current range for spiking regime (in orange, corresponding to the NDR).

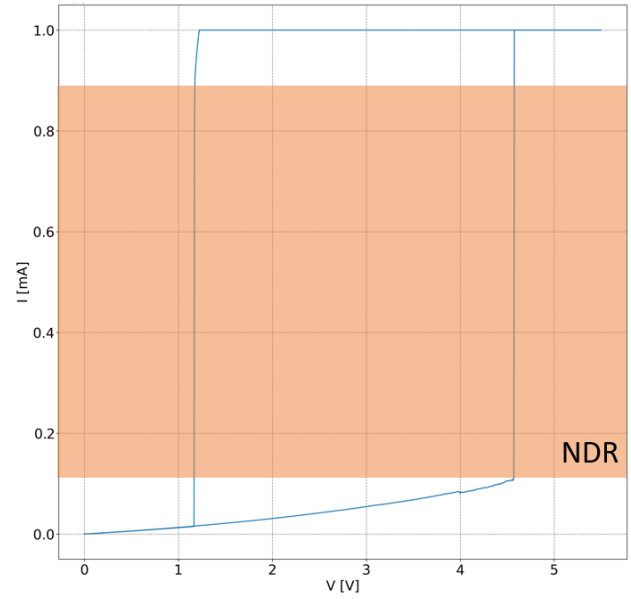


Figure 6.9: V-driven characteristic of the Cu/VO₂ device with the current range for spiking regime (in orange, corresponding to the NDR).

We acknowledge that this comparison is somewhat limited and we recommend further development for a more comprehensive analysis.

Despite being CMOS-compatible¹, copper may not be the optimal substitute for gold.

Copper is known to oxidise, resulting in reduced conductivity and unstable contacts. During performance measurements, we encountered this issue, as illustrated in Figure 6.10. On top of this, copper is known for its easy diffusion and strong interaction with silicon (Si) or SiO₂ which can lead to degradation of electrical performance in microelectronic devices [23]. Typically, a layer of tantalum nitride (TaN) is deposited around copper to prevent this diffusion [26]. Tantalum nitride is estimated to have an EI of approximately 4406 [MJ/kg]. This approximation is derived from the sum of the EI of tantalum (4400 [MJ/kg] [54]) and nitrogen (5.73 [MJ/kg] [4]).

The application of the tantalum nitride layer leads to a 5% increase in total PED, increasing from 1.03 [MJ/cm²] to 1.08 [MJ/cm²] (Figure 6.12). The PED for inputs in the metallization step rises from $1.42 \cdot 10^{-2}$ [MJ/cm²]

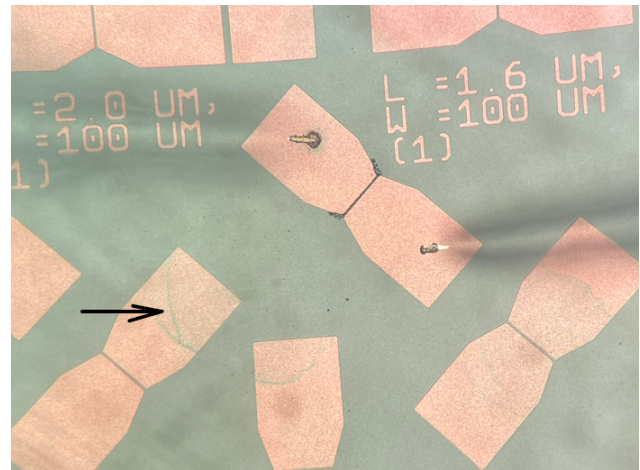


Figure 6.10: The green spot indicated by the arrow in the figure shows the oxidation of copper.

¹CMOS is the process used in the semiconductor industry to manufacture integrated circuits. The performance of CMOS devices can be severely degraded by contaminants that affect the doping of terminals or the performance of electrical gates. Therefore, a CMOS-compatible material does not affect the performance of CMOS devices [38].

to $6.68 \cdot 10^{-2}$ [MJ/cm²], resulting in a 17.8% increase in this particular step (Figure 6.11). The mass of TaN deposited for a thickness of 5 nm was estimated using the same approximation method as employed in calculating the mass of copper (as described in equation 5.1).

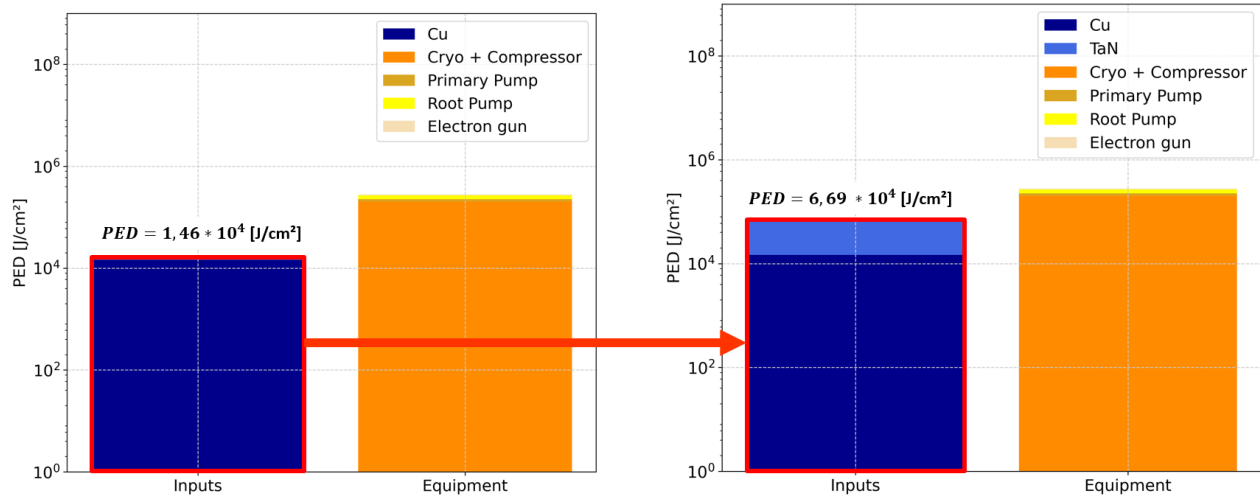


Figure 6.11: PED [J/cm²] of the metallization step copper versus copper and tantalum nitride evaporation, logarithmic scale.

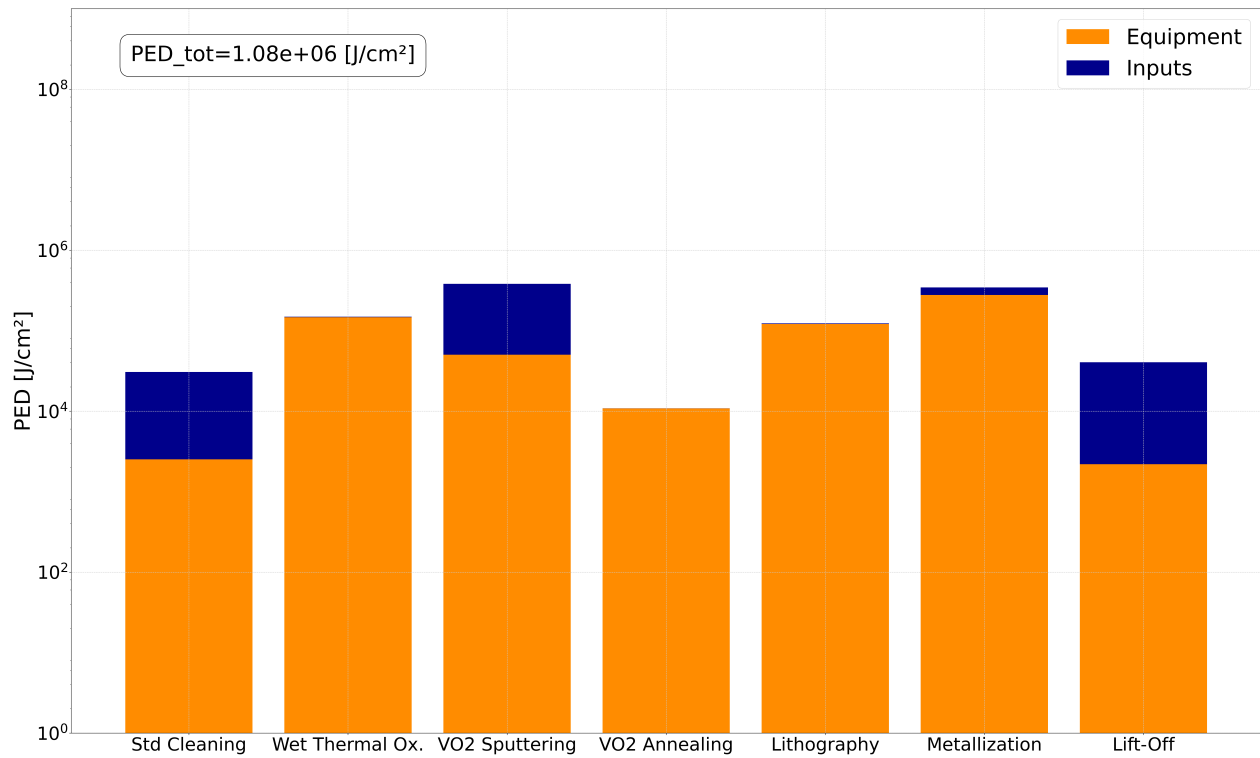


Figure 6.12: PED [J/cm²] of the complete process with copper and tantalum nitride evaporation, logarithmic scale.

6.3 Perspectives

A series of alternatives could be implemented in the process and in the microfabrication laboratory to reduce the overall impact.

Aluminum instead of copper and gold

We discussed the possibility that copper may not be the most optimal substitute for gold. Our initial plan was to deposit aluminum using the Vacotec equipment in the WINFAB cleanroom; however, due to an equipment failure, this could not be accomplished. Aluminum, even with its higher electrical resistivity than copper [35], may be suggested as an alternative to copper and gold, offering a lower EI than gold, 193.5 [MJ/kg] for Al compared to 425,000 [MJ/kg] for Au [4]. In the WINFAB laboratory, aluminum is deposited by Electron Beam Physical Vapour Deposition (EBPVD) (as gold) in the VACOTEC or VST equipment. The VST equipment exhibits lower energy consumption. The amount needed to deposit a 100 nm layer of aluminum is determined using the same method as for gold. Taking into account, as an assumption, that the VST chamber shares the same dimensions as the Vacotec chamber.

$$mass [kg] = Surface [m^2] \cdot thickness [m] \cdot density [kg/m^3] \quad (6.1)$$

with

- Surface = $2lw + 2lh + 2wh$, length (l) = 0.64 [m], width (w) = 0.84 [m], height (h) = 0.66 [m].
- Thickness (Al) = 100 [nm]
- Density (Al) = 2700 [kg/m³]

Although aluminum has a higher EI than copper, its density is lower. This leads to a lower PED for the inputs used in the metallization stage.

This modification results in a reduction of 99.93% in the metallization step's PED, decreasing it from $1.36 \cdot 10^2$ [MJ/cm²] for the gold evaporation to $9.31 \cdot 10^{-2}$ [MJ/cm²] for the aluminum evaporation (Table 6.8). This change involves decreases in both inputs and equipment as shown in Figure 6.13. For a more comprehensive overview of this aluminum evaporation stage, please refer to Section A.10 in Chapter A (appendix), which provides a detailed worksheet.

With its work function of $\phi_{Al} = 4.26$ eV ([37], [40]), aluminum can also establish an Ohmic contact for electrons with the VO₂ layer ($\phi_{VO_2} = 5.12$ eV) similar to copper and gold. Note that aluminum is also CMOS-compatible. You can find the relevant data for the three metals in Table 6.7.

	Au	Cu	Al
EI [MJ/kg]	425,000	98.3	193.5
Density [kg/m³]	19300	8940	2700
PED [MJ/cm²]	$1.36 \cdot 10^2$	$1.46 \cdot 10^{-2}$	$2.17 \cdot 10^{-3}$
Work function ϕ eV	4.95	4.60	4.26
CMOS-compatible	no	yes	yes

Table 6.7: Comparison of gold, copper and aluminum.

PECVD instead of wet thermal oxidation

Another approach to reduce the impact involves the wet thermal oxidation step. It can be potentially replaced by PECVD deposition using the Oxford Plasmalab PECVD equipment. PECVD differs from chemical vapor deposition (CVD) in that it utilizes plasma as the source of activation energy instead of relying on high temperatures. This allows for deposition to occur at significantly lower temperatures since the plasma provides the necessary energy, eliminating the reliance on thermal energy. Within the PECVD chamber, there is a flat platform where the substrate is placed and can be heated if required. Positioned on top of the chamber is a gas input, which is responsible for generating the plasma. The plasma, in turn, chemically reacts with the substrate to deposit the thin film. Additionally, the chamber features a high voltage radio frequency (RF) electrical connection linked to an electrode at the top. This RF connection supplies the power necessary to create the plasma. PECVD employs energized atoms, plasma, to carry out a chemical reaction on the surface of the substrate, resulting in the deposition of a thin film. In short, in the PECVD system, a mixture of gases is utilized to generate the plasma responsible for depositing the film onto the substrate [49]. For further details regarding the application of the PECVD technique, please refer to Chapter D (appendix).

PECVD presents several advantages over wet thermal oxidation. First, PECVD allows for precise control over layer thickness. During PECVD, a 400 nm layer is directly deposited on the wafer. In contrast, wet thermal oxidation involves the attack of oxygen atoms on Si, creating SiO₂ bonds, resulting in only 400 nm of the 380 μm of the wafer being converted into a SiO₂ layer. Furthermore, PECVD enables deposition on heat-sensitive substrates, whereas wet thermal oxidation necessitates high temperatures that may potentially damage certain substrates. Nevertheless, wet thermal oxidation possesses its own set of advantages. It offers high-quality oxide and a clean interface between the oxide and the substrate. Additionally, wet thermal oxidation eliminates the need for potentially hazardous reactive gases, unlike PECVD which employs silane (SiH₄).

By implementing this change, the PED for this particular step is reduced significantly (Figure 6.14), decreasing from $1.49 \cdot 10^{-1}$ [MJ/cm²] for wet thermal oxidation to $2.63 \cdot 10^{-2}$ [MJ/cm²] for PECVD (Table 6.8). This corresponds to a reduction of 82.35%. For a more comprehensive overview of this PECVD stage, please refer to Section A.9 in Chapter A (appendix), which provides a detailed worksheet.

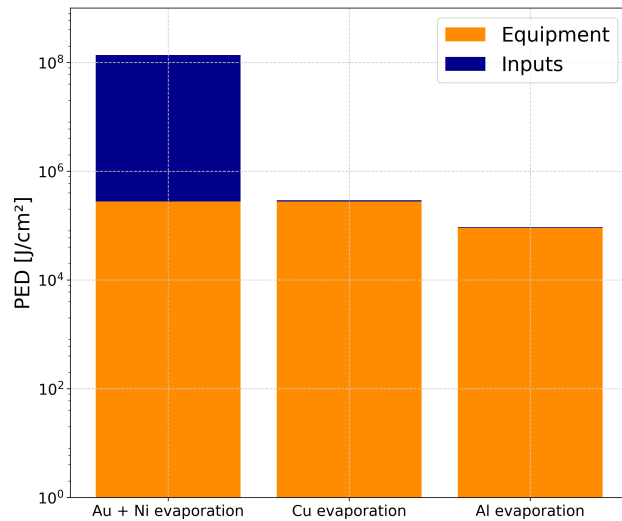


Figure 6.13: PED [J/cm²] of the metallization step for gold, copper and aluminum evaporation, logarithmic scale.

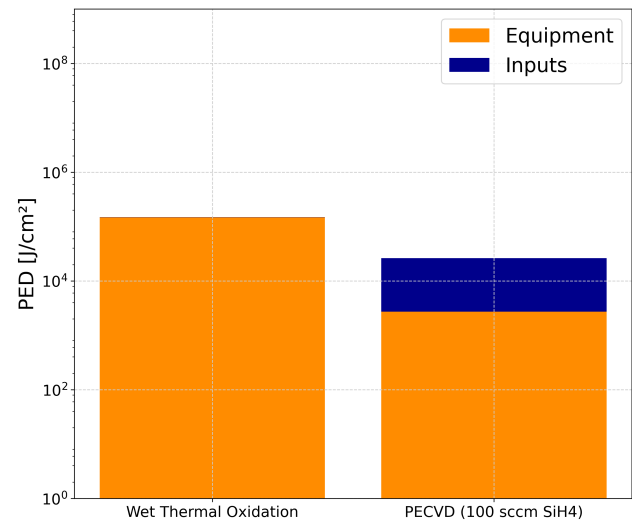


Figure 6.14: PED [J/cm²] of the oxidation step, logarithmic scale. Wet Thermal Oxidation versus PECVD.

Please note that in the case of the PECVD technique, there exist multiple recipes. The comparison conducted above utilized a recipe involving 100 sccm of SiH₄. However, an alternative recipe with a usage of 1000 sccm of SiH₄ exists, and with this particular recipe, the PECVD process becomes more energy-intensive compared to wet thermal oxidation as shown in Figure 6.15. During our collaboration with CEA-Leti, we had discussions revealing that when the equipment is fully utilized (at 100% capacity), thermal oxidation has the least impact on the criterion being studied compared to PECVD (even with a flow of SiH₄ between 100 and 500 sccm). Nevertheless, it is not recommended to employ thermal oxidation if the total capacity is not utilized. Hence, this PECVD alternative is still under consideration.

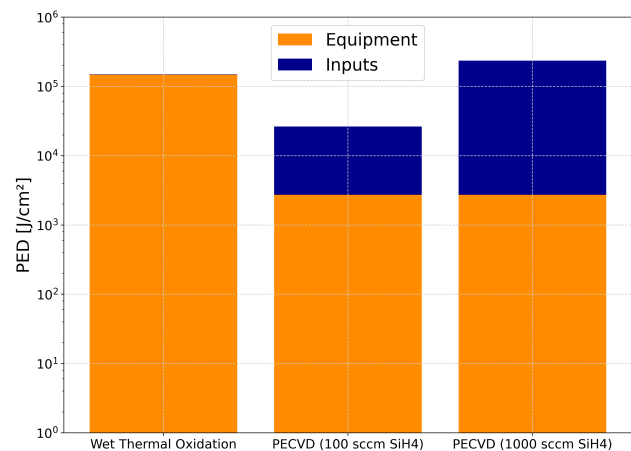


Figure 6.15: PED [J/cm²] of the wet thermal oxidation vs PECVD (100 sccm) vs PECVD (1000 sccm), logarithmic scale.

Aluminum and PECVD

Consequently, by implementing these two changes to the initial process, we observe a substantial reduction of 99.48% in the overall impact, from $1.37 \cdot 10^2$ [MJ/cm²] to $7.07 \cdot 10^{-1}$ [MJ/cm²] as shown in Figure 6.16 (and its corresponding values in Table 6.8).

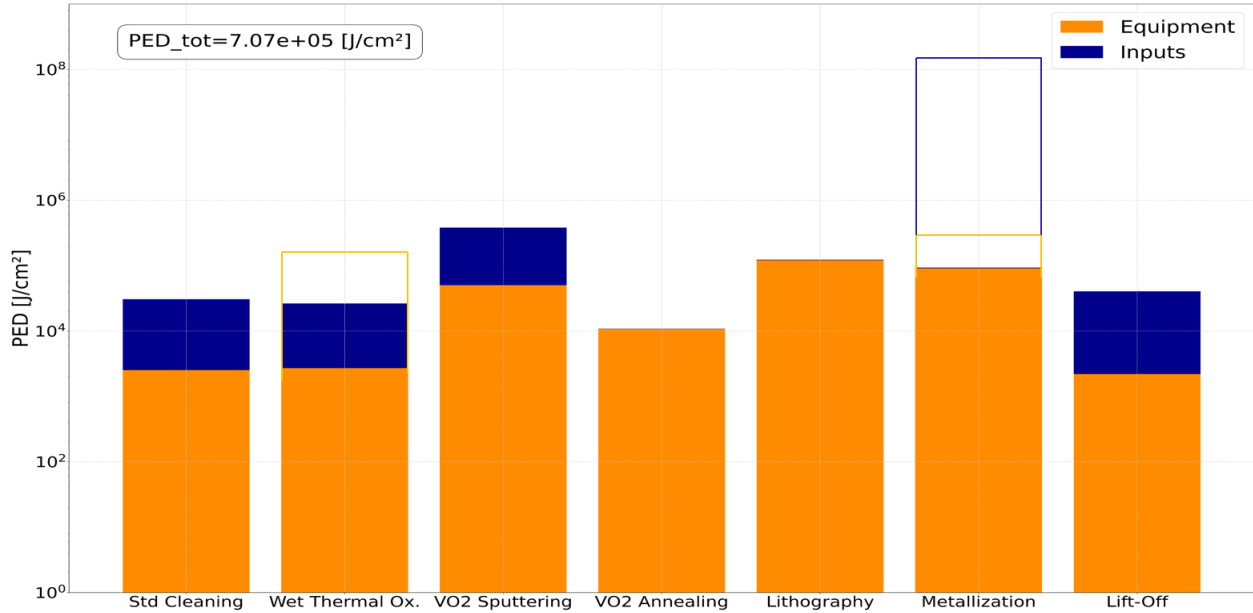


Figure 6.16: PED [J/cm²] of the complete process with aluminium evaporation and PECVD. The solid line in the graph depicts the PED [J/cm²] for gold (and nickel) evaporation and wet thermal oxidation.

PED [MJ/cm ²]	Standard Cleaning	PECVD	VO2 Sputtering	VO2 Annealing	Lithography	Metallization	Lift-Off
Inputs	$2.81 \cdot 10^{-2}$	$2.36 \cdot 10^{-2}$	$3.32 \cdot 10^{-1}$	$3.17 \cdot 10^{-5}$	$2.26 \cdot 10^{-3}$	$2.17 \cdot 10^{-3}$	$3.83 \cdot 10^{-2}$
Equipment	$2.52 \cdot 10^{-3}$	$2.71 \cdot 10^{-3}$	$5.02 \cdot 10^{-2}$	$1.08 \cdot 10^{-2}$	$1.21 \cdot 10^{-1}$	$9.10 \cdot 10^{-2}$	$2.19 \cdot 10^{-3}$
PED_{tot}	$3.06 \cdot 10^{-2}$	$2.63 \cdot 10^{-2}$	$3.82 \cdot 10^{-1}$	$1.08 \cdot 10^{-2}$	$1.23 \cdot 10^{-1}$	$9.31 \cdot 10^{-2}$	$4.05 \cdot 10^{-2}$

Table 6.8: PED [MJ/cm²] of the complete process with aluminium evaporation and PECVD.

The suggested enhancements outlined here have yet to be put into action, but they hold potential as future avenues for improvement. Since the proposed process has not undergone testing, we cannot accurately predict its performance. Nevertheless, it is expected that this new approach will effectively lower overall consumption.

Alternatives in microfabrication laboratory

In addition to minimizing the impact of the process itself, there are available alternatives within the laboratory that can contribute to reducing its environmental footprint. Two existing alternatives in WINFAB can serve as valuable sources of inspiration for other microfabrication laboratories. First, the acetone utilized during the lift-off stage undergoes filtration to enable its reuse in subsequent lift-off processes. Secondly, liquid nitrogen is delivered to WINFAB and needs to be converted into a gaseous state before being introduced into the various equipment.

Instead of requiring additional equipment for this conversion process, the extracted heat from other operational equipment such as pumps is utilized to vaporize the nitrogen, which is then transported through a pipeline in the equipment area.

Chapter 7

Conclusion

This study aimed to evaluate the performance and environmental impacts of a microfabricated device, specifically a VO₂-based device. A cradle-to-gate Life Cycle Assessment (LCA) was conducted to assess the environmental impact of the VO₂ device using the Primary Energy Demand (PED) indicator, spanning from raw material extraction to the exit of the WINFAB laboratory. The objective was to identify the hotspot and propose an alternative with lower energy consumption, while evaluating its impact on device performance. It's important to note that this study was conducted at a university research laboratory where the equipment is dedicated to different processes and may therefore present contamination problems.

To begin, the research and articles related to the device itself and LCA were reviewed in the Chapter 2. Chapter 3 provided a detailed presentation of the complete process, including the inputs and equipment used. The primary objective of this work was on conducting an LCA of the inputs and equipment used in the process (Chapter 4). The chosen impact indicator for this study was the Primary Energy Demand (PED) measured in [MJ/cm²]. The PED was calculated based on Cumulative Energy Demand (CED) and Energy Intensity (EI), and certain assumptions were made during the calculation. At first, Boyd's work [8] served as the basis for all inputs EI values. However, subsequent investigations brought to light the underestimation in her work of metal values. As a result, Boyd's work was utilized for all inputs except metals, for which the values were sourced from the EduPack software [4]. Another assumption involved applying the capacity factor measured on the KOYO furnace during the wet thermal oxidation step, revealing that the actual energy consumption of the equipment differed from the datasheet. Ultimately, the total PED was determined to be $1.37 \cdot 10^2$ [MJ/cm²], with the metallization step, primarily due to the use of gold, accounting for 99.3% of the PED ($1.36 \cdot 10^2$ [MJ/cm²]).

The second part of this work proposed an alternative to address the identified hotspot, namely the gold deposition, in order to reduce the overall environmental impact. Copper deposition was suggested as an alternative, given its lower EI (98.3 [MJ/kg] compared to 425,000 [MJ/kg]). This substitution resulted in a 99.25% reduction, with the PED decreasing from $1.37 \cdot 10^2$ [MJ/cm²] for gold evaporation to 1.03 [MJ/cm²] for copper evaporation. In this new process, the VO₂ sputtering stage became the dominant contributor to environmental impact. Furthermore, it was essential to ensure that reducing the environmental impact did not compromise device performance. Performance measurements were conducted on two wafers, one with gold evaporation and the other with copper evaporation. The measurements included assessing Ohmic contact for the two metal deposits and

observing the characteristic IV transitions of VO₂-based devices. Additional performance metrics, such as $R_{contact}$ and the ratio between R_{ins}/R_{met} (related to the size of the NDR zone), were also recorded. The results indicated that for both depositions, an Ohmic contact and the characteristic IV transitions were observed. Additionally, copper evaporation yielded a lower $R_{contact}$, indicating improved current flow across the junction. Moreover, the larger R_{ins}/R_{met} ratio for copper evaporation resulted in a larger NDR zone, which corresponds to the potential region for oscillations that we desire maximum.

However, it is worth noting that the copper solution might not be the optimal choice due to copper's diffusion properties and tendency to oxidize, which would require a layer of tantalum nitride for protection. Although the alternative proposed in this study is not ideal, it serves as a source of ideas and encourages open-mindedness among readers. Aluminum has also been suggested as an alternative material for the metallization step. An additional proposed alternative involves substituting the wet thermal oxidation method with the Plasma Enhanced Chemical Vapor Deposition (PECVD) technique. This alternative process, conducted solely in a virtual setting to provide an estimation of its impact, achieves a substantial reduction of 99.48% in the total PED, ranging from $1.37 \cdot 10^2$ [MJ/cm²] to $7.07 \cdot 10^{-1}$ [MJ/cm²].

Additionally, it is acknowledged that the absolute precision of the results is limited.

In conclusion, this work highlights the ongoing and iterative nature of LCA, where hotspots are identified, addressed, and new ones may emerge. LCAs play a crucial role in reducing the environmental impact of microelectronics. Conducting such studies prior to the market launch of new devices is essential to avoid creating products with significant environmental footprints. The hope is that this work will open new doors, broaden perspectives, and foster greater collaboration among industries, platforms, and researchers, leading to a more ecologically responsible future for microelectronics.

Appendix A

Detailed Worksheet (Inventory)

A.1 Standard Cleaning (10 wafers)

Inputs	EE [MJ/kg]	Mass [kg]	PED [MJ/cm ²]
H ₂ SO ₄ (l)	0.04	3.26	2.86 · 10 ⁻⁴
H ₂ O ₂ (l)	12	10.01	2.66 · 10 ⁻²
HF 2% (l)	18	0.04	1.36 · 10 ⁻³
DI water (l)	0	200	0
Equipment	Power [W]	Time	PED [MJ/cm ²]
Heaters for the baths	400	50 minutes, 15 seconds	1.52 · 10 ⁻³
Rinser-dryer	3300	24 seconds	9.99 · 10 ⁻⁴
PED_{tot}			3.06 · 10 ⁻²

Table A.1: Detailed worksheet of the standard cleaning step.

A.2 Wet Thermal Oxidation (20 wafers)

Inputs	EE [MJ/kg]	Mass [kg]	PED [MJ/cm ²]
N ₂ (g)	0.66	0.79	5.75 · 10 ⁻⁴
H ₂ (g)	8.5	0.04	3.79 · 10 ⁻⁴
O ₂ (g)	1.8	0.66	1.31 · 10 ⁻³
Equipment	Power [W]	Time	PED [MJ/cm ²]
Furnace heaters (KOYO)	17100	3 hours, 47 minutes	1.47 · 10 ⁻¹
PED_{tot}			1.49 · 10 ⁻¹

Table A.2: Detailed worksheet of the wet thermal oxidation step.

A.3 VO2 Sputtering (1 wafer)

Inputs	EE [MJ/kg]	Mass [kg]	PED [MJ/cm ²]
O ₂ (g)	1.8	$2.25 \cdot 10^{-4}$	$8.88 \cdot 10^{-6}$
V(s)	3715	$4.07 \cdot 10^{-3}$	$3.32 \cdot 10^{-1}$
Ar(g)	3.6	$4.71 \cdot 10^{-3}$	$3.72 \cdot 10^{-4}$
Equipment	Power [W]	Time	PED [MJ/cm ²]
Primary Pump (Load chamber)	450	27 minutes, 20 seconds + 15 minutes	$1.44 \cdot 10^{-2}$
Turbo Pump (Load chamber)	110	27 minutes, 20 seconds + 15 minutes	$3.52 \cdot 10^{-3}$
Primary Pump (Main chamber)	450	27 minutes, 20 seconds + 15 minutes	$1.44 \cdot 10^{-2}$
Turbo Pump (Main chamber)	420	27 minutes, 20 seconds + 15 minutes	$1.35 \cdot 10^{-2}$
Transfer Valve	12.18	27 minutes, 20 seconds	$2.52 \cdot 10^{-4}$
DC Source	200	27 minutes, 20 seconds	$4.14 \cdot 10^{-3}$
PED_{tot}			$3.82 \cdot 10^{-1}$

Table A.3: Detailed worksheet of the VO2 sputtering step.

A.4 VO2 annealing (20 wafers)

Inputs	EE [MJ/kg]	Mass [kg]	PED [MJ/cm ²]
Ar(g)	3.6	$8.03 \cdot 10^{-3}$	$3.17 \cdot 10^{-5}$
Equipment	Power [W]	Time	PED [MJ/cm ²]
Furnace heaters	2500	1 hour, 30 minutes	$8.51 \cdot 10^{-3}$
Pump	400	2 hours, 30 minutes	$2.27 \cdot 10^{-3}$
PED_{tot}			$1.08 \cdot 10^{-2}$

Table A.4: Detailed worksheet of the VO2 annealing step.

A.5 Lithography (1 wafer)

Inputs	EE [MJ/kg]	Mass [kg]	PED [MJ/cm ²]
DI water (l)	0	0.26	0
HMDS	3.1	$9.63 \cdot 10^{-4}$	$6.54 \cdot 10^{-5}$
Photoresist AZnLof5510 (Novolac)	3.1	$3.75 \cdot 10^{-3}$	$2.55 \cdot 10^{-4}$
Developer AZ726MIF (TMAH)	3.1	$1.27 \cdot 10^{-2}$	$8.62 \cdot 10^{-4}$
Acetone	3.1	$7.90 \cdot 10^{-3}$	$5.37 \cdot 10^{-4}$
Methanol	3.1	$7.92 \cdot 10^{-3}$	$5.38 \cdot 10^{-4}$
Equipment	Power [W]	Time	PED [MJ/cm ²]
LPIII Oven (HMDS)	1200	23 minutes	$2.09 \cdot 10^{-2}$
Suss Gamma (Robotic arm, oven, coater)	7000	approx. 6 minutes	$3.18 \cdot 10^{-2}$
Suss MA6 (UV lamp)	1000	1 hour, 30 minutes	$6.81 \cdot 10^{-2}$
PED_{tot}			$1.23 \cdot 10^{-1}$

Table A.5: Detailed worksheet of the lithography step.

A.6 Metallization - Gold Evaporation (4 wafers)

Inputs	EE [MJ/kg]	Mass [kg]	PED [MJ/cm ²]
<i>Au</i> (s)	425000	$5.85 \cdot 10^{-2}$	$1.36 \cdot 10^2$
<i>Ni</i> (s)	206.5	$1.35 \cdot 10^{-4}$	$1.53 \cdot 10^{-4}$
Equipment	Power [W]	Time	PED [MJ/cm ²]
Cryo pump + compressor	6950	4 hours, 30 minutes	$2.04 \cdot 10^{-1}$
Primary pump	700	4 hours, 30 minutes	$2.06 \cdot 10^{-2}$
Root pump	1500	4 hours, 30 minutes	$4.40 \cdot 10^{-2}$
Electron gun	3000	30 minutes	$9.79 \cdot 10^{-3}$
<i>PE</i>_{tot}			$1.36 \cdot 10^2$

Table A.6: Detailed worksheet of the gold evaporation step.

A.7 Lift-off (1 wafer)

Inputs	EE [MJ/kg]	Mass [kg]	PED [MJ/cm ²]
DI water (l)	0	0.15	0
Acetone	3.1	0.55	$3.76 \cdot 10^{-2}$
Methanol	3.1	$9.90 \cdot 10^{-3}$	$6.73 \cdot 10^{-4}$
Equipment	Power [W]	Time	PED [MJ/cm ²]
Waterbath with ultrasound vibration	580	5 minutes	$2.19 \cdot 10^{-3}$
<i>PE</i>_{tot}			$4.05 \cdot 10^{-2}$

Table A.7: Detailed worksheet of the lift-off step.

A.8 Metallization - Copper Evaporation (4 wafers)

Inputs	EE [MJ/kg]	Mass [kg]	PED [MJ/cm ²]
<i>Cu</i> (s)	98.3	$2.71 \cdot 10^{-2}$	$1.46 \cdot 10^{-2}$
Equipment	Power [W]	Time	PED [MJ/cm ²]
Cryo pump + compressor	6950	4 hours, 30 minutes	$2.04 \cdot 10^{-1}$
Primary pump	700	4 hours, 30 minutes	$2.06 \cdot 10^{-2}$
Root pump	1500	4 hours, 30 minutes	$4.40 \cdot 10^{-2}$
Electron gun	3000	30 minutes	$9.79 \cdot 10^{-3}$
<i>PE</i>_{tot}			$2.93 \cdot 10^{-1}$

Table A.8: Detailed worksheet of the copper evaporation step.

A.9 PECVD (3 wafers)

Inputs	EE [MJ/kg]	Mass [kg]	PED [MJ/cm ²]
$N_2(g)$	0.66	$1.19 \cdot 10^{-2}$	$5.73 \cdot 10^{-5}$
SiH_4 5%(g)	2321	$1.37 \cdot 10^{-3}$	$2.32 \cdot 10^{-2}$
$N_2O(g)$	193.5	$1.32 \cdot 10^{-2}$	$2.98 \cdot 10^{-4}$
Equipment	Power [W]	Time	PED [MJ/cm ²]
RF plasma	30	9 minutes, 30 seconds	$7.19 \cdot 10^{-5}$
Pump	1100	9 minutes, 30 seconds	$2.64 \cdot 10^{-3}$
PED_{tot}			$2.63 \cdot 10^{-2}$

Table A.9: Detailed worksheet of the PECVD alternative.

A.10 Metallization - Aluminum evaporation (16 wafers - VST)

Inputs	EE [MJ/kg]	Mass [kg]	PED [MJ/cm ²]
$Al(s)$	193.5	$8.18 \cdot 10^{-3}$	$2.17 \cdot 10^{-3}$
Equipment	Power [W]	Time	PED [MJ/cm ²]
Heater for the water	9750	3 hours	$8.09 \cdot 10^{-2}$
Primary pump	440	3 hours	$3.74 \cdot 10^{-3}$
Turbo Pump	750	3 hours	$6.38 \cdot 10^{-3}$
Electron gun	2000	3 hours	$1.70 \cdot 10^{-2}$
PED_{tot}			$9.31 \cdot 10^{-2}$

Table A.10: Detailed worksheet of the aluminum evaporation in VST alternative.

Appendix B

PEL103 measuring device.

The positioning of the PEL103 measuring device involves placing loops around the cables to capture the currents, while connecting the clamps to the ferrules as shown in Figure B.1.

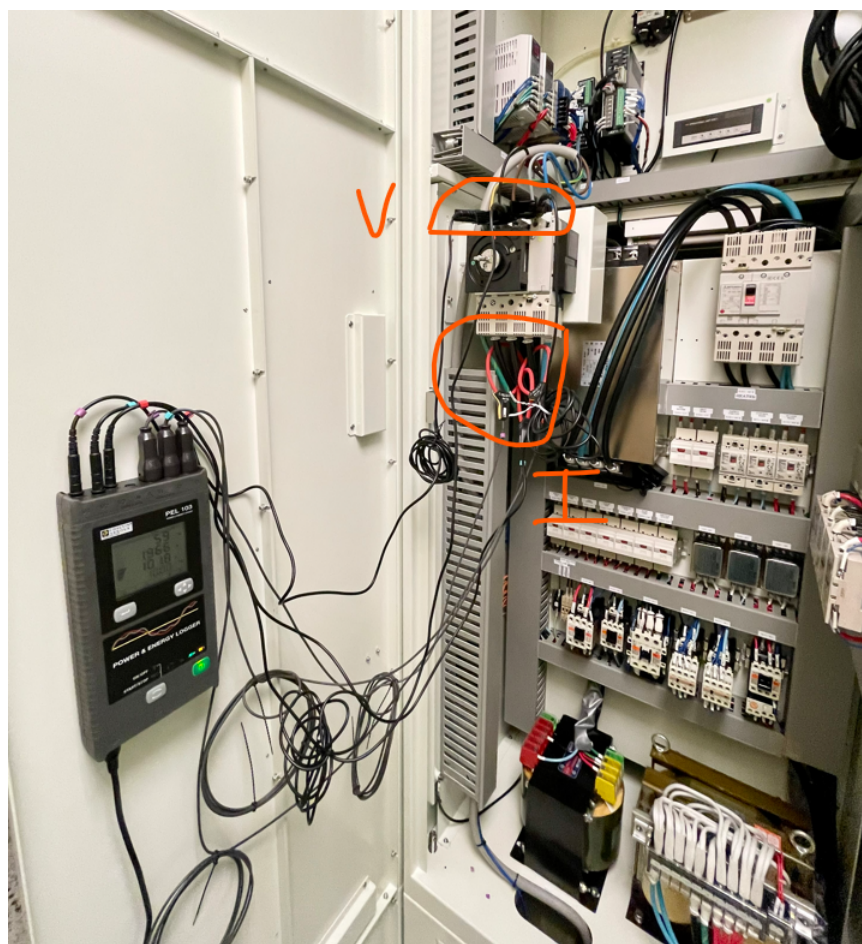
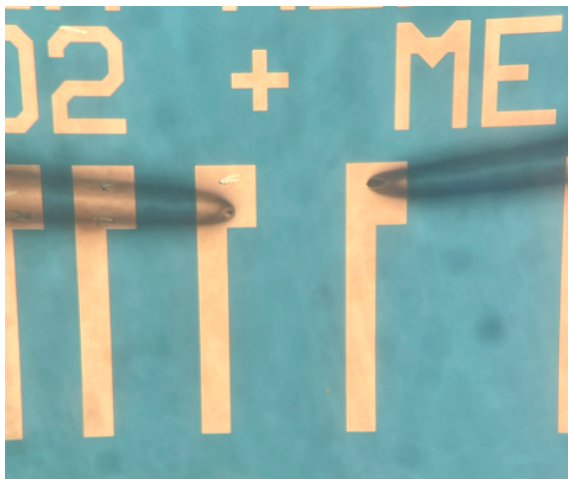


Figure B.1: Positioning of the PEL103 measuring device.

Appendix C

VO₂ appearance between insulator and metallic state.



(a) VO₂ as insulator, 25°C.



(b) VO₂ as metal, 110°C.

Figure C.1: VO₂ appearance.

Appendix D

PECVD

To utilize PECVD, the following steps are typically followed [49]:

1. Chamber Preparation: Initially, the chamber is evacuated using a mechanical pump to establish a clean deposition environment.
2. Gas Introduction: The desired gases are introduced into the chamber.
3. Pressure Stabilization: Within a short duration, typically less than a minute, the pressure inside the chamber is adjusted and stabilized (around 1mTorr).
4. High Voltage Application: The high voltage is applied to the chamber electrode, resulting in the ionization of the gas molecules. This ionization process enhances the chemical reactivity of the source gas molecules.
5. Thin Film Deposition: The chemically reactive gas molecules then combine to form a thin layer of material on the substrate. The film grows consistently, allowing for the achievement of a desired thickness by running the process for a specific duration.
6. Deposition Termination: To cease the deposition of the thin film, the RF voltage is turned off, and the gas flow is stopped.
7. Chamber Evacuation: Once the thin film deposition is complete, the chamber is pumped down again to remove all gases and byproducts generated during the deposition process.
8. Pressure Equalization: The chamber is filled with nitrogen until the pressure inside matches the ambient room pressure.
9. Chamber Opening and Sample Removal: Finally, the chamber can be safely opened, and the sample with the deposited thin film can be extracted.

I hereby declare that I have used artificial intelligence tools such as ChatGPT as authorised by the EPL to assist with writing (correction or revision of texts, source of inspiration, etc.).

Bibliography

- [1] Agence de la transition écologique ADEME. *L'analyse du cycle de vie*. URL: <https://expertises.ademe.fr/economie-circulaire/consommer-autrement/passer-a-laction/dossier/lanalyse-cycle-vie/quest-lacv>.
- [2] Paul A. Anderson. "The Work Function of Copper". In: *Phys. Rev.* 76 (3 Aug. 1949), pp. 388–390. DOI: 10.1103/PhysRev.76.388. URL: <https://link.aps.org/doi/10.1103/PhysRev.76.388>.
- [3] Paul A. Anderson. "Work Function of Gold". In: *Phys. Rev.* 115 (3 Aug. 1959), pp. 553–554. DOI: 10.1103/PhysRev.115.553. URL: <https://link.aps.org/doi/10.1103/PhysRev.115.553>.
- [4] ANSYS, Inc., Cambridge, UK. *Ansys Granta EduPack*.
- [5] Chauvin Arnoux. *PEL103 POWER-ENERGY LOGGER*. URL: https://catalog.chauvin-arnoux.com/fr_fr/pel103-power-energy-logger.html.
- [6] Ingwild Baudry. "Caractérisation des process de fabrication microélectroniques pour l'éco-conception des futures technologies (partenaire industriel STMicroelectronics)". Theses. Université de Grenoble, Oct. 2013. URL: <https://theses.hal.science/tel-00957329>.
- [7] Noémie Bidoul et al. "Static and Dynamic Stochastic Analysis of a Temperature-Sensitive VO₂ Spiking Neuron". May 2023.
- [8] Sarah Boyd. *Life-Cycle Assessment of Semiconductors*. Mar. 2011, pp. 1–226. ISBN: 978-1-4419-9987-0. DOI: 10.1007/978-1-4419-9988-7.
- [9] James Edward Hoffmann - Britannica. *gold processing*. URL: <https://www.britannica.com/technology/gold-processing/Refining>.
- [10] Lanli Chen et al. "Exploring the work function variability and structural stability of VO₂ (1 1 0) surface upon noble metal (Ag, Au, Pt) adsorption and incorporation". In: *Applied Surface Science* 450 (Apr. 2018). DOI: 10.1016/j.apsusc.2018.04.197.
- [11] Aurelian Crunteanu et al. "Electric field-assisted metal insulator transition in vanadium dioxide (VO₂) thin films: Optical switching behavior and anomalous far-infrared emissivity variation". In: *Proc. SPIE 9364, Oxide-based Materials and Devices VI, pp.93640J1-J11 edited by Ferechteh H. Teherani, David C. Look, David J. Rogers* 9364 (Apr. 2015), 93640J1–J11. DOI: 10.1117/12.2076260.
- [12] Aurelian Crunteanu et al. "Voltage- and current-activated metal-insulator transition in VO₂-based electrical switches: A lifetime operation analysis". In: *Science and Technology of Advanced Materials* 11 (Dec. 2010), p. 065002. DOI: 10.1088/1468-6996/11/6/065002.

-
- [13] Marc Currie et al. "Asymmetric hysteresis in vanadium dioxide thin films". In: *Optical Materials Express* 9 (Sept. 2019). DOI: 10.1364/OME.9.003717.
- [14] Thibault P. Delhaye et al. "Bottom-Up Life-Cycle Assessment of MEMS Piezoresistive Pressure Sensors." In: *Proceedings, IEEE2021* (Aug. 2021), pp. 1–6. DOI: 10.1109/dtip54218.2021.9568683.
- [15] Liqiu Deng, Callie Babbitt, and Eric Williams. "Economic-balance hybrid LCA extended with uncertainty analysis: Case study of a laptop computer". In: *Journal of Cleaner Production - J CLEAN PROD* 19 (July 2011), pp. 1198–1206. DOI: 10.1016/j.jclepro.2011.03.004.
- [16] *Effet tunnel*. URL: https://fr.wikipedia.org/wiki/Effet_tunnel.
- [17] Electrical4u. *Work Function: Equation and Relation To Threshold Frequency*. 2020. URL: <https://www.electrical4u.com/work-function/>.
- [18] happ.e by ENGIE. *QUELLE EST LA CONSOMMATION ÉLECTRIQUE D'UN PC ?* 2022. URL: <https://www.happ-e.fr/actualites/les-eco-gestes/quelle-est-consommation-electrique-dun-pc>.
- [19] Cogen Europe. *EU Primary Energy Factor for Electricity: key to ensure well-informed choices, achieve real energy savings and reduce consumer energy bills*. URL: https://www.cogeneurope.eu/images/2017_05_26_COGEN_Europe_Primary_Energy_Factor_Position.pdf.
- [20] Shereen Farhana. "Transfer Length Measurements For Different Metallization Options And Processing Of Gallium Tin Zinc Oxide (Gszo) Tfts". Theses. North Carolina A andT State University, 2011. URL: <https://digital.library.ncat.edu/theses/31>.
- [21] fournisseurs-electricite.com. *Consommation PC et ordinateur portable, allumé ou pas*. 2023. URL: <https://www.fournisseurs-electricite.com/guides/consommation/ordinateur>.
- [22] Sami Franssila. "Introduction to Microfabrication". In: *Introduction to Microfabrication* (Nov. 2010). DOI: 10.1002/9781119990413.
- [23] Nicole Fréty et al. "Copper Diffusion Into Silicon Substrates Through TaN and Ta/TaN Multilayer Barriers". In: *Journal of Phase Equilibria and Diffusion* 27 (Dec. 2006), pp. 590–597. DOI: 10.1007/BF02736560.
- [24] M. Garcia Bardon et al. "DTCO including Sustainability: Power-Performance-Area-Cost-Environmental score (PPACE) Analysis for Logic Technologies". In: *2020 IEEE International Electron Devices Meeting (IEDM)*. 2020, pp. 41.4.1–41.4.4. DOI: 10.1109/IEDM13553.2020.9372004.
- [25] gtuttle.net. "Contact resistance and TLM measurements". PowerPoint Presentation. 2012. URL: https://gtuttle.net/fabrication/topics/tlm_measurements.pdf.
- [26] Thermo Fisher Scientific Inc. *Nitride de tantale, 99,5 % (métaux)*, Thermo Scientific Chemicals. 2023. URL: <https://www.fishersci.fr/shop/products/tantalum-nitride-99-5-metals-basis-thermo-scientific/11302188>.
- [27] Organisation internationale de normalisation ISO. *ISO 14040:2006 Management environnemental — Analyse du cycle de vie — Exigences et lignes directrices*. URL: <https://www.iso.org/fr/standard/38498.html>.
- [28] Organisation internationale de normalisation ISO. *ISO 14040:2006 Management environnemental — Analyse du cycle de vie — Principes et cadre*. URL: <https://www.iso.org/fr/standard/37456.html#:~:text=L'ISO%5C%2014040%5C%3A2006%5C%20traite,de%5C%20chacune%5C%20de%5C%20ses%5C%20phases..>

- [29] Concepción Jiménez-González, Seungdo Kim, and Michael Overcash. "Methodology for Developing Gate-to-Gate Life Cycle Information". In: *The International Journal of Life Cycle Assessment* 5 (May 2000), pp. 153–159. DOI: 10.1007/BF02978615.
- [30] Yujie Ke et al. "Vanadium Dioxide: Vanadium Dioxide: The Multistimuli Responsive Material and Its Applications (Small 39/2018)". In: *Small* 14 (Sept. 2018). DOI: 10.1002/smll.201870178.
- [31] Gil-Ho Kim et al. "Conductance Control in VO₂ Nanowires by Surface Doping with Gold Nanoparticles". In: *ACS applied materials and interfaces* 6 (Aug. 2014). DOI: 10.1021/am504229n.
- [32] Hyun-Tak Kim et al. "Mechanism and observation of Mott transition in VO₂-based two- and three-terminal devices". In: *New Journal of Physics* 6 (May 2004), p. 52. DOI: 10.1088/1367-2630/6/1/052.
- [33] Seungdo Kim and Michael Overcash. "Energy in chemical manufacturing processes: Gate-to-gate information for life cycle assessment". In: *Journal of Chemical Technology and Biotechnology* 78 (Sept. 2003), pp. 995–1005. DOI: 10.1002/jctb.821.
- [34] Niranjani Krishnan et al. "A Hybrid Life Cycle Inventory of Nano-Scale Semiconductor Manufacturing". In: *Environmental science and technology* 42 (May 2008), pp. 3069–75. DOI: 10.1021/es071174k.
- [35] T. Laurila et al. "Chemical stability of Ta diffusion barrier between Cu and Si". In: *Thin Solid Films* 373 (Sept. 2000), pp. 64–67. DOI: 10.1016/S0040-6090(00)01102-0.
- [36] Prof. Patricia Luis. "Life Cycle Assessment (LCA)". Moodle. 2020.
- [37] Herbert B. Michaelson. "The work function of the elements and its periodicity". In: *Journal of Applied Physics* 48 (1977), pp. 4729–4733.
- [38] LNF - University of Michigan. *Material restrictions*. URL: https://lnf-wiki.eecs.umich.edu/wiki/Material_restrictions.
- [39] MicroChemicals. *HMDS*. URL: https://www.microchemicals.com/products/adhesion_promotion/hmds.html.
- [40] E. W. J. Mitchell and J. W. Mitchell. "The Work Functions of Copper, Silver and Aluminium". In: *Proceedings of the Royal Society of London Series A* 210.1100 (Dec. 1951), pp. 70–84. DOI: 10.1098/rspa.1951.0231.
- [41] Jorge Morales Pedraza. "Chapter 4 - Current Status and Perspective in the Use of Coal for Electricity Generation in the North America Region". In: *Conventional Energy in North America*. Ed. by Jorge Morales Pedraza. Elsevier, 2019, pp. 211–257. ISBN: 978-0-12-814889-1. DOI: <https://doi.org/10.1016/B978-0-12-814889-1.00004-8>. URL: <https://www.sciencedirect.com/science/article/pii/B9780128148891000048>.
- [42] Joyeeta Nag and Jr. Haglund R. F. "Synthesis of vanadium dioxide thin films and nanoparticles". In: *Journal of Physics Condensed Matter* 20.26, 264016 (July 2008), p. 264016. DOI: 10.1088/0953-8984/20/26/264016.
- [43] nexAir. *What Gases Work Best for Annealing?* URL: <https://www.nexair.com/learning-center/what-gases-work-best-for-annealing/>.

-
- [44] Terry Norgate and Nawshad Haque. "Using life cycle assessment to evaluate some environmental impacts of gold production". In: *Journal of Cleaner Production* 29-30 (2012), pp. 53–63. ISSN: 0959-6526. DOI: <https://doi.org/10.1016/j.jclepro.2012.01.042>. URL: <https://www.sciencedirect.com/science/article/pii/S0959652612000947>.
- [45] Philip Nuss and Matthew J. Eckelman. "Life Cycle Assessment of Metals: A Scientific Synthesis". In: *PLOS ONE* 9.7 (July 2014), pp. 1–1. DOI: 10.1371/journal.pone.0101298. URL: <https://doi.org/10.1371/journal.pone.0101298>.
- [46] *Ohmic contact*. URL: https://en.wikipedia.org/wiki/Ohmic_contact.
- [47] Thibault Pirson et al. "The Environmental Footprint of IC Production: Review, Analysis, and Lessons From Historical Trends". In: *IEEE Transactions on Semiconductor Manufacturing* 36.1 (2023), pp. 56–67. DOI: 10.1109/TSM.2022.3228311.
- [48] EE311 notes/ Saraswat. "Metal/Semiconductor Ohmic Contacts".
- [49] Duke University - SMIF. *Introduction to PECVD*. 2020. URL: https://www.youtube.com/watch?v=9CGuysJoSCO&ab_channel=DukeUniversity-SMIF.
- [50] Ahum Sohn et al. "Evolution of local work function in epitaxial VO₂ thin films spanning the metal-insulator transition". In: *Applied Physics Letters* 101 (Nov. 2012). DOI: 10.1063/1.4766292.
- [51] PureAire Monitoring Systems. *Nitrogen Use in the Fabrication of MEMS*. 2020. URL: <https://www.pureairemonitoring.com/nitrogen-use-in-the-fabrication-of-mems/>.
- [52] Paul Teehan. "Integrative approaches to environmental life cycle assessment of consumer electronics and connected media". PhD thesis. University of British Columbia, 2014. DOI: <http://dx.doi.org/10.14288/1.0167496>. URL: <https://open.library.ubc.ca/collections/ubctheses/24/items/1.0167496>.
- [53] Brigham Young University. *METAL-SEMICONDUCTOR OHMIC AND SCHOTTKY CONTACTS*. 2023. URL: <https://cleanroom.byu.edu/ohmic-schottky>.
- [54] Ester van der Voet et al. *Environmental challenges of anthropogenic metals flows and cycles*. English. France: United Nations Environment Programme, 2013. ISBN: 978-92-807-3266-5.
- [55] Siegert Wafer. *Typical Silicon Wafer Specifications*. URL: https://www.siegertwafer.com/Silicon_Wafers.html.
- [56] Selina Weber et al. "Life Cycle Assessment of a Vanadium Redox Flow Battery". In: *Environmental Science and Technology* 52 (Aug. 2018). DOI: 10.1021/acs.est.8b02073.
- [57] Gang Xu et al. "Electron injection assisted phase transition in a nano-Au-VO₂ junction". In: *Applied Physics Letters* 93 (Aug. 2008), pp. 061911–061911. DOI: 10.1063/1.2972106.
- [58] Rui Yuan et al. "A calibratable sensory neuron based on epitaxial VO₂ for spike-based neuromorphic multisensory system". In: *Nature Communications* 13 (July 2022), p. 3973. DOI: 10.1038/s41467-022-31747-w.

UNIVERSITÉ CATHOLIQUE DE LOUVAIN
École polytechnique de Louvain

Rue Archimède, 1 bte L6.11.01, 1348 Louvain-la-Neuve, Belgique | www.uclouvain.be/epl